Department of Electrical Engineering

A Wavelet-based Method for Estimating Damping in Power Systems

Jukka Turunen

Aalto University

DOCTORAL DISSERTATIONS

Aalto University publication series
DOCTORAL DISSERTATIONS 16/2011

A Wavelet-based Method for Estimating Damping in Power Systems

Jukka Turunen

Doctoral dissertation for the degree of Doctor of Science in Technology to be presented with due permission of the School of Electrical Engineering for public examination and debate in Auditorium S1 at the Aalto University School of Electrical Engineering (Espoo, Finland) on the 25th of March 2011 at 12 noon.

Aalto University
School of Electrical Engineering
Department of Electrical Engineering
Power Transmission Systems

Supervisor
Professor Liisa Haarla

Instructor
Professor Liisa Haarla

Preliminary examiners
Prof. Dr.-Ing. Christian Rehtanz, Technische Universität Dortmund, Germany
Dr. Petr Korba, ABB Corporate Research, Switzerland

Opponent
Associate Professor Olof Samuelsson, Lunds Universitet, Lunds Tekniska Högskola, Sweden

Aalto University publication series
DOCTORAL DISSERTATIONS 16/2011

ISBN 978-952-60-4051-6 (pdf)
ISBN 978-952-60-4050-9 (printed)
ISSN-L 1799-4934
ISSN 1799-4942 (pdf)
ISSN 1799-4934 (printed)

Aalto Print
Helsinki 2011

The dissertation can be read at http://lib.tkk.fi/Diss/2011/isbn9789526040516/

Publication orders (printed book):
jukka.turunen@aalto.fi

Author
Jukka Turunen

Name of the doctoral dissertation
A Wavelet-based Method for Estimating Damping in Power Systems

Publisher School of Electrical Engineering

Unit Department of Electrical Engineering

Series Aalto University publication series DOCTORAL DISSERTATIONS 16/2011

Field of research Electrical Transmission Systems

Manuscript submitted 30.11.2010 **Manuscript revised** 10.01.2011

Date of the defence 25.03.2011 **Language** English

☒ **Monograph** ☐ **Article dissertation (summary + original articles)**

Abstract

This thesis presents a novel approach to electromechanical oscillation damping estimation under the ambient conditions of a power system. The power system is said to operate under the ambient conditions when it is only subjected to ever present small excitations such as constantly varying load. The damping estimation method is based on the wavelet transform and the random decrement technique.

The thesis reviews the properties of the wavelet transform that are essential in damping estimation, defines criteria for optimal mother wavelet selection in damping estimation, and identifies the possible mother wavelets in damping estimation of the Nordic power system. It also studies the optimal selection of other parameters and defines values for them.

Both the simulated and measured power system data is analyzed with the damping estimation method in the thesis. The results show that when the parameter selections (especially the mother wavelet function and the time window length) of the damping estimation method are done correctly and a signal with good observability of the mode is used, the damping can be estimated close to the known damping of the simulation model using the ambient-excited oscillation data. The damping estimates are more accurate when the real damping of the oscillation mode is low; i.e. when it is more important to system stability. The measurement noise of the analyzed signals does not have much effect on the estimates.

It is shown that the method can be used to observe the degraded damping due to incorrect operation of the power system damping controller. In addition, the method can possibly be applied to verification of the power system simulation model. Although the performance of the method is studied for the Nordic power system case, it is recognized that the method is applicable to other power system, too.

Keywords Ambient oscillation, damping estimation, electromechanical oscillation, PMU, power oscillation, power system, random decrement technique, wavelet transform, WAMS

ISBN (printed) 978-952-60-4050-9 **ISBN (pdf)** 978-952-60-4051-6

ISSN-L 1799-4934 **ISSN (printed)** 1799-4934 **ISSN (pdf)** 1799-4942

Pages 141 **Location of publisher** Espoo **Location of printing** Helsinki **Year** 2011

The dissertation can be read at http://lib.tkk.fi/Diss/2011/isbn9789526040516/

Tekijä(t)
Jukka Turunen

Väitöskirjan nimi
Wavelet-pohjainen menetelmä vaimennuksen estimointiin voimajärjestelmissä

Julkaisija Sähkötekniikan korkeakoulu

Yksikkö Sähkötekniikan laitos

Sarja Aalto-yliopiston julkaisusarja VÄITÖSKIRJAT 16/2011

Tutkimusala Sähkönsiirtojärjestelmät

Käsikirjoituksen pvm 30.11.2010 **Korjatun käsikirjoituksen pvm** 10.01.2011

Väitöspäivä 25.03.2011 **Kieli** Englanti

☒ **Monografia** ☐ **Yhdistelmäväitöskirja (yhteenveto-osa + erillisartikkelit)**

Tiivistelmä

Tämä väitöskirja esittelee uuden lähestymistavan sähkövoimajärjestelmän sähkömekaanisen heilahtelun vaimennuksen arviointiin, kun voimajärjestelmän herätteenä toimivat aina sähköverkossa läsnä olevat pienet muutokset, kuten muutokset kuormituksessa. Vaimennuksen arviointimenetelmä perustuu wavelet-muunnokseen ja random decrement -tekniikkaan.

Väitöskirja esittelee wavelet-muunnoksen ominaisuudet, jotka ovat oleellisia vaimennuksen arvioinnissa; määrittelee kriteerit optimaalisen wavelet-funktion valinnalle vaimennuksen arvioinnissa ja määrittää mahdolliset wavelet-funktiot Pohjoismaisen voimajärjestelmän vaimennuksen arviointiin. Se tutkii myös muiden parametrien optimaalista valintaa ja määrittää niille arvot.

Vaimennuksen arviointimenetelmällä analysoidaan tässä väitöskirjassa sekä simuloitua että mitattua voimajärjestelmädataa. Tulokset osoittavat, että kun menetelmän parametrivalinnat (erityisesti wavelet-funktio ja aikaikkunan pituus) tehdään oikein ja käytetään signaalia, jolla on hyvä heilahtelumoodin havaittavuus, vaimennusarviot ovat lähellä simulaatiomallin tunnettua vaimennusta, käytettäessä voimajärjestelmän normaalia heilahteludataa. Vaimennusarviot ovat tarkempia, kun heilahtelumoodin todellinen vaimennus on pieni ja vaimennus on tärkeämpi järjestelmän stabiiliuden kannalta. Analysoitavien signaalien mittauskohinalla ei ole suurta vaikutusta arvioihin.

Väitöskirjassa osoitetaan, että menetelmää voidaan käyttää havaitsemaan väärin toimivan vaimennussäätäjän aiheuttama huonontunut vaimennus. Lisäksi menetelmää voidaan mahdollisesti soveltaa simulaatiomallin verifioinnissa. Vaikka menetelmän suorituskykytarkastelut suoritettiin Pohjoismaisen voimajärjestelmän tapauksessa, on menetelmä sovellettavissa myös muihin voimajärjestelmiin.

Avainsanat Sähkömekaaninen heilahtelu, sähkövoimajärjestelmä, tehoheilahtelu, vaimennusestimointi, wavelet-muunnos

ISBN (painettu) 978-952-60-4050-9 **ISBN (pdf)** 978-952-60-4051-6

ISSN-L 1799-4934 **ISSN (painettu)** 1799-4934 **ISSN (pdf)** 1799-4942

Sivumäärä 141 **Julkaisupaikka** Espoo **Painopaikka** Helsinki **Vuosi** 2011

Luettavissa verkossa osoitteessa http://lib.tkk.fi/Diss/2011/isbn9789526040516/

Preface

From a personal point of view, this thesis is a straight continuation from the author's Master's thesis which was carried out at the Finnish transmission system operator, Fingrid, in 2005. The thesis considered the applicability of commercial electromechanical oscillation damping monitoring systems in the Nordic power system. The main findings of the Master's thesis were that the variability of the damping estimates is high and therefore the real damping and changes in the power system oscillation modes damping level are hard to observe reliably.

From a broader perspective, this thesis is a part of the work towards a better understanding and management of the electromechanical oscillations in the Nordic power system that has been going on since the end of the 1990's when prolonged inter-area oscillations were observed in Finland. The work was started with the linear analysis and the dynamic simulation studies in order to find out the possibilities to better damp the oscillations with the controls and the grid reinforcements. Based on these studies Fingrid took several actions to increase damping of the 0.3 Hz inter-area mode because the controllability of the mode was found to be the highest in the Finnish part of the Nordic power system (Elenius et al. 2005). These actions were, for instance, the addition of series capacitors to 400 kV lines in Northern Finland, the retuning of power system stabilizers of the largest generators in Southern Finland, the design and implementation of a new power oscillation damper for the HVDC link between Finland and Sweden, and the addition of power oscillation dampers for the HVDC link between Finland and Estonia as well as for the static var compensator device in Southern Finland (Turunen et al. 2008). The actions considerably increased the available power transfer capacity from Finland towards the rest of the Nordic power system.

After the above mentioned measures were taken to improve the damping of the oscillations, the focus was put onto monitoring the oscillations. The first idea of Fingrid was to have a system that warns the system operator if prolonged or growing oscillations exist. However, critical oscillations occur very seldomly and the operator has very little time to react after a warning. Therefore the next idea was to estimate the damping under ambient operation of the power system, i.e. when the system is subjected only to the small excitations caused mainly by the constantly varying loads. This idea was supported by the fact that commercial software, that later emerged to be the now called wide area monitoring systems (WAMS), became available for this purpose. Also the commercial availability of the high frequency measurement devices and especially the phasor measurement units (PMU) enabled this development.

A test period of about two years was conducted during which the applicability of the commercially available damping monitoring systems was analyzed at Fingrid and especially in the author's Master's thesis. Because the damping estimates turned out to be highly variable, the utilization of the damping monitoring systems was difficult and gave an input to the further research on the subject. The emphasis of this reseach as well as of this thesis has been on more accurate damping estimation. The end of this path has not been reached yet and the research on the topic continues.

Acknowledgements

The author acknowledges especially Professor Liisa Haarla from Aalto University School of Electrical Engineering for supervision of the work and all the support during the whole research project. The current and past members of the management group of the research project: Tuomas Rauhala, Katariina Saarinen, Harri Kuisti, Mikko Koskinen, Jussi Jyrinsalo, Timo Kaukonen, Minna Laasonen, and Maarit Uusitalo from Fingrid and Jarno Lamponen from Aalto University School of Electrical Engineering are acknowledged for valuable discussions and for providing industrial expertise, simulation models, and measurement data. Professor Matti Lehtonen from Aalto University School of Electrical Engineering and researcher Jegatheeswaran Thambirajah from Imperial College London are acknowledged for the ideas and co-operation during the course of the research project.

The author wants to thank also Doctor Nelson Martins from Cepel (Centro de Pesquisas de Energia Elétrica, Brazil), Professor Kjetil Uhlen from NTNU (Norwegian University of Science and Technology), Professors Nina Thornhill and Bikash Pal from Imperial College London, and Doctor Mats Larsson from ABB Corporate Research Switzerland for co-operation during different periods of the research project. William Martin is acknowledged for proofreading the final version of the manuscript.

Contents

List of Abbreviations

AC	Alternating Current
AVR	Automatic Voltage Regulator
Bior	Biorthogonal wavelet family
Cgau	Complex Gaussian wavelet family
Cmor	Complex Morlet wavelet family
Cmor1-0.5	Complex Morlet wavelet of order 1-0.5
Cmor1-1	Complex Morlet wavelet of order 1-1
Cmor1-1.3	Complex Morlet wavelet of order 1-1.3
Cmor1-1.5	Complex Morlet wavelet of order 1-1.5
Cmor1-5	Complex Morlet wavelet of order 1-5
Coif	Coiflets wavelet family
CWT	Continuous Wavelet Transform
Db	Daubechies wavelet family
Db28	Daubechies wavelet of order 28
Dmey	Discrete Meyer wavelet family
DSA	Dynamic Security Assessment
DWT	Discrete Wavelet Transform
Fbsp	Complex frequency b-spline wavelet family
Fenno-Skan	HVDC link between Southern Finland and Sweden
Gaus	Gaussian wavelet family
Gaus20	Gaussian wavelet of order 20
Gaus28	Gaussian wavelet of order 28
Gaus4	Gaussian wavelet of order 4
Gaus44	Gaussian wavelet of order 44
HVDC	High Voltage Direct Current
Mexh	Mexican hat wavelet family
Meyr	Meyer wavelet family
Morl	Morlet wavelet family
n – 1 criterion	Operational principle used commonly in power systems, states that power system should withstand any single fault in the system
PDC	Phasor Data Concentrator
PMU	Phasor Measurement Unit
POD	Power Oscillation Damper

pp	Percentage point
PSS®E	Power System Simulator for Engineering
Rbio	Reverse biorthogonal wavelet family
RDS	Random Decrement Signature
RDT	Random Decrement Technique
Shan	Complex Shannon wavelet family
SNR	Signal-to-Noise Ratio
std	Standard deviation
STFT	Short Time Fourier Transform
SVC	Static Var Compensator
Sym	Symlets wavelet family
TSO	Transmission System Operator
WAMS	Wide Area Monitoring System
WT	Wavelet Transform

List of Symbols

a	A scale parameter of a wavelet
A_A	Exponent of approximation accuracy of a wavelet function
a_i	The wavelet scales from the lower frequency bound to the upper frequency bound with the dense enough spacing to achieve high enough resolution for frequency estimation
a_m	Estimated mode scale
b	Position of a time-frequency atom / translation parameter of a wavelet
B_A	Absolute bias
b_j	The wavelet positions from the beginning of the time window to the end of the time window with the spacing of signal sampling period
B_R	Relative bias
c	Frequency of a time-frequency atom
$C(a,b)$	A wavelet coefficient with the scale parameter a and with the translation parameter b
$C(a_i, b_i)$	Wavelet coefficients with the scale parameters a_i and position parameters b_i
$C_{env}(t)$	Wavelet coefficient envelope (in case of a real wavelet) or the wavelet coefficient modulus (in case of a complex wavelet)
C_m	Wavelet coefficients at the estimated frequency
$C_{m,\,imp}$	Wavelet coefficients after applying the RDT
$e(t)$	Input which excites the electromechanical oscillations in a power system (e.g. constantly varying loads)
V_E	Estimated value
f	Frequency
f_c	Center frequency of a wavelet
f_m	Estimated mode frequency
g	Time-frequency atom

h	Threshold used in the RDT
N	Number of samples averaged in the RDT
P_{noise}	Average power of the noise in a signal
P_{signal}	Average power of a signal (without mean value)
r	Sample number
V_{R}	Real value
S	Short time Fourier transform
SNR	Signal-to-noise ratio in linear scale
t_r	Time instances when the signal crosses the triggering condition of the RDT
W	Wavelet transform
T_{d}	Time difference between the two points of the wavelet coefficient envelope or the wavelet coefficient modulus between which the damping is calculated
T_{sp}	Selection point of the damping estimate or the time instant from the beginning of the approximate impulse response, needed for the damping calculation
$y(t)$ and $y(t+T_{\text{d}})$	Magnitudes of successive peaks of an impulse response/ Measurable output signal of the power system
y_0	Sample of the signal
Δ	Signal sampling period
$\delta = \ln\left(\frac{y(t+x)}{y(t)}\right)$	Logarithmic decrement
ζ	Damping ratio
ζ_{m}	Estimated damping ratio of the mode
σ	Real part of a pole
σ_{noise}	Standard deviation of the noise in a signal
σ_{signal}	Standard deviation of a signal
σ_t^2	Temporal variance
σ_ω^2	Frequency variance

τ	Sample length used in the RDT/Time constant
ψ	A wavelet (or mother wavelet)
$\hat{\psi}$	Fourier transform of the wavelet function ψ
$\psi_{a,b}(t) = \frac{1}{\sqrt{a}}\psi\left(\frac{t-b}{a}\right)$	A daughter wavelet of the mother wavelet ψ with a scale parameter a and with a translation parameter b
$\psi_{\text{d.e.}}$	Wavelet function used in the impulse response's damping estimation
$\psi_{\text{f.e.}}$	Wavelet function used in the frequency estimation
$\psi_{\text{m.e.}}$	Wavelet function used in the mode extraction
$\psi^{\text{Gaus4}}_{a_4,b_4}$	Gaussian wavelet of order 4 with the scale parameter a_4 and with the translation parameter b_4
$\psi^{\text{Gaus20}}_{a_{20},b_{20}}$	Gaussian wavelet of order 20 with the scale parameter a_{20} and with the translation parameter b_{20}
$\psi^{\text{Gaus44}}_{a_{44},b_{44}}$	Gaussian wavelet of order 44 with the scale parameter a_{44} and with the translation parameter b_{44}
ω_{c}	Center frequency of a wavelet
ω_{n}	Natural frequency of an oscillation mode
$\omega_{\text{t}} = \omega_{\text{n}}\sqrt{1-\zeta^2}$	Frequency of oscillation/ Imaginary part of a pole
$\|\|$	Absolute value
$*$	Complex conjugate
$\langle\ \rangle$	Inner product
$\bar{}$	Mean value

1 Introduction

1.1 Motivation

The traditional way to manage the stability of a power system is based on extensive simulation studies. However, the studies can only be done for a limited set of operating conditions. In principle, the dynamic security assessment (DSA) tools could tackle the challenge arising from differences in the simulated operating condition of the power system and the realized operating condition of the real power system. DSA tools are based on simulation of the set of critical contingencies in an operating condition of the power system that is automatically updated to reflect the real operating condition of the power system (Pourbeik & Morison 2007). However, the simulation studies and the DSA tools require that the simulation model reflects the behavior of the real power system accurately enough. In practice, there are many factors causing differences between the dynamic behavior of the simulated power system and the real power system. For example, specific information of the load dynamics is often unknown for the TSO. In addition, in a large power system simulation model there is often missing or incorrect data, which cause discrepancies between the simulated and the real dynamic behavior of the power system. Components are added and updated in the power system but the simulation model might remain unupdated in some cases. Another source of incorrect data is the modeling errors.

Due to the differences between the simulated and real operating conditions of the power system as well as between the simulation model and the real behavior of the grid, a specific marginal has to be maintained between the allowed power transfer capacity and the theoretical maximum power transfer capacity, to maintain sufficient system security. Even so, instabilities of the power systems have been recorded in the past, basically due to the discrepancies between the simulated and the real dynamic behavior of the power systems (Venkatasubramanian 2003). On the other hand, market forces may pose stress on the TSOs to increase the inter-area power transfer capacities of the power system to allow functional electricity markets. At the same time due to the environmental, political, and economic reasons limitations are imposed on building new transmission lines and, by the means, on increasing the inter-area transfer capacities of the power system.

The challenges in grid operation and planning pointed out above have led the TSOs to seek for new and innovative ways to manage the power system stability issue, use the grid efficiently, and keep the security high. One of the approaches is the development of methods for estimating damping from the power system measurements. This is studied in this thesis, and a new method for damping estimation is introduced.

1.2 The Research Problem

Accurate damping estimation using the measured power system signals under the ambient conditions of the power system is the research problem of the thesis. In

addition to measured signals, simulated signals are used to study the characteristics of the damping estimation method. The operational experience achieved of some commercial damping monitoring systems which have been analyzing Finnish transmission system data has shown that there is a need for improved accuracy of damping estimation (Turunen et al. 2008).

In addition, it is recognized in many other publications too that if only ambient excitations excite the modes and if real-time monitoring capability is required with fast reaction to changes in damping level, the damping estimates tend to have too large a variance for operational use. The artificial probing can be used to reduce the variance of the damping estimates (Anderson et al. 2005, Wies et al. 2007, Wiltshire et al. 2007, Hauer et al. 2009, Ledwich et al. 2008, Turunen et al. 2008, Zhou et al. 2006a, Zhou et al. 2006b, Trudnowski & Pierre 2009, Pierre et al. 2010). However, in this thesis the damping estimation is based on the ambient oscillations that are inherent to the power system.

1.3 Objectives

The main objective of this thesis is to develop a new measurement-based method for estimating the inter-area oscillation damping under the ambient conditions of the power system. Damping estimation enables maximal utilization of the power transfer capacity of the grid while maintaining high system security.

1.4 Scope of the Research

The thesis studies the estimation of both damping and the frequency of electromechanical oscillations. This belongs under the topic of angle stability management of power systems. The scope is only on the inter-area modes (oscillation frequencies from 0.1 to 1 Hz) and especially on the damping estimation of the Nordic power system's 0.3 Hz mode because it is the limiting factor when defining the maximum power transfer capacity from Finland to Sweden.

The estimation of damping and frequency is based on measured signals, usually the phasor measurement unit (PMU) measurements. In addition to measurements, simulated signals are used to study the characteristics of the damping estimation method. Estimation of damping and frequency is studied under the ambient conditions, where only normal load variations excite the oscillations; the cases of transient oscillations and external probing are not included.

1.5 Research Methods

Computational methods are used for selecting the parameters of the method, and to study the performance of the method. A commercial software, Matlab®, is used in

carrying out the computations and another commercial software, PSS®E, to conduct the simulations of this thesis. The simulations are done using the existing simulation model of the Nordic power system and the simulations are used for producing data for the performance analyses of the method. Experimental methods are used for studying the performance of the method with the measured data. Statistical methods are used for studying the accuracy of the damping estimates.

1.6 Previous Work

Damping estimation under the ambient conditions has been a topic of great interest over the last decade or so (Pourbeik & Rehtanz 2007, Doraiswami & Liu 1993, Pierre et al. 1997, Ledwich & Palmer 2000, Hemmingsson et al. 2001, Banejad & Ledwich 2002, Wies et al. 2003, Zhang & Ledwich 2003, Hemmingsson 2003, Korba et al. 2003, Wies et al. 2004, Anderson et al. 2005, Zima et al. 2005, Glickman et al. 2005, Zhou et al. 2006a, Wies et al. 2006a, Wies et al. 2006b, Korba 2007, Larsson et al. 2007, Wies et al. 2007, Ledwich 2007, Ghasemi & Cañizares 2007, Zhou et al. 2007, Glickman et al. 2007, Wiltshire et al. 2007, Leirbukt et al. 2008, Trudnowski et al. 2008, Trudnowski 2008, Uhlen et al. 2008, Zhou et al. 2008, Liu & Venkatasubramanian 2008, Laila et al. 2009, Larsson & Laila 2009, Korba & Uhlen 2010, Thambirajah et al. 2010b, Vanfretti et al. 2010). In these publications, several different methods for damping estimation under the ambient conditions of the power system have been presented. However, the methods presented in all of the above mentioned papers differ substantially from the method of this thesis. Unlike this thesis, none of the methods are based on utilization of the wavelet transform in damping estimation.

Most of the methods, like the least squares (Wies et al. 2004, Zhou et al. 2007), regularized robust recursive least squares (Zhou et al. 2008), Yule-Walker with autoregressive (Pierre et al. 1997) and autoregressive moving average model (Wies et al. 2003), the Kalman filter with autoregressive model (Korba et al. 2003), and the subspace method (Zhou et al. 2006a, Larsson & Laila 2009), are parametric; they assume a certain model and fit the parameters of the model to minimize the difference between the model output and the system output (Thambirajah et al. 2010a). The main drawback with the parametric methods is that they require the assumption of the model structure. In addition, some models like the autoregressive and autoregressive moving average require the selection of model orders. The selection affects the estimation results (Wies et al. 2003). Incorrect assumption of the model structure and/or order might lead to incorrect damping estimates. Usually, the parametric methods also assume that the power system is excited by white noise (Thambirajah et al. 2010a). However, this assumption can be considered valid in a power system where the number of loads is large and the individual loads are small compared to the system size.

Some other methods like the autocorrelation approach (Ledwich & Palmer 2000), damping estimation from spectral estimates (Hemmingsson 2003), Welch periodogram methods and the method presented in this thesis are non-parametric; they work directly on the data (Thambirajah et al. 2010a).

Several factors affect the usefulness of a damping estimation method in practical applications. First of all, the damping estimation method should produce accurate

estimates. Second, the estimates should react to changes in real damping fast enough. Both the requirement of accuracy and speed of reaction depend on the application the method is applied to: for example, real-time damping monitoring, tuning of power system stabilizers and power oscillation dampers, and for power system planning purposes. The third factor affecting the usefulness of a damping estimation method is the ease of tuning the method for a specific power system or application. The fourth is the reliability or robustness of the estimates during normal operation and during abrupt changes of the power system.

In developing the damping estimation method of this thesis the emphasis has been on the accurate and robust damping estimates. The speed of reaction and the ease of tuning have been secondary objectives. However, in general the tuning process of the non-parametric methods, like the one in this thesis, is less complicated than that of the parametric methods. Although the method is non-parametric by nature (it does not assume a specific system model), some parameters need to be selected.

In some other methods and especially in the Kalman filter approach (Korba et al. 2003, Korba 2007) the emphasis is on fast estimation of changes in damping when the mode is well excited. However, the performance of the Kalman filter approach is limited when the excitation of the mode is low (Turunen et al. 2008).

Anderson et al. (2005), Larsson & Laila (2009), Liu & Venkatasubramanian (2008), Trudnowski et al. (2008), and Trudnowski & Pierre (2009) report case studies of the performance of their respective methods. The performance analyses are based on the case studies of some particular data sets, the results are presented in multiple different ways, and there usually are multiple variable parameters in the methods. The objective comparison of the results is therefore very difficult. However, Liu & Venkatasubramanian (2008), Trudnowski et al. (2008), and Trudnowski & Pierre (2009) present similar kinds of results to those given in this thesis; i.e. the damping estimates are more accurate for a poorly damped mode than for well damped modes. The results or observations of several papers indicate that the mean values of the damping estimates are not always conservative (e.g. Wies et al. 2003, Anderson et al. 2005, Trudnowski et al. 2008, Turunen et al. 2008). In real-time operation, the conservative estimates are beneficial because they do not lead to reduced system security.

The wavelet transform has previously been used to study various power system transients. It has also been used in visualization purposes in WAMS software (Kim & Aggarwal 2001, Cirio et al. 2006, Ruiz-Vega et al. 2005). In damping estimation, the wavelet transform has been used mainly in case of transient oscillations (Kang & Ledwich 1999, Hashiguchi et al. 2003, Mei et al. 2006, Bronzini et al. 2007). Hashiguchi et al. (2003) studied briefly the damping and natural frequency of local generator oscillation excited by random load variations. Extensive analysis of utilizing the wavelet transform in inter-area oscillation damping estimation under the ambient conditions has not been provided before this thesis.

In addition, several methods use only the transient oscillations of the power system in determining the damping (Poon & Lee 1988, Hauer 1991, Pierre et al. 1992, Grund et al. 1993, Trudnowski et al. 1998, Trudnowski et al. 1999, Sanchez-Gasca & Chow 1999, Ruiz-Vega et al. 2003, Ruiz-Vega et al. 2004, Crow & Singh 2005, Messina & Vittal 2006, Messina et al. 2006, Terzija et al. 2009). However, the damping estimation

under ambient conditions, the topic of this thesis, is not considered in these publications.

Some methods have been implemented in commercial or non-commercial Wide-Area Measurement Systems (WAMS) software and are in operational or experimental use in various countries (Pourbeik & Rehtanz 2007, Sattinger et al. 2006, Wilson 2007, Hauer et al. 2009, Cai et al. 2005, Ledwich et al. 2008, Leirbukt et al. 2006, Su & Jau 2007, Turunen et al., 2008). These publications discuss implementation of the existing methods in WAMS and the main emphasis of them is not on developing new methods for damping estimation, which is the focus of this thesis.

1.7 Scientific Contribution

The main scientific contribution of this thesis is a new method to estimate the damping and frequency of the power system electromechanical oscillation mode under the ambient conditions of the power system. The method estimates the damping from the power system signals which are usually measured but can be simulated too. The method is based on utilizing the *wavelet transform* and the *random decrement technique*. The frequency estimation is based on the wavelet transform only and the damping estimation is based on a combination of the wavelet transform and the random decrement technique.

The thesis presents a detailed study of the *optimal parameters* for the method, especially the *optimal mother wavelet selection*. First, the general criteria for the optimal mother wavelet selection in the mode extraction and frequency estimation are defined and the criteria are quantitatively specified for the studied Nordic power system case. The feasible mother wavelets in the damping estimation of the impulse response are also studied in the thesis; this wavelet selection is not dependent on the power system.

The thesis studies the *damping estimation method's ability to estimate the known damping* of the dominant 0.3 Hz inter-area mode of the Nordic power system simulation model. Random variations in the loads excite the oscillation modes of the system, imitating the ambient conditions of the real power system. The characteristics of the damping estimation method are studied also in the real Nordic power system case from which the measurements are available via the wide area monitoring system.

1.8 Outline of the Thesis

Chapter 1 presents an introduction to the thesis. In the introduction, the motivation for the research project, the research problem, objectives, and scope of the research are presented. Also a short review of the previous work and description of how it differs from the work of this current thesis is presented. In addition, descriptions of the power system electromechanical oscillation, damping quantity, existing damping estimation methods, the Nordic power system, and the wavelet transform are presented.

Chapter 2 presents the main result of the thesis, a new damping estimation method for assessing the damping from the measurements under the ambient conditions of the power system. In Chapter 3, the selection of correct parameters for the method is studied. One of the most important parameter selections, the optimal wavelet function selection, is studied in this chapter too. Chapter 4 describes how the performance analysis of the damping estimation method is conducted both in the case of simulated and measured power system data. Also the issues of measurement noise and different damping conditions of the power system are addressed in the performance analysis. Chapter 5 presents the results of the performance analysis.

Chapters 6 and 7 present the discussion and conclusions of the thesis, respectively. Also some future work areas are pointed out in Chapter 7.

1.9 Electromechanical Oscillations, Damping Quantity and Damping Estimation Methods

This section describes which types of electromechanical oscillations there are in the power systems and the main focus of ambient inter-area oscillations is described in more detail. In addition, it is defined which damping quantity is used, and how the damping estimation method of this thesis is positioned in the general classification of different means to manage the stability of the power system.

1.9.1 Power System Electromechanical Oscillations

Introduction

Power system electromechanical oscillation is an inherent property of an AC transmission system. The oscillations cannot be eliminated altogether but in some power systems (e.g. with short lines) they do not cause any problems due to high damping. Under certain operating conditions the oscillations set the limits for power transfer capacity and may pose a serious threat to system stability.

There are different types of electromechanical oscillations and they can be classified by their interaction characteristics: inter-area mode oscillations, local plant mode oscillations, intraplant mode oscillations, torsional (subsynchronous) mode oscillations, and control mode oscillations. The electromechanical oscillations can also be classified by the operating condition of the power system: ambient (spontaneous) oscillations, transient oscillations, and forced oscillations. Ambient, transient, and forced oscillations (Figure 1 and Figure 2) are excited by constantly varying loads, large transients, and processes which are exogenous to conventional stability control loops, respectively. (Paserba 1996, Pal & Chaudhuri 2005, Kundur 1993).

In this thesis only the ambient inter-area oscillations are studied and the oscillation type is described in more detail in the following section.

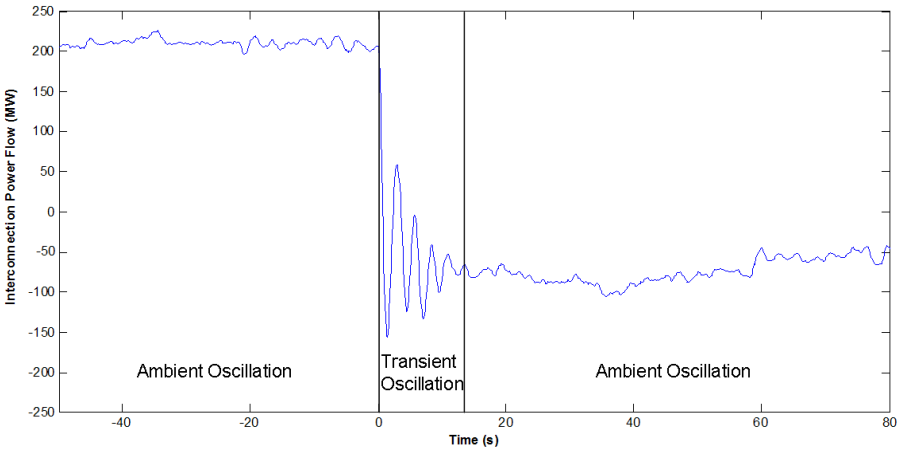

Figure 1. Examples of ambient and transient inter-area oscillations in the measured power flow of a line. The transient oscillation is excited by a sudden power change of an HVDC link. The ambient oscillations are excited mainly by constantly varying loads.

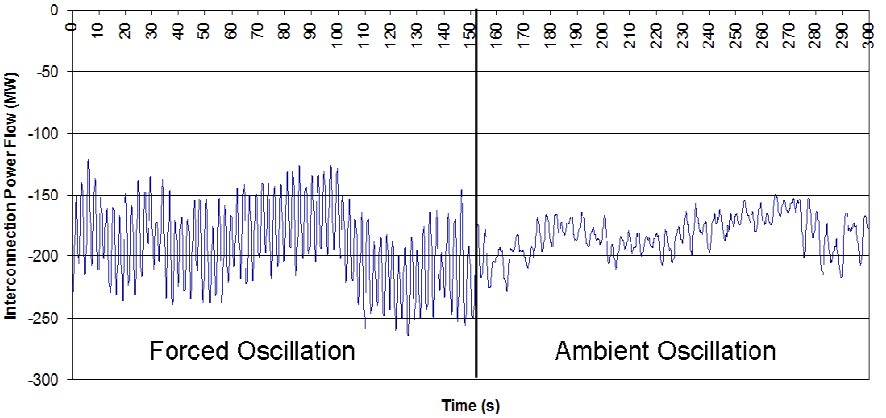

Figure 2. Examples of forced and ambient inter-area oscillations in the measured power flow of a line. The forced oscillation is excited by modulating the power of an HVDC link. The ambient oscillations are excited mainly by constantly varying loads.

Ambient Inter-Area Oscillations

In the expression "*ambient inter-area oscillation*", the term "ambient" denotes that the oscillations are excited by the multitude of sources that are integral part of the power system. The main excitation under ambient conditions comes from the combined effect of varying loads, which are randomly varying by nature. In addition, minor transients such as minor changes in production, minor switching events, or minor faults can be considered as ambient excitation of the electromechanical oscillations. With these inputs, a power system is said to operate *under the ambient conditions* and the response of the power system to these inputs is the *ambient response*. The term "inter-area" refers

to the oscillations in which a coherent group of generators in one part of the system swings against other generators in other parts of the system (Pal & Chaudhuri 2005, Kundur 1993). The frequency range of the inter-area oscillations is from 0.1 to 1 Hz (Paserba 1996). Inter-area oscillations are observed in many system quantities over a large part of the power system (Pal & Chaudhuri 2005). They are observed in the systems where two or more groups of closely coupled machines are interconnected by weak ties (Kundur 1993).

Inter-area oscillation is a complex and non-linear phenomenon and its damping characteristic is dictated by the strength of the transmission path, the nature of the loads, the power flow through the interconnection, and the interaction of loads with the dynamics of generators and their associated controls (Pal & Chaudhuri 2005, Messina 2009). Usually the oscillations are stable but if the system is stressed too much the Hopf bifurcation may occur where the real parts of a complex conjugate eigenvalue pair cross the imaginary axis and the system becomes unstable (Mithulananthan et al. 2003).

A weak transmission path means high effective impedance between the oscillating generator groups. The high impedance causes the amortisseur windings of the generators to lose their effect on the inter-area oscillation damping. Also the adverse interactions among the automatic controls, especially the automatic voltage regulators (AVRs), decrease inter-area oscillation damping. Even without the adverse effects among the automatic controls, the uncontrolled system's damping for inter-area oscillations is commonly poor when the transmission path is weak. Additionally, when the loading of the interconnecting lines grow, the damping decreases, mainly because the angle difference between the oscillating generator groups grow and thus the voltage oscillations at the generator terminals grow, causing the AVRs to act and produce negative damping. (Paserba 1996)

In certain conditions the inter-area oscillations restrict the allowable power transfer through the tie lines and thus cause economical losses (Messina 2009). For example, in the Nordic power system the inter-area oscillations limit the power transfer capacity from Finland to Sweden.

Ambient inter-area oscillations (Figure 1 and Figure 2) occur in the power system due to poor damping and they are excited mainly by the constantly varying loads. Usually the oscillations are small in amplitude and thus the power system behavior can be assumed linear and the associated damping of the oscillation modes is the small-signal damping of the modes (Kundur 1993). In Figure 1, an example of a transient oscillation (caused by a power change of an HVDC link) and in Figure 2 an example of a forced oscillation (caused by modulation of an HVDC link) is presented, together with the ambient oscillation, for the comparison of different kinds of oscillations.

1.9.2 Damping Quantity

In this thesis, the damping is quantified with the damping ratio. The damping ratio is a quantity related to the linear systems. Because the power system is assumed to behave (approximately) linearly when the ambient inter-area oscillations are considered, the damping ratio is a suitable quantity for the purpose.

The damping ratio can be determined via the logarithmic decrement of a second order system impulse response[1] with the equation

$$\zeta = \frac{\delta}{\sqrt{(2\pi)^2 + \delta^2}} \left(\approx -\frac{\delta}{\omega T_\mathrm{d}} \text{ if } \delta < 0.2 \right), \tag{1}$$

where $\delta = \ln\left(\frac{y(t+T_\mathrm{d})}{y(t)}\right)$ is the *logarithmic decrement*. $y(t)$ and $y(t+T_\mathrm{d})$ are the magnitudes of successive peaks of the impulse response, T_d is a period of the oscillation, and ω is the angular frequency of the oscillation.

It is common to express the damping ratio in percent. Hence $\zeta = 0.1$ may be expressed as the damping ratio of 10 %.

1.9.3 Damping Estimation Methods

In practice, power system electromechanical oscillation stability and damping are estimated with time-domain simulations, linear analysis or signal analysis. The first two methods rely on the mathematical model of the power system (Kundur 1993) but the last is used to estimate damping directly from the power system signals. Signal analysis is the main topic of this thesis. Time-domain simulations and linear analysis are also used.

In the following the damping estimation methods are briefly described, their use in this thesis is characterized, and their benefits and drawbacks are specified.

Time-domain Simulations

Time-domain simulations need the individual models of the generators, automatic voltage regulators (AVR), turbine-governors and the system loads by the differential and algebraic equations. The network is modeled by the algebraic equations. The equations form a non-linear mathematical model of the system. The analytical solution of the non-linear system model is generally not possible and it is usually solved with numerical integration methods to simulate the system behavior in the time domain. (Machowski et al. 1997) The simulations are used[2] here in producing data for the performance analysis of the damping estimation method. The simulations are beneficial because they enable the calculation of reference damping for comparisons.

A benefit of the time-domain simulations is that a correct system model leads to very realistic results of the power system behavior. The main drawback of the time-domain

[1] Second order system impulse response is the output of a second order system to an impulse input. A second order system has only one oscillation mode.

[2] Usually the time-domain simulation method is used to resolve the question of whether or not a power system will recover successfully after being subjected to severe transients such as three phase faults. It is also used to test that the controls designed using linear analysis methods do fulfill the design criteria also in a nonlinear environment (Rogers 2000).

simulation method is that deficiencies in the system model lead to conservative transfer limits and/or to reduced system security.

Linear Analysis

For the linear analysis, usually the same system model is used as for the time-domain simulations but the non-linear differential and algebraic equations are linearized around the equilibrium point and a set of linear differential and algebraic equations is obtained. Linear analysis[3] is utilized here in describing the oscillation characteristics (frequency response and a mode shape) of the Nordic power system.

Many important components (generators, AVRs, governors, loads) in a power system have very non-linear characteristics. However, when the power system is operating under the ambient conditions, the resulting oscillations are essentially linear allowing the use of linear analysis methods in assessing oscillation stability (and damping) (Rogers 2000, Pal & Chaudhuri 2005).

The main benefit of the linear analysis is that it enables the use of standard linear analysis tools. The main drawback of the linear analysis is that the power system is essentially a non-linear system and the results achieved with the linear analysis are applicable only when the assumption of linear behavior is valid.

Signal Analysis

The concept of signal analysis in damping estimation includes a multitude of methods. Common for all of the methods is that they rely, instead of system model, only on the signals of the power system. The signals are usually measured from the power system, but simulated signals are also used here to study the characteristics of the damping estimation method.

Some of the methods assume the oscillations to be linear while others do not carry this assumption (Messina 2009). The signals to be used for damping estimation are those which include information of the specific oscillation mode. At the node points of the oscillations such signals are the inter-area power transfers between the oscillating areas whereas at the antinode points of the oscillations the signals are voltage angle differences between the oscillating areas, speed deviations of the participating generators and the active powers of the participating generators.

The methods of signal analysis hold an enormous potential to provide critical information for early detection, mitigation, and avoidance of large-scale cascading failures and could form the basis of smart, wide-area automated analysis and control systems (Messina 2009, Li et al. 2009). In principle the methods can be used directly in

[3] Linear analysis enables the use of standard linear analysis tools. Eigenvalues can be calculated easily and the determination of different modes' damping and frequency is straightforward. From the system eigenvectors e.g. mode shapes, participation factors, modal controllability and observability can be determined (Pal & Chaudhuri 2005).

the system stability monitoring. The results of the signal analysis methods can be compared with the simulated results of the same scenario and used to develop the system model to better reflect the actual system behavior.

The main benefit of the signal analysis methods is that they do not rely on the system model in the damping estimation. In theory, more realistic results are thus achieved than from the simulation-based methods. The main drawback of the signal analysis methods is that they might produce inaccurate results.

1.10 The Nordic Power System

1.10.1 Description and Modeling

The Nordic power system, which is studied in this thesis, is a synchronous power system consisting of the grids of Finland, Sweden, Norway and Eastern Denmark (Figure 3). There is also an internal HVDC link between Southern Finland and Southern Sweden (Fenno-Skan). There are several HVDC connections from the Nordic power system to Eastern and Western European as well as to Russian grids.

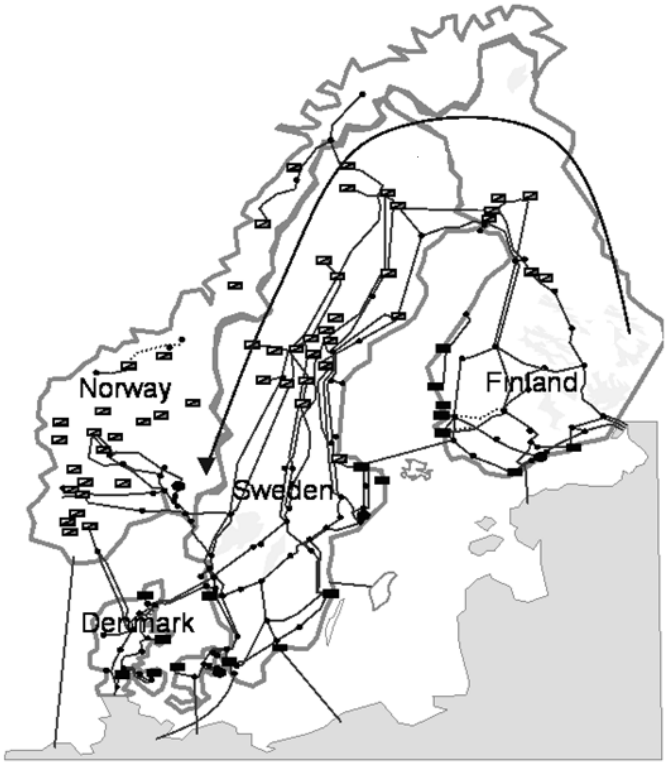

Figure 3. The Nordic power system with only the 400 kV and HVDC lines shown. The long arrow indicates the power transfer in an export situation as seen from the Finnish grid.

A detailed dynamic simulation model used by the Nordic transmission system operators (TSO) is used in this thesis. The simulation model consists of about 6000 buses, 1700 machines and 2600 loads. The number of state variables is about 17000.

1.10.2 Oscillation Characteristics

In the Nordic system, oscillations typically arise when the power is exported from Southern Finland (a smaller system) to Southern Sweden (a larger system) via interconnecting Northern AC lines. The distance between the oscillating generator groups can thus be about 2000 km.

In order to illustrate the oscillation characteristics of the Nordic power system, the dynamic simulation model is linearized and linear analysis methods are applied. The illustration is done in a power flow situation in which power transfer from Finland to Sweden is high.

The frequency response (Figure 4) shows that there are two main inter-area oscillation modes: about 0.3 Hz and about 0.5 Hz. The mode shape of the 0.3 Hz mode (Figure 5) indicates that the Finnish generators oscillate against the other generators of the Nordic power system. In the 0.5 Hz mode, typically generators of Southern Norway and Finland oscillate in phase against the rest of the system (Uhlen et al. 2003, Elenius et al. 2005).

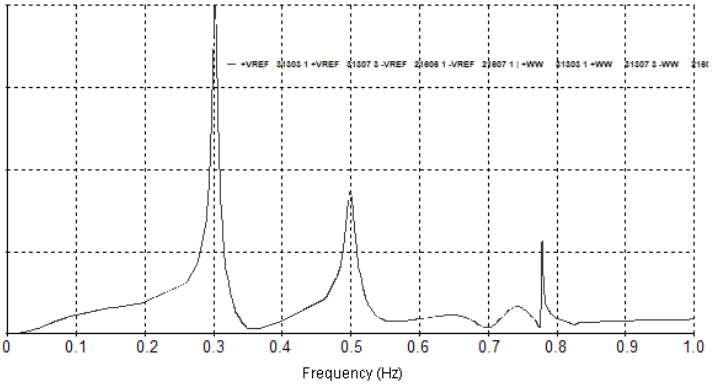

Figure 4. Frequency response of the Nordic power system when power transfer from Finland to Sweden is high.

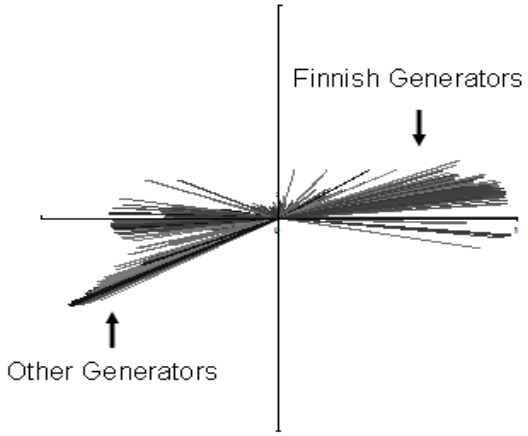

Figure 5. Mode shape of the Nordic power system 0.3 Hz mode when power transfer from Finland to Sweden is high.

1.11 Wavelet Transform

The wavelets and the wavelet transform (WT) are addressed in this section. Definition of a wavelet and different wavelet types are reviewed. Also, the wavelet transform properties are presented.

1.11.1 Wavelet Function and Wavelet Transform

General Description

A wavelet ψ (or mother wavelet) is a function of zero average

$$\int_{-\infty}^{\infty} \psi(t)dt = 0, \tag{2}$$

which is dilated with a scale parameter a, and translated by b to produce the daughter wavelets:

$$\psi_{a,b}(t) = \frac{1}{\sqrt{a}}\psi\left(\frac{t-b}{a}\right). \tag{3}$$

Different types of wavelets are often grouped into wavelet families according to their properties. The wavelet families, whose applicability in damping estimation is studied in this thesis, are the typical wavelet families, those which are included in the Matlab® Wavelet Toolbox™ version 4.1. These include biorthogonal (Bior), complex Gaussian (Cgau), complex Morlet (Cmor), coiflets (Coif), Daubechies (Db), discrete Meyer (Dmey), complex frequency b-spline (Fbsp), Gaussian (Gaus), Mexican hat (Mexh), Meyer (Meyr), Morlet (Morl), reverse biorthogonal (Rbio), complex Shannon (Shan) and symlets (Sym) wavelet families (Misiti et al. 2009). Some examples of different types of wavelets are presented in Appendix B.

The wavelet transform of $y(t)$ at the scale a and position b is computed by correlating $y(t)$ with a wavelet function ψ

$$Wy(a,b) = C(a,b) = \int_{-\infty}^{\infty} y(t)\frac{1}{\sqrt{a}}\psi^*\left(\frac{t-b}{a}\right)dt, \tag{4}$$

where $C(a,b)$ is the wavelet coefficient (approximately directly proportional to the amplitude of a specific mode) with the scale a (inversely proportional to the wavelet center frequency) and position b and ψ^* is the complex conjugated wavelet function (Mallat 1999). $y(t)$ denotes the original signal in continuous time, t, and it can be any signal in a power system which includes information of the studied oscillation. Those signals include, for example, the interconnecting line power flow between oscillating systems, the angular speed of an oscillating generator and the voltage angle difference between oscillating systems.

Center Frequency of the Wavelet Function

A commonly used term in this thesis is the *center frequency of the wavelet function*, f_c. It is defined as the frequency that maximizes the Fourier transform of the wavelet function ψ:

$$f_c = \left\{ f \;\middle|\; \max \hat{\psi}(f) = \hat{\psi}(f_c) \right\}, \tag{5}$$

where f is frequency and $\hat{\psi}$ is the Fourier transform of the wavelet function (Mallat 1999). An illustration of the center frequency of a wavelet function is presented in Figure 6.

When the wavelet scale (parameter a) is changed, the wavelet center frequency changes accordingly. If the scale is increased (the wavelet function is stretched), the center frequency of the wavelet function is decreased and vice versa. In this thesis, a wavelet function with a specific center frequency is referred to as the specific frequency wavelet. If, for instance, the wavelet function is scaled to have a center frequency of 0.3 Hz it is referred to as "0.3 Hz wavelet."

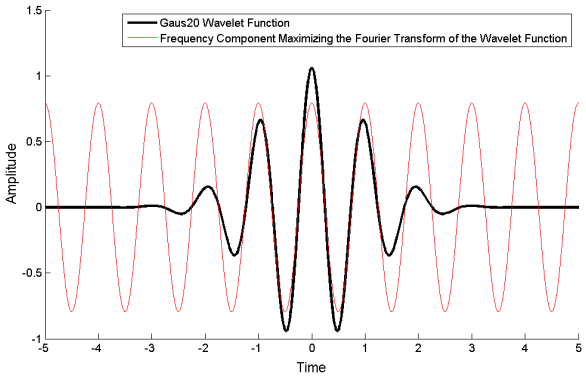

Figure 6. An illustration of the center frequency of a Gaus20 wavelet function.

Continuous and Discrete Wavelet Transform

By definition, continuous wavelet transform (CWT) is calculated such that both the parameters a and b are continuous variables in the interval of interest. In practice, though, both a and b are discrete when sampled data is analyzed. The wavelet transform is still referred to as continuous if a is an arbitrarily selected set of scales (selected according to frequency band in question and the needed resolution in frequency) and b is set by the signal sampling interval.

To reduce the amount of data produced by the wavelet transform it is possible to use the discrete wavelet transform (DWT) that uses a certain subset of scales, a, and positions, b. Using DWT, the signal reconstruction will be as accurate as using CWT (Mallat

1989). However, the subset of scales that is used in DWT sets the frequency bands of the analysis. Therefore, to enable study of any frequency component in the electromechanical oscillation frequency range (0.1–2 Hz) CWT is used in this thesis.

An example of the continuous wavelet transform at a specific frequency (wavelet function center frequency is 0.3 Hz) is presented in Figure 7. The Gaus20 wavelet function, Figure 7b, slides through the original signal, Figure 7a, with the steps governed by the signal sampling interval. The wavelet coefficient is calculated at each time instant. The resulting wavelet coefficients, Figure 7c, are (approximately) linearly dependent on the amplitude of the frequency component (or mode) of interest at each time instant and therefore the mode damping information is (approximately) preserved in the wavelet transform.

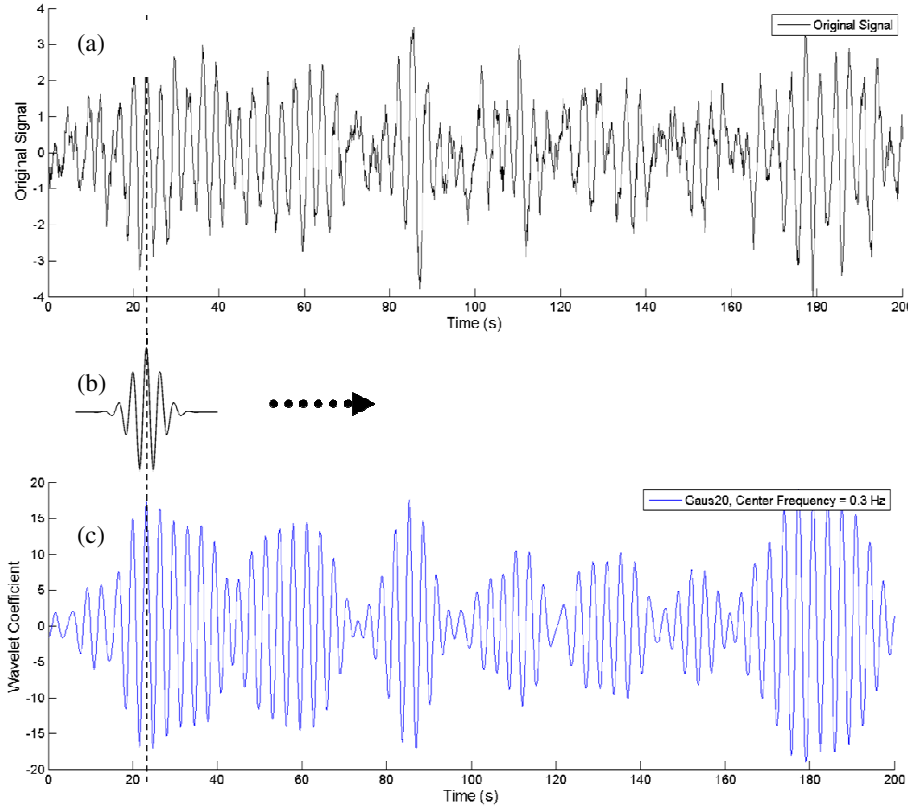

Figure 7. Continuous wavelet transform at a specific frequency. (a) presents the original signal, (b) the Gaus20 wavelet function with the center frequency of 0.3 Hz, and (c) the wavelet coefficients [Equation (4)].

Different frequency components of the original signal, Figure 7a, are studied by scaling (stretching or compressing) the wavelet function. The scaling is done by changing the parameter *a*. When the continuous wavelet transform is used, any scale can be selected. As an example, the wavelet coefficients with the 0.5 Hz Gaus20[4] wavelet are presented

[4] Gaus20 wavelet function having the center frequency of 0.5 Hz.

in Figure 8. The 0.5 Hz component is much smaller in the original signal than the 0.3 Hz component because the 0.5 Hz wavelet coefficients are much smaller than the 0.3 Hz wavelet coefficients.

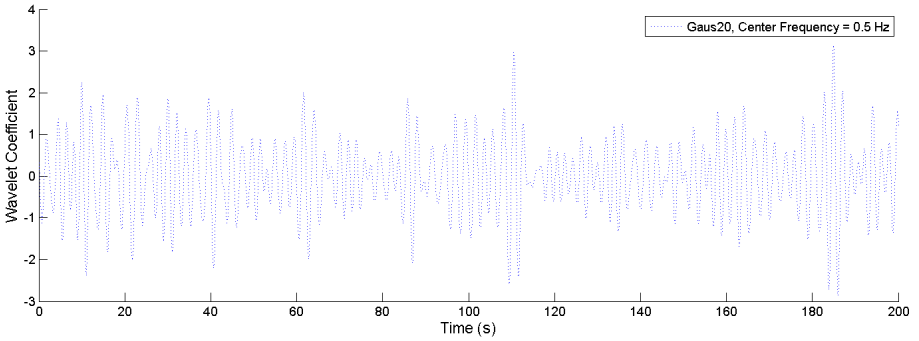

Figure 8. Wavelet coefficients of the original signal (Figure 7) when the 0.5 Hz Gaus20 (Gaus20 wavelet function with the center frequency of 0.5 Hz) wavelet function is used.

If the wavelet coefficients are calculated with a specific frequency range, the results can be presented as a three dimensional figure (Figure 9). The 0.3 Hz component is clearly dominant in the original signal of Figure 7.

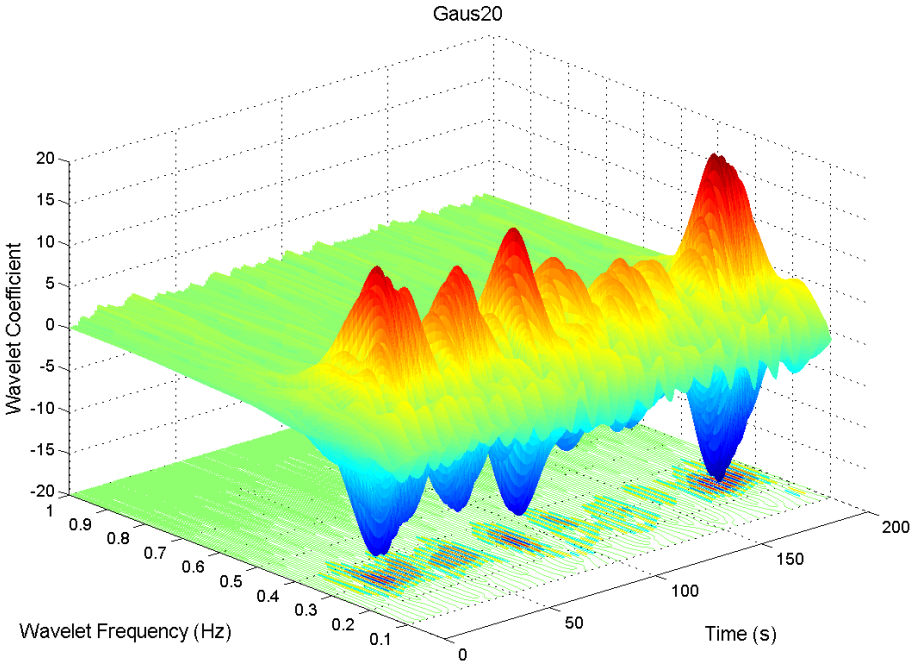

Figure 9. Wavelet coefficients of the original signal (Figure 7) with Gaus20 wavelet function in the wavelet frequency range from 0.1 to 1 Hz.

Properties of Wavelet Transform

The wavelet transform can be used in damping estimation because it can (with certain accuracy) extract the amplitudes of various frequency components of the signal along the time axis (Daubechies 1992, Mallat 1999). After that, the damping of the frequency components (modes) can be identified. Wavelet transform has some common properties with short time Fourier transform (STFT). The transforms and their properties are compared in Appendix D.

The accuracy (or resolution) of the wavelet transform to measure time-frequency variations of spectral components is limited by Heisenberg's uncertainty principle. This is illustrated in Figure 10 in which Heisenberg boxes of three wavelets of different lengths are presented. A Heisenberg box describes the time-frequency resolution of a wavelet in the time-frequency plane such that its width along time is σ_t and the width along frequency is σ_ω (Mallat 1999). A wavelet has a good frequency or time resolution when it has a narrow Heisenberg box in the frequency or time domain, respectively. The uncertainty principle is illustrated in Appendix C using the original signal in Figure 7.

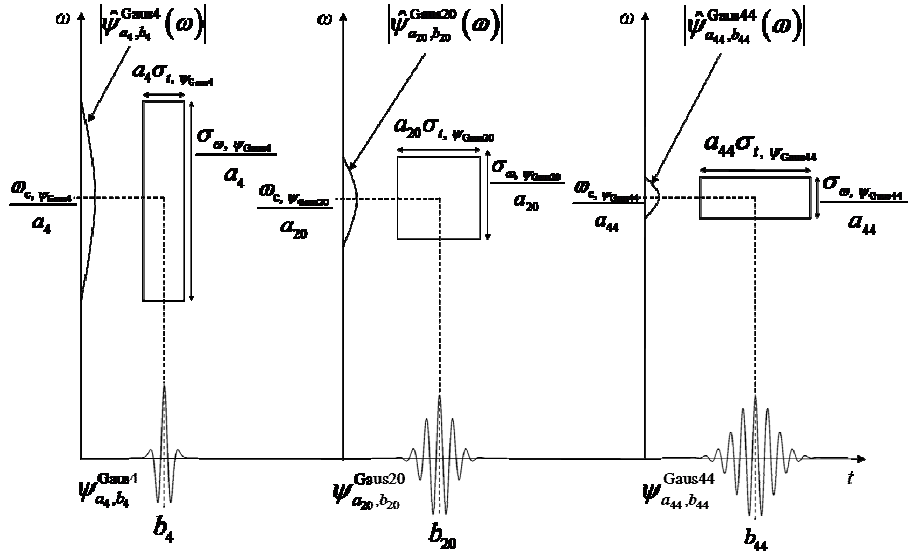

Figure 10. Heisenberg boxes of three wavelets ($\psi^{\text{Gaus4}}_{a_4,b_4}$, $\psi^{\text{Gaus20}}_{a_{20},b_{20}}$, $\psi^{\text{Gaus44}}_{a_{44},b_{44}}$) with the same center frequency (ω_c). Longer wavelets ($\psi^{\text{Gaus20}}_{a_{20},b_{20}}$, $\psi^{\text{Gaus44}}_{a_{44},b_{44}}$) have better frequency resolution (lower Heisenberg box in the direction of ω) but poorer time resolution (wider Heisenberg box in the direction of t). $\hat{\psi}$ is the Fourier transform of the wavelet function ψ. (Mallat 1999)

Both wavelet characteristics, time and frequency resolution, affect the damping information of the mode after the wavelet transform is performed. Therefore, it is

important to use mother wavelets with good enough frequency resolution to separate the modes from each other but having as good as possible time resolution also.

In addition to different modes, the analyzed signals in the damping estimation of the electromechanical oscillations always have a certain amount of measurement noise. The noise is due to the measurement errors of the analyzed quantities (voltages, currents, and frequencies). The measurement errors are mainly caused by the inaccuracies of the measurement transformers and the PMUs. The ability of different mother wavelets to separate the noise from the actual mode is different but generally the wavelet transform is quite insensitive to noise in the analyzed signals (Kang & Ledwich 1999).

1.12 Random Decrement Technique

The random decrement technique (RDT) is an output-only[5] system identification method. It was first introduced in (Cole 1973) and studied then after in (Chang 1975) and has been applied extensively in the fields of structural (Ibrahim 1977) and mechanical (Siviter & Pollard 1985) engineering. Recently it has been applied also for estimating the damping of electromechanical oscillations in power systems (Thambirajah et al. 2010b).

RDT is an averaging technique in the time domain, analogous to the Welch Periodogram method (Welch 1967) in the frequency domain. The averaging technique yields a trend known as the random decrement (RD) signature, which is an estimation of the correlation function of a Gaussian process. In order to extract the RD signature from a signal, RDT uses a threshold, h, so that every time the signal, $y(t)$, crosses the threshold, a sample of the signal of length τ, $y(t_s:t_s + \tau)$, is collected. The samples collected in a specific time window are averaged yielding the RD auto signature $D_{YY}(\tau)$. Under the assumption that the power system is linear and excited with Gaussian distributed random variations, the RD auto signature, $D_{YY}(\tau)$, is proportional to the free decay or impulse response of the system (Brincker et al. 1992). Therefore, the approximate impulse response, $r_{imp,a}(t)$, is

$$r_{\mathrm{imp,a}}(t) \approx D_{\mathrm{YY}}(\tau) = \frac{1}{N}\sum_{s=1}^{N} C_{\mathrm{m}}(t_s : t_s + \tau), \tag{6}$$

where N is the total number of samples collected using the threshold, s is the sample number, t_s is the time instance when the single-mode ambient response, $C_m(\cdots)$, crosses the threshold, τ is the length of each sample (and corresponding approximate impulse response).

[5] Output-only method processes only the output signals of the system; it does not need the input signals in the estimation process.

The main assumptions of the random decrement technique are that the system dynamic behavior is linear and that the system is excited with random variations that are Gaussian distributed.

Demonstration of the RDT is shown in Figure 11, Figure 12, and Figure 13. The wavelet-filtered signal, C_m, with the threshold of $\sqrt{2} \cdot \text{std}(C_m)$, where std is the standard deviation, is shown in Figure 11. The first six samples and the 30th (last) sample of C_m which fulfill the threshold condition are shown in Figure 12. The RDS after the corresponding number of samples averaged is shown in Figure 13. It is seen in Figure 13 that after all the collected 30 samples the RDS has approached the shape of the impulse response.

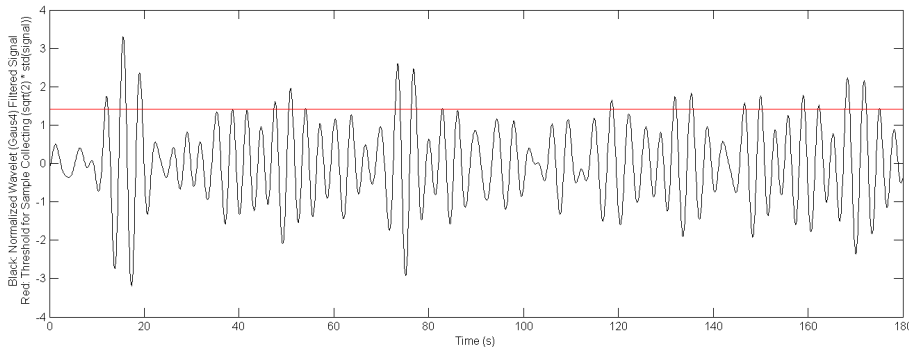

Figure 11. Signal with a three minutes time window and the threshold used in the random decrement technique.

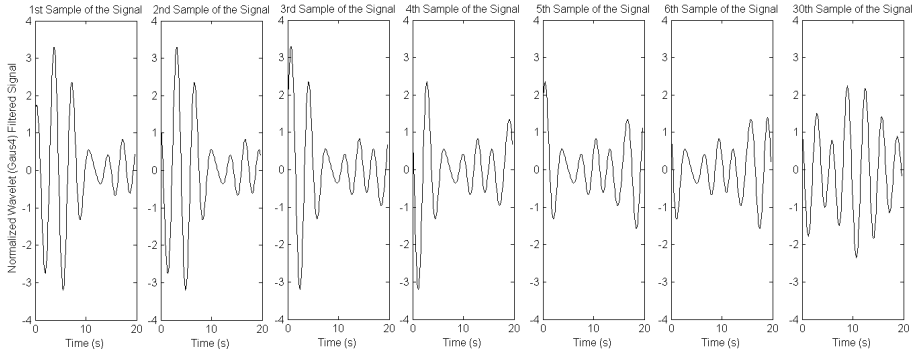

Figure 12. Examples of samples of the signal in Figure 11.

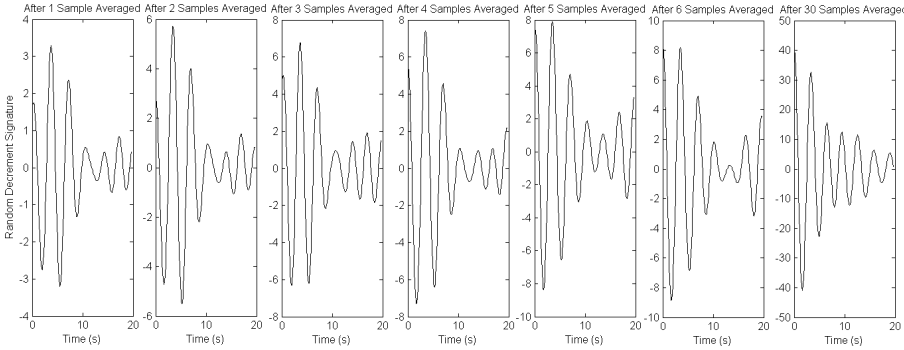

Figure 13. Approximate impulse response after 1, 2, 3, 4, 5, 6, and 30 samples averaged, respectively.

2 Damping Estimation Method

2.1 General Description

The developed damping estimation method is based on the wavelet transform and the random decrement technique. The *wavelet transform* is applicable in damping estimation because it can extract the amplitudes of various frequency components of the signal as a function of time with an accuracy defined by the time and frequency resolutions of the wavelet. The *random decrement technique* is applicable in estimating the damping from the ambient response of the power system[6]. The method is a univariate[7] method and therefore it is important to select for the analysis a signal with good observability of the specific mode. Usually, the observability of the oscillation mode in a specific signal is fairly constant (observability does not change with operating condition because it is related to the physical structure of the power system) and known from the linear analysis of the system model. This is the case also for the Nordic power system.

The block diagram of the method is presented in Figure 14. The method analyses a sampled signal $y(t)$ by using a frequency band and a time window length. The time window length is the duration of data from which the damping and frequency estimates are calculated. The time window slides forward along the analyzed signal using the steps defined by the update time. After each step, the estimates for damping and frequency are updated. The method consists of four blocks:

- mode frequency estimation,
- mode extraction,
- estimation of the mode's approximate impulse response, and
- mode damping estimation from the approximate impulse response.

[6] The random decrement technique is described in Section 1.12.
[7] Univariate method utilizes only one signal in the estimation process.

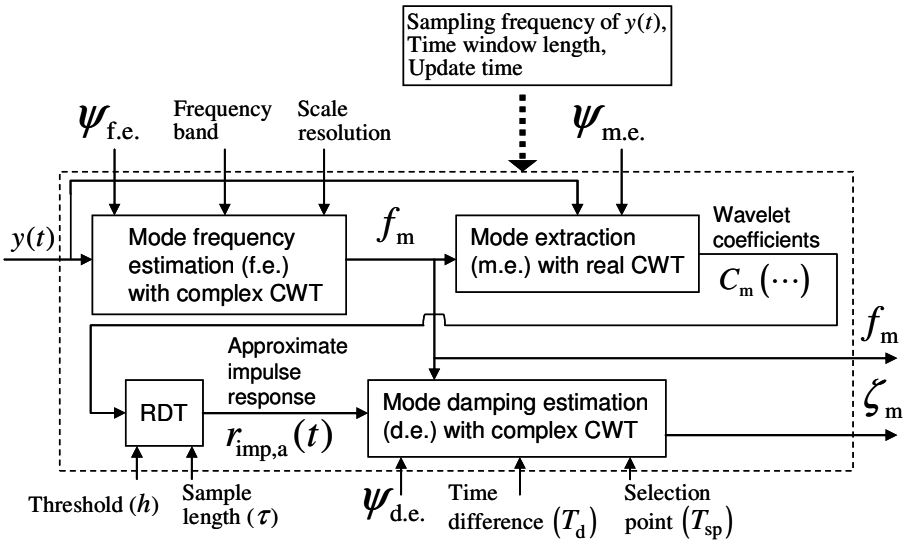

Figure 14. Block diagram of the damping estimation method. CWT is continuous wavelet transform and RDT is random decrement technique. Input y(t) is the analyzed signal, ψ is the selected wavelet function, and outputs f_m and ζ_m are the estimated mode frequency and damping, respectively.

2.2 Steps of the Damping Estimation Method

2.2.1 Frequency Estimation with Complex Continuous Wavelet Transform

The mode frequency is estimated in a specified time window and frequency band with the complex continuous wavelet transform. First, the analyzed signal, $y(t)$, is wavelet transformed:

$$C(a_i,b_j)=\frac{1}{\sqrt{a_i}}\int_{-\infty}^{\infty} y(t)\psi_{\text{f.e.}}^{*}\left(\frac{t-b_j}{a_i}\right)dt\,, \tag{7}$$

where parameters a_i are the wavelet scales from the lower frequency bound to the upper frequency bound with dense enough spacing to achieve high enough resolution for frequency estimation. Parameters b_j are the wavelet positions from the beginning of the time window to the end of the time window with the spacing of signal sampling period. Time is t, $\psi_{\text{f.e.}}$ is the wavelet function used in the frequency estimation, and $C(a_i,b_j)$ are the wavelet coefficients with the specific scale and position parameters.

The wavelet scale a_{m} that produces the highest average wavelet coefficient modulus,

$$a_{\mathrm{m}} = \left\{ a_i \;\middle|\; \max \overline{\left|C(a_i, b_j)\right|}_{b_j} = \overline{\left|C(a_{\mathrm{m}}, b_j)\right|}_{b_j} \right\}, \tag{8}$$

is selected as the scale of the mode. The scale is converted to the mode frequency, f_{m}:

$$f_{\mathrm{m}} = \frac{f_{\mathrm{c}}(\psi_{\mathrm{f.e.}})}{a_{\mathrm{m}}(\psi_{\mathrm{f.e.}}) \cdot \Delta}, \tag{9}$$

where $f_{\mathrm{c}}(\psi_{\mathrm{f.e.}})$ is the center frequency of the wavelet function $\psi_{\mathrm{f.e.}}$ [Equation (5)] and Δ is the signal sampling period.

2.2.2 Mode Extraction with Real Continuous Wavelet Transform

After knowing the mode frequency, f_{m}, the mode is extracted from the analyzed signal, $y(t)$, with the real continuous wavelet transform by calculating the resulting wavelet coefficients:

$$C_{\mathrm{m}}\left(a_{\mathrm{m}}(\psi_{\mathrm{m.e.}}), b\right) = \frac{1}{\sqrt{a_{\mathrm{m}}(\psi_{\mathrm{m.e.}})}} \int_{-\infty}^{\infty} y(t) \psi_{\mathrm{m.e.}} \left(\frac{t-b}{a_{\mathrm{m}}(\psi_{\mathrm{m.e.}})} \right) dt \,. \tag{10}$$

The wavelet coefficients, C_{m}, are (approximately) linearly dependent on the instantaneous value of the mode at different time instances, b (Daubechies 1992). Therefore, the mode damping information is (approximately) preserved during the mode extraction. The mode extraction resolution is limited by Heisenberg's uncertainty principle[8] (frequency resolution vs. time resolution). The parameter $a_{\mathrm{m}}(\psi_{\mathrm{m.e.}})$ is the wavelet scale corresponding to the estimated mode frequency, f_{m}, with the equation

$$a_{\mathrm{m}}(\psi) = \frac{f_{\mathrm{c}}(\psi)}{f_{\mathrm{m}} \cdot \Delta}, \tag{11}$$

where $f_{\mathrm{c}}(\psi)$ is the center frequency of the mode extraction wavelet function, $\psi_{\mathrm{m.e.}}$, and Δ is the signal sampling period.

2.2.3 Impulse Response from Ambient Response with the Random Decrement Technique

After extracting the mode of interest from the signal, the result is the power system's ambient response at the mode frequency. Because it is not possible to determine the

[8] Heisenberg's uncertainty principle is discussed in Section Wavelet Transform Properties of Section 1.11.1.

damping of the mode directly from the single-mode ambient response, the random decrement technique (RDT) is used to estimate the approximate single-mode impulse response from the single-mode ambient response. From the estimated impulse response, the damping of the mode can be estimated.

Under the assumption that the power system is linear and excited with Gaussian distributed random variations, the RD auto signature, $D_{YY}(\tau)$, is proportional to the free decay or impulse response of the system (Brincker et al. 1992). Therefore, the approximate impulse response, $r_{imp,a}(t)$, is

$$r_{\text{imp,a}}(t) \approx D_{\text{YY}}(\tau) = \frac{1}{N}\sum_{s=1}^{N} C_{\text{m}}(t_s : t_s + \tau), \tag{12}$$

where N is the total number of samples collected using the threshold, s is the sample number, t_s is the time instance when the single-mode ambient response, $C_m(\cdots)$, crosses the threshold, and τ is the length of each sample (and corresponding approximate impulse response).

The main assumptions of the random decrement technique are that the power system dynamic behavior is linear and that the system is excited with random variations that are Gaussian distributed. The assumptions can be considered valid when the system is operating under the ambient conditions. Then the oscillations are small and approximately linear. The random load variations can be considered approximately Gaussian distributed based on the central limit theorem[9] (Cam 1986) because the number of loads in a power system is large.

2.2.4 Mode Damping Estimation from the Approximate Impulse Response with Complex Continuous Wavelet Transform

The damping of the mode is estimated from the approximate impulse response, $r_{imp,a}(t)$, utilizing the complex continuous wavelet transform. At first the complex wavelet coefficients, $C_{imp}(\cdots)$, at different time instances, b, are calculated:

$$C_{\text{imp}}(a_{\text{m}}(\psi_{\text{d.e.}}), b) = \frac{1}{\sqrt{a_{\text{m}}(\psi_{\text{d.e.}})}} \int_{-\infty}^{\infty} r_{\text{imp,a}}(t)\psi^{*}_{\text{d.e.}}\left(\frac{t-b}{a_{\text{m}}(\psi_{\text{d.e.}})}\right) dt, \tag{13}$$

where $a_m(\psi_{d.e.})$ is the wavelet scale corresponding to the estimated mode frequency, f_m, calculated with Equation (11), and $\psi_{d.e.}$ is the wavelet function used in the damping estimation.

[9] Central limit theorem states that the sum of independent and identically distributed random variables with finite mean and variance approaches the normal distribution (Gaussian distribution) when the number of random variables increases, irrespective of the distribution of the random variables.

The damping ratio of the mode, ζ_m, is finally calculated by using wavelet coefficients, $C_{imp}(\cdots)$, from two different time instances:

$$\zeta_m = -\frac{100}{2 \cdot \pi \cdot f_m \cdot T_d} \ln \frac{\left| C_{imp}\left(T_{sp} + T_d/2 \right) \right|}{\left| C_{imp}(T_{sp} - T_d/2) \right|}, \tag{14}$$

where T_d is the difference between the positions (or time instants), b, of the wavelet coefficients C_{imp} in the damping calculation, and T_{sp} is the time instant from the beginning of the approximate impulse response (selection point), needed for the damping calculation. The absolute value of the complex wavelet coefficient corresponds to the amplitude of the approximate impulse response at a certain time instance.

3 Parameters of the Damping Estimation Method

In this chapter, the parameter selections of the different blocks of the damping estimation method are considered. At first the general parameters which are common for the damping estimation method are presented.

3.1 General Parameters

The highest possible signal *sampling frequency* is in practice set by the PMU measurement frequency. However, usually a significantly lower sampling frequency is enough for the inter-area modes in the range from 0.1 to 2 Hz and specifically for the inter-area mode of 0.3 Hz. For these reasons, a signal sampling frequency of 10 Hz is assumed throughout this thesis.

In addition to the sampling frequency, the method has two other general parameters: time window length and update time. The *time window length* is the duration of data from which the damping and frequency estimates are calculated. The time window slides forward along the analyzed signal using the steps defined by the *update time*. After each step, the estimates for damping and frequency are updated. The time window length affects the damping estimation results and this effect is studied in Chapter 4 of the thesis. The update time does not affect the damping estimates themselves but it only sets the time interval of updating the estimates. A fixed 5 second update time is used in this thesis and the different time window lengths between 1 and 32 minutes are used.

3.2 Parameters of the Frequency Estimation and Mode Extraction

The parameters of the frequency estimation are: scale resolution, frequency band, and the wavelet function. In the mode extraction, only the wavelet function needs to be selected. These parameter selections are addressed in the following.

3.2.1 General Parameters of the Frequency Estimation

The *scale resolution* or spacing of scales should be high enough for accurate frequency estimation. Here, the scale resolution of 0.1, which corresponds to the frequency interval of 0.0006 Hz at the 0.3 Hz frequency, is used. The scale resolution leads to an insignificant error in the frequency estimation.

The *frequency band* should be selected such that it includes the mode of interest. Therefore, the selected frequency band is 0.2–0.4 Hz because it includes the 0.3 Hz mode, which is of interest in this thesis.

3.2.2 Selecting Wavelet Function for Frequency Estimation and Mode Extraction

In order for some wavelet to be good in damping estimation it should be able to reproduce the amplitude of a specific mode accurately enough along the time axis. If the amplitude at a specific frequency was known at every time instant, the damping ratio of the specific mode, ζ, could be calculated (with certain accuracy) from the ring-down signals (or transients) of the power system oscillation caused by some disturbance using

$$\zeta = -\frac{100}{\omega_n T_d} \ln \frac{C_{env}(t+T_d)}{C_{env}(t)}, \tag{15}$$

where ω_n is the undamped angular frequency of the mode. $C_{env}(t)$ is the wavelet coefficient envelope (in case of a real wavelet)[10] or the wavelet coefficient modulus (in case of a complex wavelet)[11] of the mode frequency wavelet at time t. T_d is the time difference between the two points of the wavelet coefficient envelope or the wavelet coefficient modulus between which the damping is calculated. In addition, if the amplitude at a specific frequency was known at every time instant, the damping of the specific mode could be calculated using the ambient-excited oscillations with further processing.

A property of the wavelet transform in damping estimation is the tradeoff between the time and frequency resolutions. The tradeoff means that if fast reaction to changes in amplitude in the time domain is required, a short wavelet must be used, which possibly causes the nearby modes to interfere with each other in the frequency domain, see Figure 15. On the other hand, if a good separation of the modes in the frequency domain is required, we must use a long wavelet, which gives a slow reaction to changes in amplitude and therefore leads to slow damping estimation in the time domain, see Figure 16. Too low a time resolution prevents the damping estimation both in the case of transient and ambient oscillations. This is basically because the oscillations disappear and new oscillations appear during the wavelet length and the damping information of the oscillations is (at least partially) lost.

[10] Real continuous wavelet transform produces the real wavelet coefficients that are approximately linearly dependent on the instantaneous value of the mode at different time instances. Therefore, the damping ratio can be calculated from the envelope of the wavelet coefficients.

[11] Complex continuous wavelet transform produces the complex wavelet coefficients. Moduli of these coefficients are approximately linearly dependent on the amplitude of the mode at different time instances. Therefore, the damping ratio can be calculated from the complex wavelet coefficient moduli.

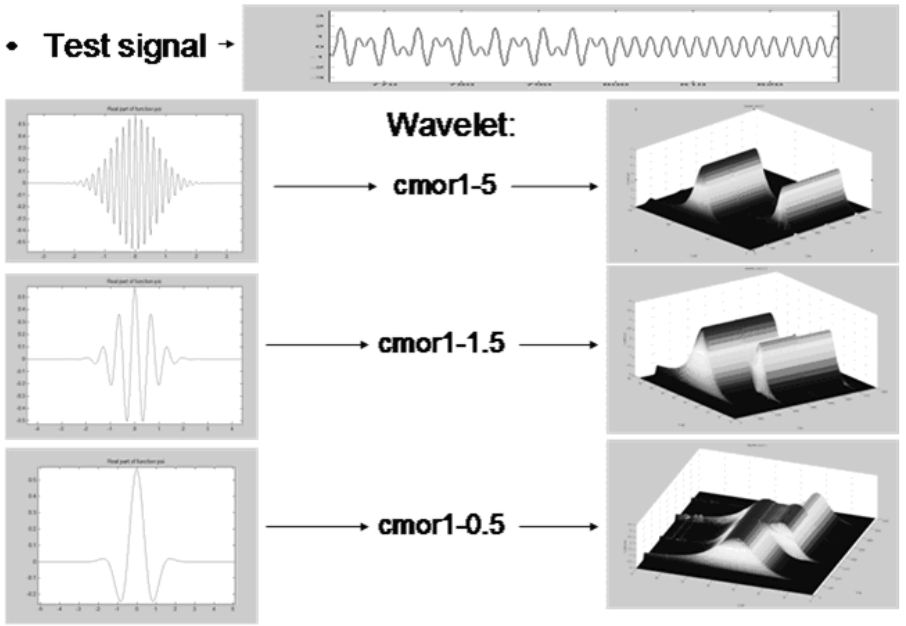

Figure 15. The effect of the wavelet length on the ability of separating the modes from each other (frequency resolution). A long wavelet (Cmor1-5) separates the modes better than the shorter ones (Cmor1-1.5 and Cmor1-0.5). Only a fraction of the test signal is presented.

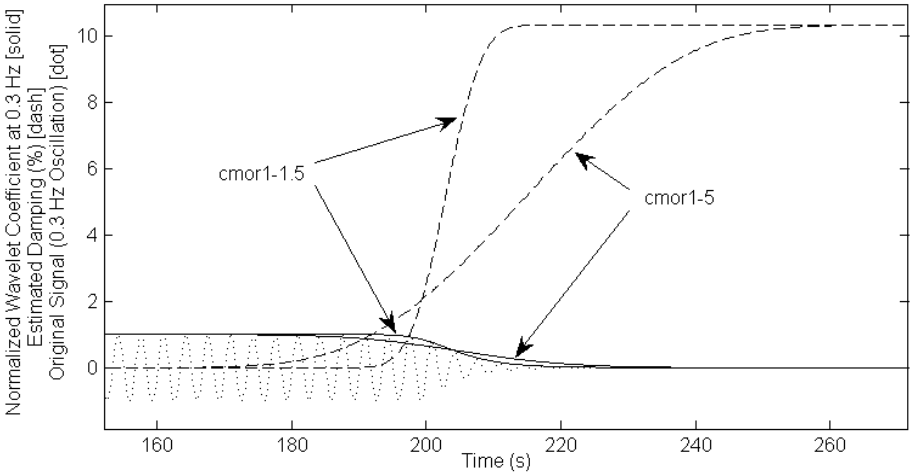

Figure 16. The effect of the wavelet length on the reaction time of changing amplitude (time resolution). A long wavelet (Cmor1-5) reacts to the changing amplitude much slower than the shorter one (Cmor1-1.5).

Another property of some mother wavelets is that the wavelet coefficient does not necessarily peak at the same wavelet frequency as the signal frequency is, see Figure 17.

This causes problems in determining the oscillation frequency. Therefore, mother wavelets, which cause the wavelet coefficient to peak at the desired frequency, should be used.

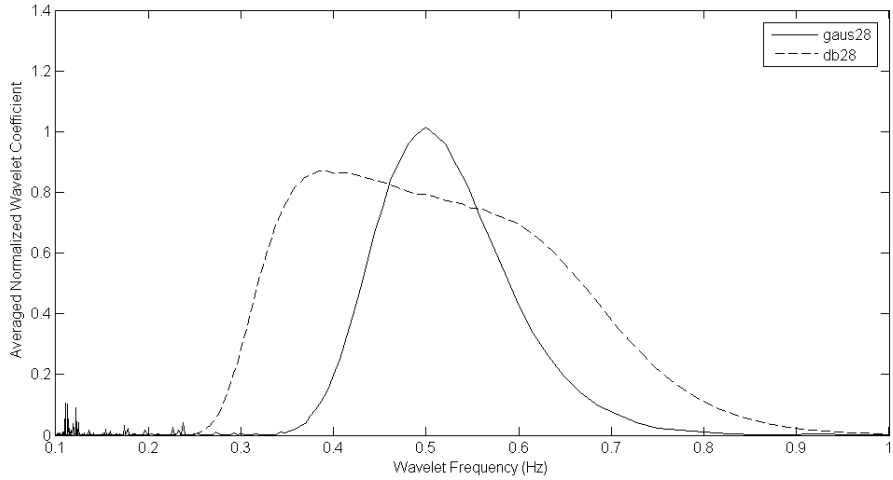

Figure 17. The wavelet coefficient as a function of the wavelet frequency when the 0.5 Hz undamped sinusoidal signal is analyzed. The Gaus28 wavelet peaks at the signal frequency whereas the Db28 wavelet peaks at a lower frequency.

Based on the observations above, when selecting the best mother wavelet in electromechanical oscillation damping estimation, it is important that the following conditions are fulfilled:

1) The wavelet should separate the different oscillation modes well enough (frequency resolution)
   - This is important because there possibly are several oscillation modes present in the power system
2) The wavelet should react quickly enough to changes in amplitude (time resolution)
   - This is important because damping is related to the changes in amplitude
3) The wavelet coefficient should peak at the signal frequency
   - This is important in the frequency estimation, which is based on selecting the maximum wavelet coefficients

3.2.3 Wavelet Function Selection for the Frequency Estimation and Mode Extraction in the Nordic Power System Case

In this section, the optimal mother wavelet selection is further studied in the case of oscillation damping estimation of the Nordic power system with inter-area oscillation modes at about 0.3 Hz and 0.5 Hz. The optimal mother wavelet should react to changes in amplitude fast enough but it should also separate the modes at 0.3 Hz and 0.5 Hz well enough.

In order to be able to quantitatively compare different wavelets, the frequency and time resolution criteria need to be specified precisely. For this purpose, a test signal having only a frequency component of 0.3 Hz and damping of 10 % is analyzed with an example wavelet.

Here, the upper frequency resolution is defined as the frequency interval (in Hz) towards greater frequencies that it takes the normalized wavelet coefficient to decrease to 10 % of the peak value. Similarly, the lower frequency resolution is the frequency interval towards smaller frequencies that it takes the normalized wavelet coefficient to decrease to 10 % of the peak value, Figure 18. A wavelet with high frequency resolution has small values for the upper and lower frequency resolutions, i.e. a narrow peak in the frequency domain.

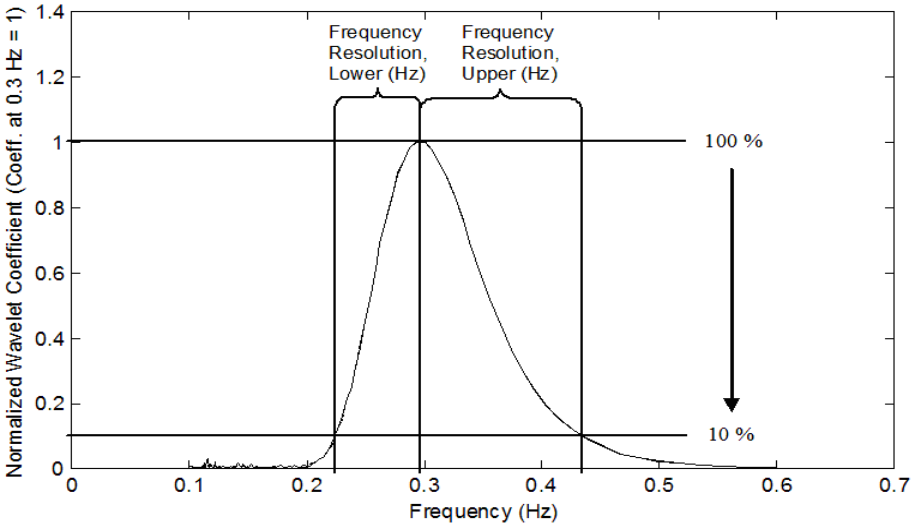

Figure 18. Specification of the upper and lower frequency resolution in this thesis. The test signal has only a frequency component of 0.3 Hz.

The time resolution is defined as the time that it takes for damping estimate (estimated using Equation (15) with the time difference, T_d, of half cycle of oscillation) to change from 0.5 % to 9.5 % when the damping of the test signal changes from 0 % to 10 %, Figure 19. A wavelet with the high time resolution has a small value for the time resolution, i.e. a fast reaction in the time domain.

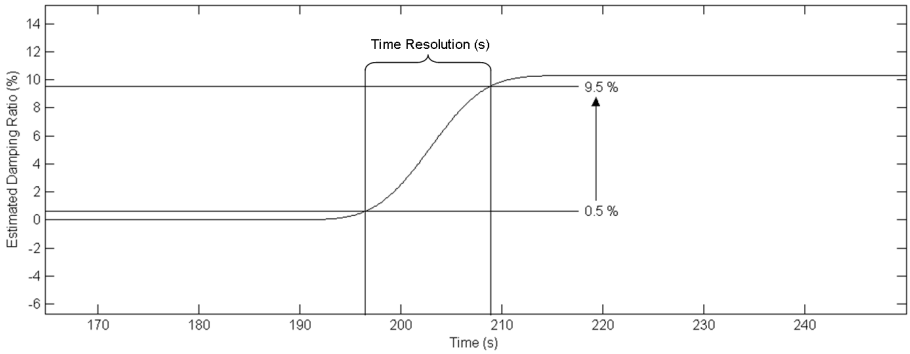

Figure 19. Specification of the time resolution in this thesis. Damping of the test signal changes instantaneously from 0 % to 10 %.

Now, when the frequency and time resolutions are specified quantitatively, the criteria for selection of optimal mother wavelets in damping estimation of the Nordic power system can be defined:

1) ***Frequency resolution***
   - ***a.*** The lower frequency resolution of the wavelet for the 0.5 Hz signal must be less than 0.2 Hz. This is to guarantee that the 0.5 Hz mode does not interfere with the 0.3 Hz mode.
   - ***b.*** The upper frequency resolution of the wavelet for the 0.3 Hz signal must be less than 0.2 Hz. This is to guarantee that the 0.3 Hz mode does not interfere with the 0.5 Hz mode.
2) ***Time resolution***
   - ***a.*** The time resolution of the wavelet for the 0.3 Hz signal must be equal or less than 16.7 s (equals about 5 cycles of 0.3 Hz oscillation). This is to prune the wavelets with poor time resolution.
3) ***Frequency estimation capability***
   - ***a.*** When the test signal frequency is 0.5 Hz, the wavelet coefficient must peak in the range of 0.49-0.51 Hz. This is to guarantee the frequency estimation capability.

The mother wavelets that pass the criteria are the Gaussian (Gaus), complex Gaussian (Cgau), and complex Morlet (Cmor) wavelets shown in Figure 20 with the related 0.3 Hz and 0.5 Hz time and frequency resolutions. The number after the wavelet name in Figure 20 is related to the wavelet length. The smaller the number the shorter the wavelet is. All these mother wavelets are possible ones for damping estimation of the Nordic power system. In practice, the 0.5 Hz mode is nearly unobservable in Finland at most times and therefore it is often possible to use even shorter wavelets than presented in Figure 20. Shorter wavelets are preferred because they have better time resolution.

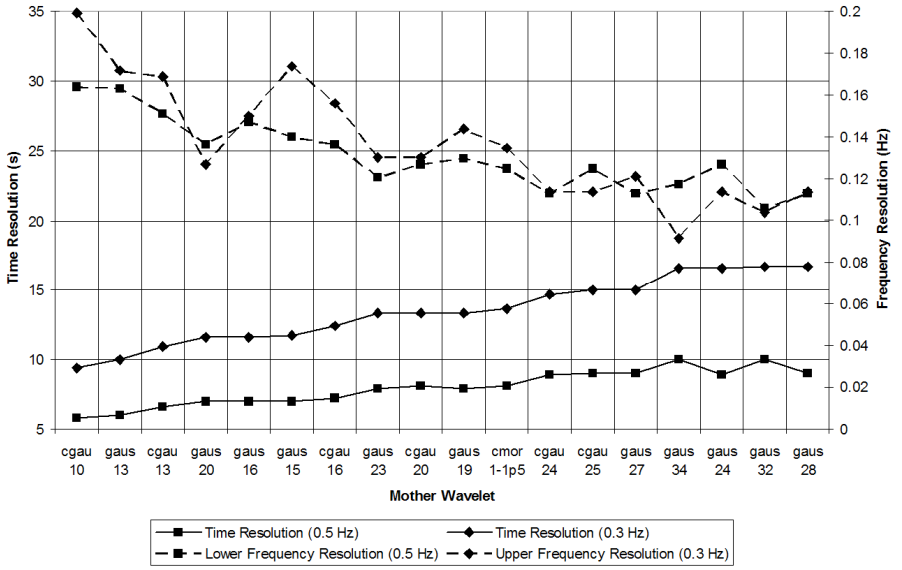

Figure 20. The time and frequency resolutions of the mother wavelets which passed the criteria set for the optimal mother wavelets in damping estimation of the Nordic power system.

In this thesis, Cmor1-1.5 wavelet is used in the *frequency estimation* because it fulfills the criteria above and it is a complex wavelet. Three different wavelet functions are used for the *mode extraction* in this thesis: Gaus4, Gaus20, and Gaus44. Of these wavelets, only the Gaus20 wavelet function fulfills the criteria above. However, the effect of using a longer and shorter wavelet on the damping estimation results is illustrated with the other two wavelets. The wavelets are of significantly different length and have thus very different frequency and time resolutions.

3.3 Parameters of the Random Decrement Technique

Parameters of the random decrement technique are the *length of the samples*, τ, and the *threshold* value, h. The selection of these parameters is done such that the results of the simple simulation model, described in Figure 21, are analyzed with the damping estimation method using different RDT parameter values. The simulation model consists of the single pole pair transfer function that is excited with the Gaussian white noise. The output of the transfer function is analyzed with the damping estimation method presented in Figure 14.

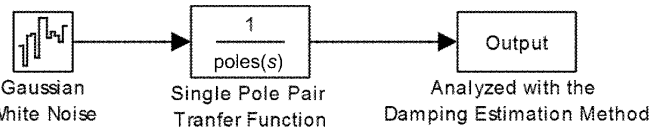

Figure 21. The simple simulation model: a single complex conjugate pole pair transfer function model.

Damping estimation results with the sample lengths from 4 to 8 cycles and with the threshold values from -2.5 to 2.5 when the real damping is 5 %, are presented in Figure 22. The damping estimate mean value is close to the real damping of 5 % and the standard deviation is low when the sample length, τ, is six oscillation cycles and when the threshold value is approximately 1.4. These values are used for the sample length and threshold in this thesis. If the threshold value is lower (higher) the number of samples the method collects during a time window is higher (lower) but the samples are of poorer (better) quality. The threshold value of 1.4 is a good compromise between the quality and number of samples collected during a time window.

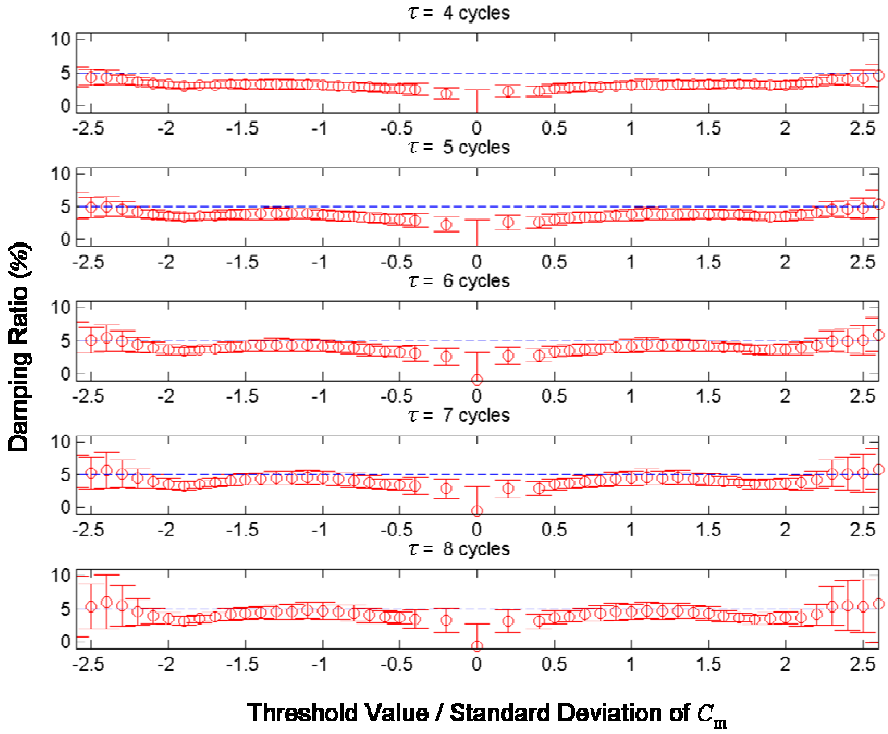

Figure 22. Damping estimates with different sample lengths, τ, and threshold values when the real damping ratio is 5 %. The circles describe the mean values of the damping estimates and the errorbars show the standard deviations of the estimates.

3.4 Parameters of the Mode Damping Estimation from the Approximate Impulse Response

In analyzing the damping from the approximate impulse response, the *wavelet function*, *time difference* between the wavelet coefficient moduli, T_d, and *selection point* of damping estimate, T_{sp}, are important parameters and studied here. Another parameter to be considered is the *accuracy of the wavelet's approximation*. The accuracy is dependent on the number of points used in the approximation in the wavelet's support domain[12], in other words what is the wavelet's sampling frequency. This is an internal parameter of the continuous wavelet transform but it has some effect on the damping estimates. Therefore, the approximation accuracy of the wavelet is considered in the following. In addition, the effect of *frequency deviation* between the analyzing wavelet and the signal is studied because it has some effect on the damping estimates.

3.4.1 Effect of Time Difference between the Selected Wavelet Coefficients on the Damping Estimates with Different Wavelets

The time difference between the selected wavelet coefficients, T_d, [Figure 14, Equation (14)] affects the damping estimation results. The maximum time difference is limited by the fact that a wavelet has to be well enough in the domain of the impulse response. When the time difference between the two wavelets increases, a larger part of the wavelets' domain is outside of the impulse response's domain. This behavior is dependent on the wavelet length. The maximum allowed time difference for the short wavelets is greater than for the long wavelets. The effect of time difference, T_d, on the damping estimates is studied in the following in case of an ideal exponentially decaying sinusoidal signal. An example of the analysis is first presented, after which the results are considered for multiple time differences between the selected wavelet coefficients using three different wavelet functions. The analysis is done for damping ratios of the impulse response from 1 %–10 %.

Example of the Analysis

An ideal exponentially decaying sinusoidal signal (or impulse response) and the time difference between the wavelet coefficients, T_d, used in the damping calculation is shown in Figure 23. The damping ratio of the impulse response is 6 % and frequency is 0.3 Hz.

[12] Wavelet's support domain is the time interval during which the wavelet function is numerically defined. Outside the support domain wavelet function has a value of zero.

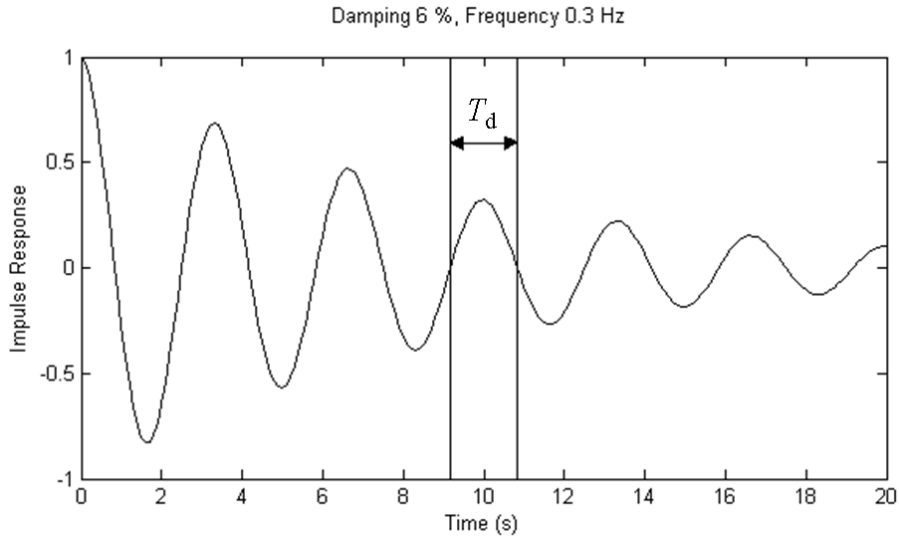

Figure 23. Impulse Response with 6 oscillation cycles. Frequency of the impulse response is 0.3 Hz and damping is 6 %. Time difference between the selected wavelet coefficients, T_d, is shown.

Three complex wavelets (Cmor1-1, Cmor1-1.3, and Cmor1-1.5) of the Morlet wavelet family are used in the analysis. The real parts of the wavelet function ψs are shown in Figure 24, Cmor1-1 being the shortest and Cmor1-1.5 the longest wavelet. These wavelets were selected for the analysis because their length is approximately sufficient for damping estimation from the impulse response which length is six cycles. Their applicability is studied in detail in the following sections.

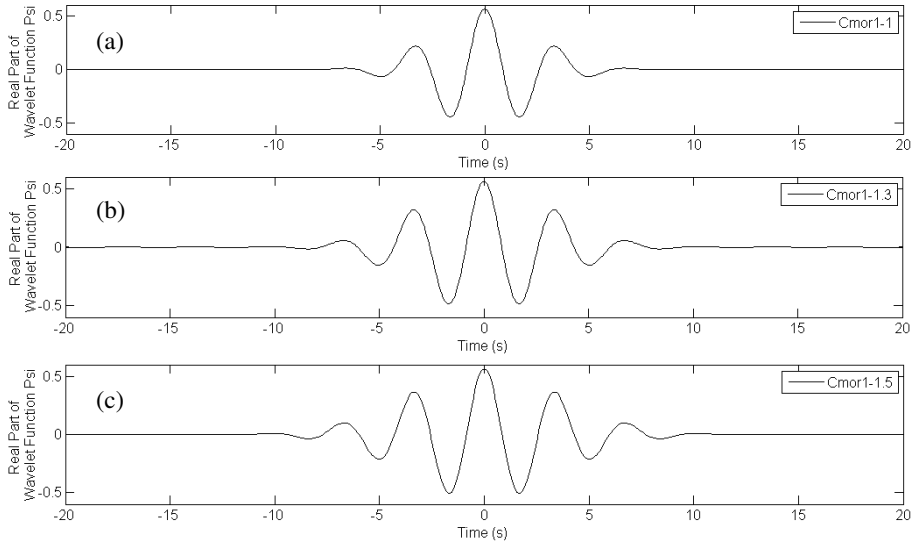

Figure 24. Complex Morlet wavelets Cmor1-1 (a), Cmor1-1.3 (b), and Cmor1-1.5 (c) used in the analyses.

Wavelet coefficient modulus[13] as a function of time for the example impulse response (Figure 23) with the Cmor1-1 wavelet is shown in Figure 25. The modulus is first growing although the impulse response is decaying because the wavelet is entering the domain of the impulse response. The corresponding damping estimate (Figure 26) with the time difference, T_d, of 0.5 oscillation cycles is thus negative. At some point (about 3 s in Figure 25 for the example impulse response and the wavelet) the modulus reaches the maximum and right after begins to decay because the impulse response is decaying. The corresponding damping estimate reaches the value zero and turns to positive at this point. The modulus continues to decay with a higher damping ratio because the wavelet is still entering the domain of the impulse response (Figure 25 and Figure 26). At some point, the damping reaches almost a constant level because the wavelet is almost entirely in the domain of the impulse response[14], and then after starts to increase again because the wavelet starts to go out of the impulse response's domain.

There is a time lag in the damping estimate compared to the wavelet coefficient modulus because the damping is calculated from two wavelet coefficient moduli with Equation (15) and the time of the damping estimate is defined as the time of the leading wavelet coefficient modulus. The damping estimate is defined to be zero before both wavelet coefficient moduli are available for the damping calculation.

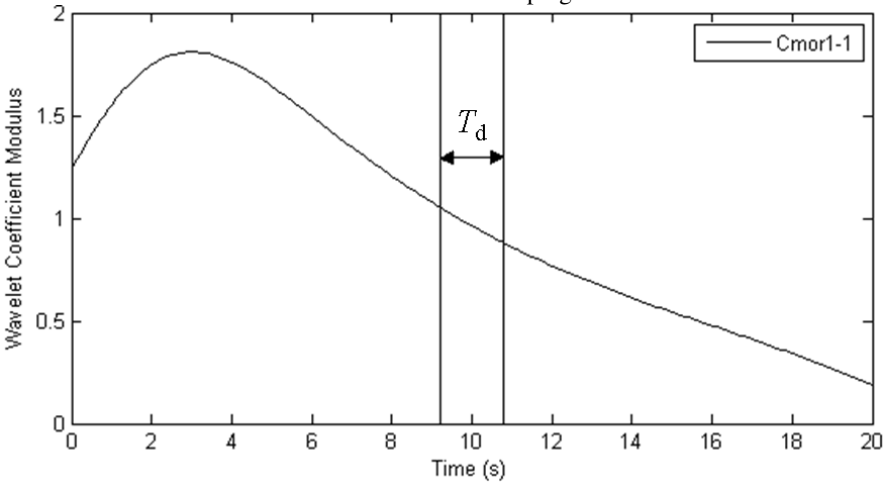

Figure 25. Wavelet coefficient modulus of the example impulse response (Figure 23) with the Cmor1-1 wavelet. Time difference between the selected wavelet coefficients, T_d, is shown.

[13] Wavelet coefficient modulus is the absolute value of the complex wavelet coefficient.
[14] This is the point when the damping estimate approximately equals the damping of the impulse response.

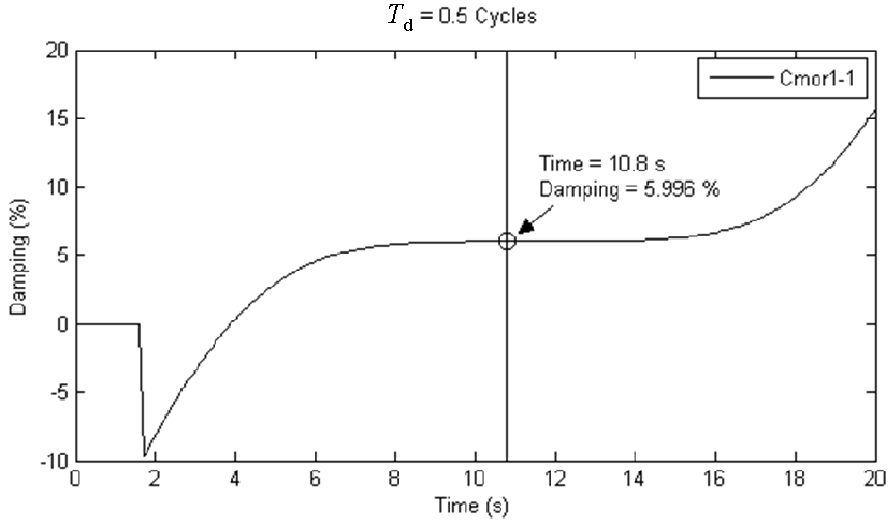

Figure 26. Damping estimate calculated from the wavelet coefficient modulus (Figure 25) of the example impulse response (Figure 23) with the time difference, T_d, of 0.5 oscillation cycles. Damping value and time instance highlighted in the figure is the midpoint of the damping values.

Analysis Results with Multiple Time Differences between the Selected Wavelet Coefficients and with Different Wavelets

Damping estimates with the Cmor1-1, Cmor1-1.3, and Cmor1-1.5 wavelets (shown in Figure 24), with 10 different damping ratios of the impulse response (1 %–10 %) and with the time difference, T_d, from 0.1 to 3 oscillation cycles are shown in Figure 27. The biases of the damping estimates as a function of the time difference, T_d, are shown in Figure 28. The biases as a function of the impulse response's damping ratio are shown in Figure 29 (relative biases in Figure 30). The biases as a function of different wavelets are shown in Figure 31 and Figure 32.

For the shortest wavelet (Cmor1-1), the damping estimates are very little biased even when the time difference, T_d, is long and the damping ratio is high (Figure 27a, Figure 28a, Figure 29, Figure 30, Figure 31, and Figure 32). When the length of the wavelet, the time difference T_d, or the damping of the impulse response increases, the bias from the real damping value increases. The bias increases because the wavelets go more out of the impulse response's domain. Here, bias is defined as absolute bias

$$B_A = V_E - V_R, \tag{16}$$

where B_A is absolute bias, V_E is estimated value, and V_R is real value.

If the bias was defined as relative bias (B_R)

$$B_{\mathrm{R}} = \frac{V_{\mathrm{E}} - V_{\mathrm{R}}}{V_{\mathrm{R}}}, \tag{17}$$

it would be nearly equal for different damping ratios of the impulse response (Figure 30).

Although a short wavelet and short time difference T_{d}, give good results for the ideal impulse response, the longer wavelet and longer time difference have certain advantages which are not reflected in the ideal case. A longer wavelet gives better frequency resolution, which is beneficial if there are other modes present in the impulse response and a longer wavelet is less sensitive to noise. A longer time difference gives more difference in the wavelet coefficient moduli and therefore a more reliable damping estimate because the effect of random excursions in the impulse response is minimized.

However, a significant benefit of a short wavelet is that it allows the use of a long time difference T_{d}, and gives still low bias in the damping estimate (Figure 27a, Figure 28a, and Figure 32). It can be seen from the figures that although the time difference of three oscillation cycles is used in case of the Cmor1-1 wavelet, the bias is still about the same as for the Cmor1-1.3 wavelet with the time difference of 0.5 oscillation cycles. The bias for the Cmor1-1.5 with the time difference of 0.5 cycles is about three times larger than the corresponding bias for the Cmor1-1 with the time difference of 3 oscillation cycles.

The biases are acceptable for the Cmor1-1 wavelet with all the studied time differences from 0.1 to 3 oscillation cycles. The biases are possibly acceptable also for the longer wavelets (Cmor1-1.3 and Cmor1-1.5) when the time difference is kept relatively low ($T_{\mathrm{d}} < 2$ for the Cmor1-1.3 and $T_{\mathrm{d}} < 0.5$ for the Cmor1-1.5).

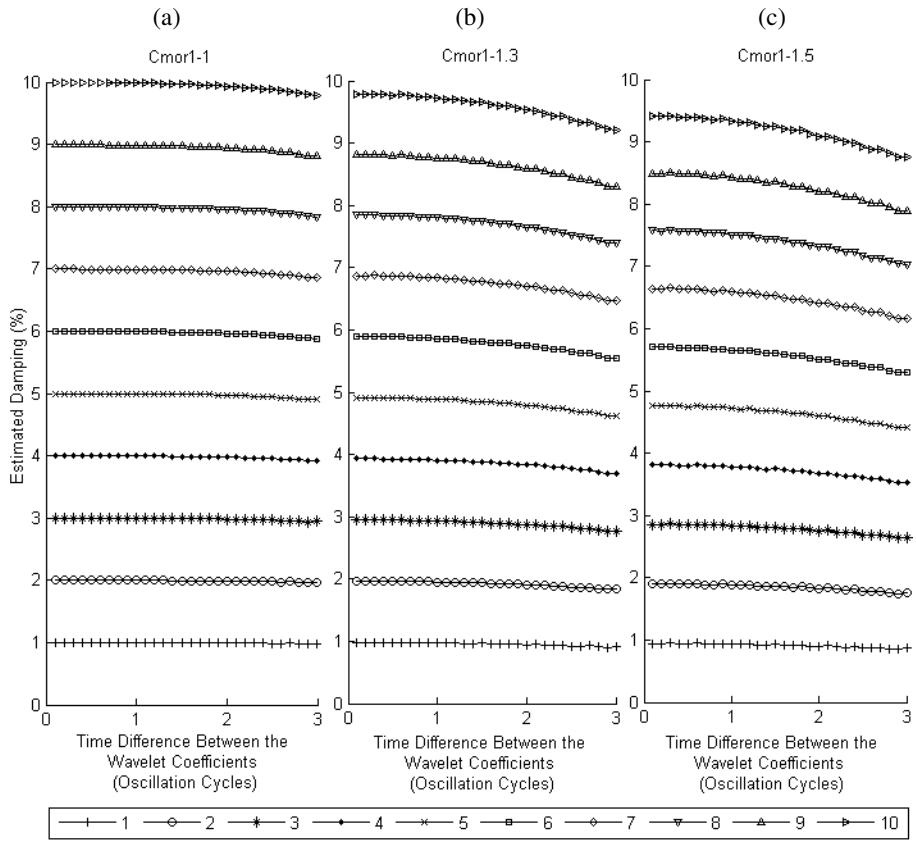

Figure 27. Estimated damping as a function of time difference between the selected wavelet coefficients in the damping estimation, T_d. The results are presented for the three wavelets Cmor1-1 (a), Cmor1-1.3 (b), and Cmor1-1.5 (c). The legend value shows the real damping of the impulse response for each curve.

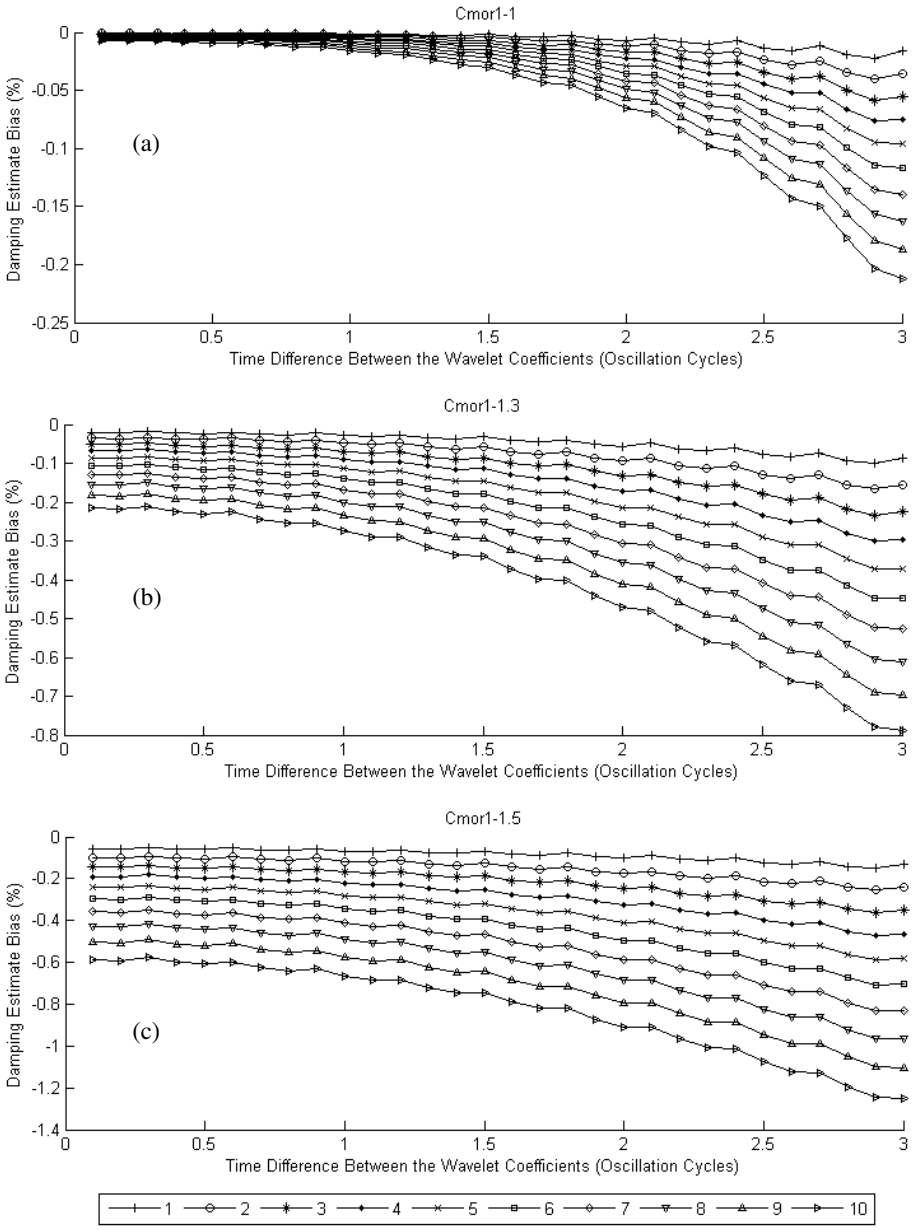

Figure 28. Damping estimate bias as a function of time difference between the selected wavelet coefficients in the damping estimation, T_d. The results are presented for the three wavelets Cmor1-1 (a), Cmor1-1.3 (b), and Cmor1-1.5 (c). The legend value shows the real damping of the impulse response for each curve.

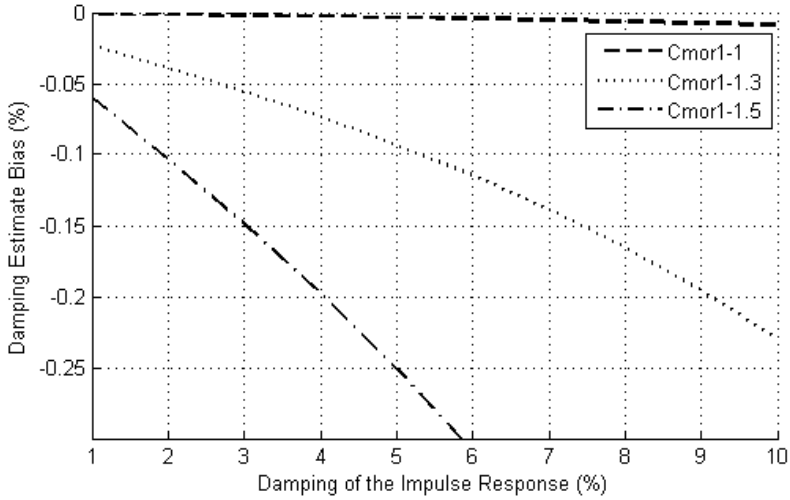

Figure 29. Damping estimate bias as a function of real damping of the impulse response. The time difference between the selected wavelet coefficients in the damping estimation, T_d, is 0.5 oscillation cycles. The results are presented for the three wavelets Cmor1-1, Cmor1-1.3, and Cmor1-1.5.

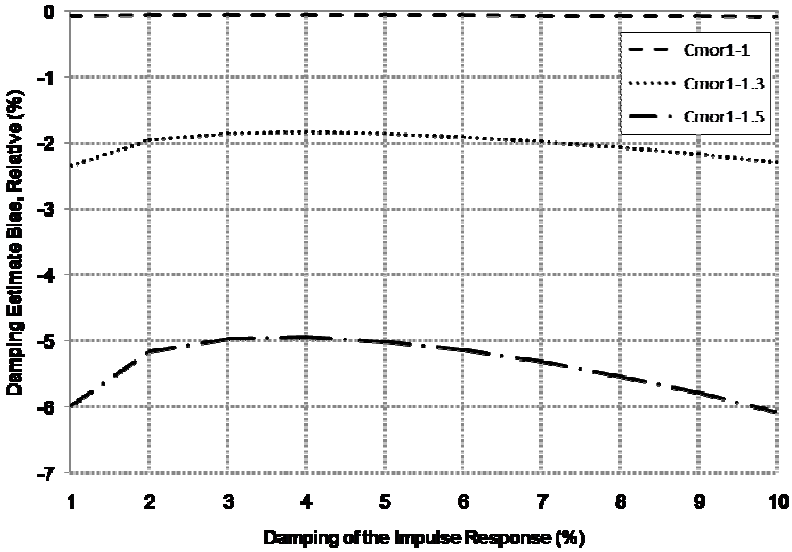

Figure 30. Relative damping estimate bias as a function of real damping of the impulse response. The time difference between the selected wavelet coefficients in the damping estimation, T_d, is 0.5 oscillation cycles. The results are presented for the three wavelets Cmor1-1, Cmor1-1.3, and Cmor1-1.5.

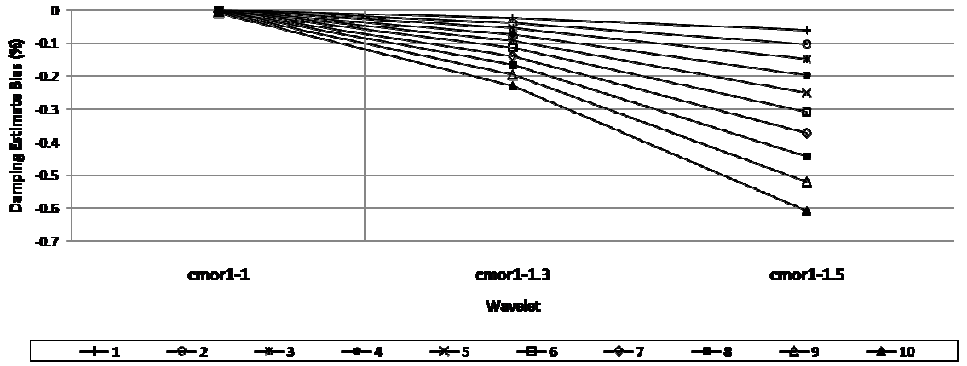

Figure 31. Damping estimate bias as a function of wavelet length. The time difference between the selected wavelet coefficients in the damping estimation, T_d, is 0.5 oscillation cycles. The legend value shows the real damping of the impulse response for each curve.

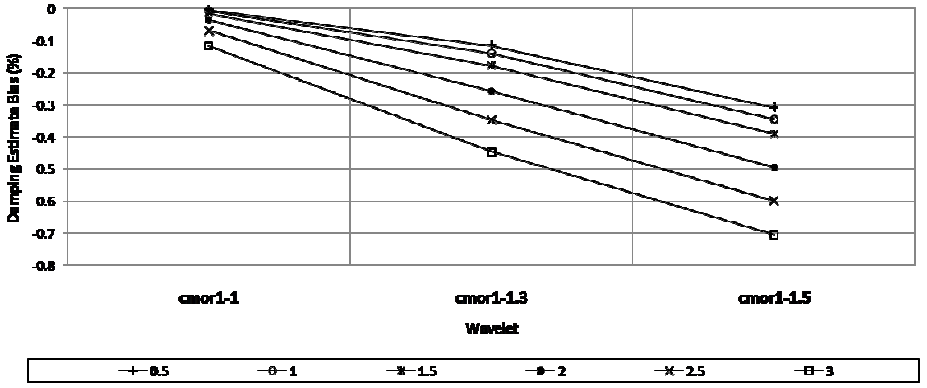

Figure 32. Damping estimate bias as a function of wavelet length. Damping of the impulse response is 6 %. The legend value shows the time difference between the selected wavelet coefficients in the damping estimation, T_d, for each curve.

Two different wavelet functions are used in the impulse response's damping estimation in this thesis: Cmor1-1 and Cmor1-1.5. Although the Cmor1-1 wavelet gives better results for the ideal impulse response, the effect of using a longer wavelet on the damping estimation results is illustrated with the Cmor-1.5 wavelet. The time difference, T_d, between the selected wavelet coefficients in the impulse response's damping estimation is selected to be 0.5 oscillation cycles.

3.4.2 Effect of Selection Point on the Damping Estimates

The selection point, T_{sp}, of the damping estimate [Figure 14, Equation (14)] affects the damping estimation results. Here, its effect is studied in the case of an ideal impulse response. Intuitively, the best selection point for a damping estimate is the point when

the two wavelets[15] are symmetrically located at each side of the center of the impulse response curve. To verify the assumption, two cases are studied below. The one in which the rightmost wavelet is located in the center of the impulse response curve (Figure 33a) and the other in which the leftmost wavelet is located in the center of the impulse response curve (Figure 33b). Both damping estimate groups differ substantially more from the real damping values than the group where the wavelets were located symmetrically at each side of the center of the impulse response curve (Figure 27a). This is the case especially with longer time difference, T_d. For a short time difference the effect of selection point is small for the studied Cmor1-1 wavelet and the effect of it grows with longer wavelets.

When the approximate impulse response of a specific inter-area mode is estimated with the damping estimation method (Figure 14), it is possible that the first part of the approximate impulse response is more reliable than the last part[16]. Therefore, the selection point when the rightmost wavelet is in the middle of the impulse response curve, might be justifiable in practice, although it gives worse (but still acceptable) results in the ideal case. Therefore, both selection points are used in this thesis: the midpoint and the point in which the rightmost wavelet is in the middle of the impulse response. The effect of using these selection points on the damping estimates is studied.

[15] Damping estimate is calculated from the wavelet coefficients at two different locations according to Equation (14).

[16] The first part might be more reliable than the last part because the amplitude is larger and therefore the effect of random excursions is minimized.

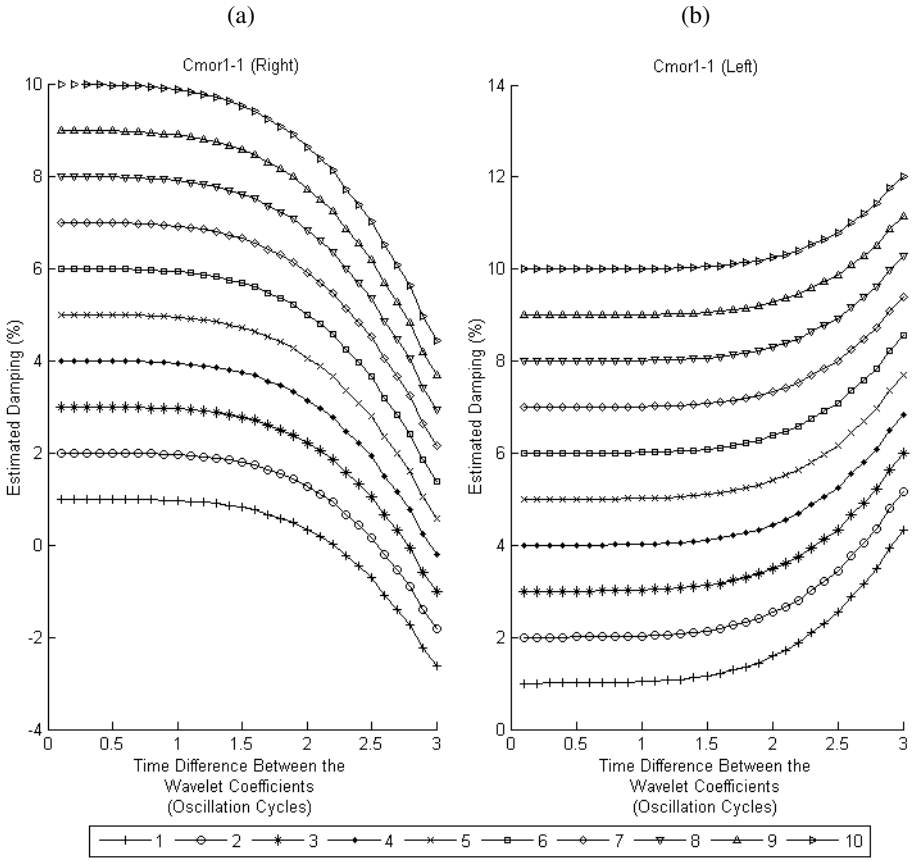

Figure 33. Damping estimates as a function of time difference between the selected wavelet coefficients in the damping estimation, T_d, when the rightmost wavelet is in the middle of the impulse response (a) and when the leftmost wavelet is in the middle of the impulse response (b). The results are presented for the Cmor1-1 wavelet. The legend value shows the real damping of the impulse response for each curve.

3.4.3 Effect of Deviation between the Frequency of the Approximate Impulse Response and the Estimated Frequency on the Damping Estimates

The estimated frequency, f_m, is not an actual parameter of the block which estimates the damping from the approximate impulse response (Figure 14). However, it is an input of the block and for each time window its value is fixed and can be considered as a parameter. This section studies how much the deviation between the frequency estimate, f_m, and frequency of the actual impulse response affects the damping estimates. The estimated frequency, f_m, is converted to the corresponding scale of the wavelet function used in the mode damping estimation from the approximate impulse response, $\psi_{d.e.}$, with

Equation (11). However, the effect that the difference between the frequency estimate and the actual mode frequency has on the *mode extraction*, is *not* studied here.

The study is done in such a way that the wavelet center frequency is kept constant at 0.3 Hz and the impulse response's frequency is varied in the range from 0.25 Hz to 0.35 Hz. The results are presented for different damping ratios (from 1 % to 10 %) and for the Cmor1-1, Cmor1-1.3, and Cmor1-1.5 wavelets (Figure 34a, b, and c, respectively).

The effect of frequency deviation is significant on the damping estimates for all the studied wavelets and damping ratios. In addition, the damping estimate is almost linearly dependent on the impulse response's frequency in case of the short wavelet Figure 34a.

In the results of Figure 35, the real frequency of the impulse response is used as the frequency, f_m, in the equation of the damping ratio [Equation (14)]. In this case, the frequency deviation has very little effect on the damping estimates especially in the case of the short wavelet (Figure 35a). The wavelet center frequency is 0.3 Hz in this case, too.

The conclusion is that the frequency mismatch between the impulse response and the wavelet center frequency does not affect much the damping of the wavelet coefficient, but it has an effect via the equation of the damping ratio [Equation (14)].

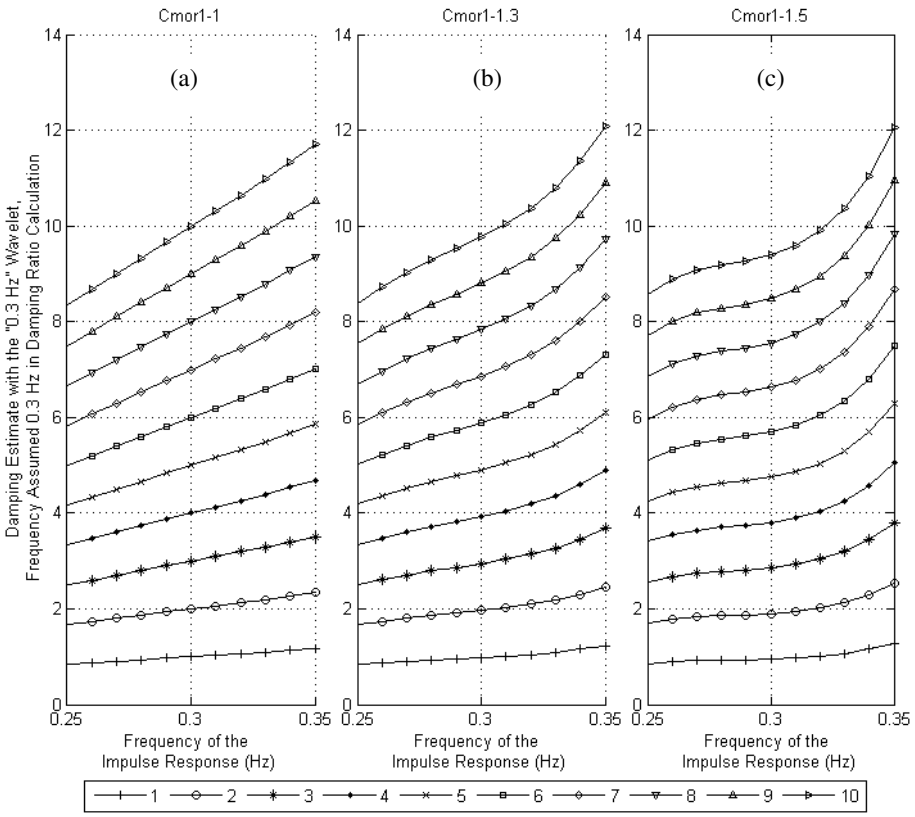

Figure 34. Estimated damping as a function of impulse response's frequency when the estimated frequency is 0.3 Hz and therefore the wavelet center frequency is kept constant at 0.3 Hz in each case. The time difference between the selected wavelet coefficients in the damping estimation, T_d, is 0.5 oscillation cycles. The results are presented for the three wavelets Cmor1-1 (a), Cmor1-1.3 (b), and Cmor1-1.5 (c). The legend value shows the real damping of the impulse response for each curve.

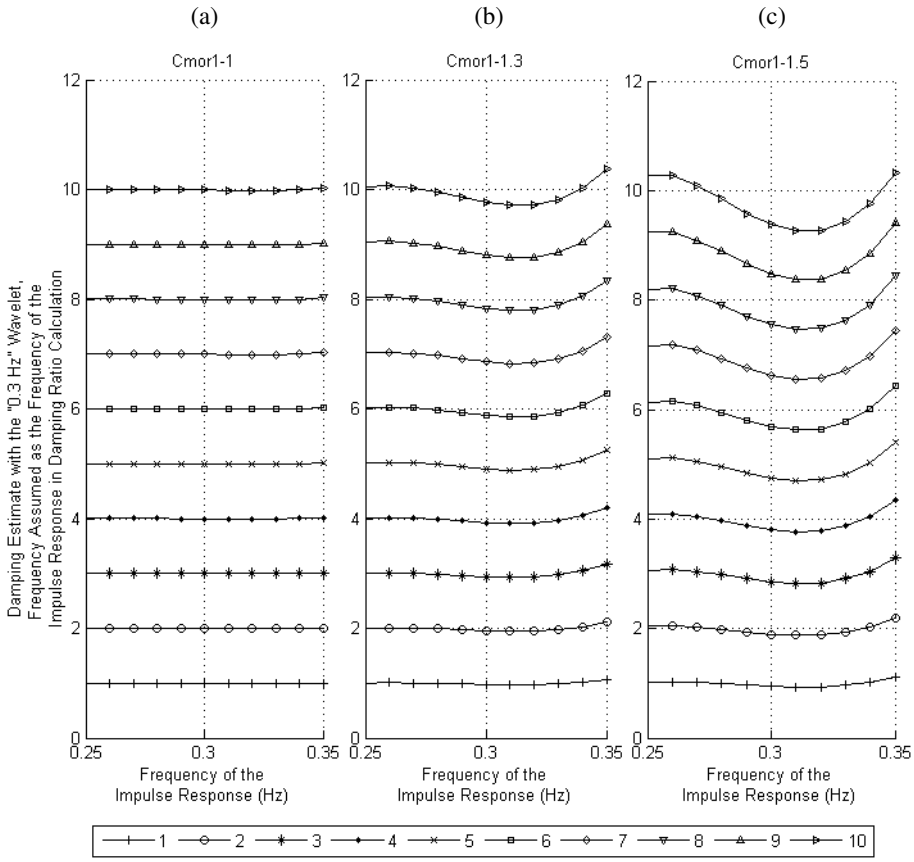

Figure 35. Estimated damping as a function of impulse response's frequency when the impulse response's frequency is used in the damping ratio calculation. Wavelet center frequency is kept constant at 0.3 Hz in each case. The time difference between the selected wavelet coefficients in the damping estimation, T_d, is 0.5 oscillation cycles. The results are presented for the three wavelets Cmor1-1 (a), Cmor1-1.3 (b), and Cmor1-1.5 (c). The legend value shows the real damping of the impulse response for each curve.

3.4.4 Effect of Wavelet's Approximation Accuracy on the Damping Estimates

The wavelet's numerical approximation accuracy is not explicitly shown as a parameter of the block which estimates the damping from the approximate impulse response (Figure 14). This is because the approximation accuracy is an internal parameter of the Matlab®'s algorithm for the continuous wavelet transform (CWT). However, this parameter might have an effect on the damping estimates. In all the previous studies very high numerical approximation accuracy was used for the wavelets to achieve as reliable results as possible. In practice, though, the numerical approximation accuracy of the wavelet affects the computational speed of the damping estimation algorithm. Therefore sufficient accuracy, not higher, should be used. Matlab®'s algorithm for

continuous wavelet transform implicitly uses the numerical approximation accuracy of 2^{10} points in the wavelet's domain.

The name *continuous wavelet transform* implies that the wavelet transform is made continuously both in the direction of time translation (parameter a_i in Equation (7)) and in the direction of scale (or frequency, parameter b_j in Equation (7)). However, practical power system data is numerical and therefore the calculations are made using numerical calculations instead of analytic calculations. Therefore, continuous wavelet transform is done using a finite set of parameters a_i and b_j. Also the wavelet function itself is a numerical approximation of the underlying analytic waveform and the approximation accuracy (or sampling interval) of it affects the damping estimation results.

Accuracies of 2^6, 2^8, 2^{10}, 2^{12}, 2^{14}, 2^{16}, 2^{18}, and 2^{20} data points in the wavelet's support domain from -8 to 8 are studied. Examples of wavelets' numerical approximations for the accuracies of 2^6, 2^8, and 2^{10} data points for the Cmor1-1.5 wavelet are shown in Figure 36, Figure 37, and Figure 38, respectively.

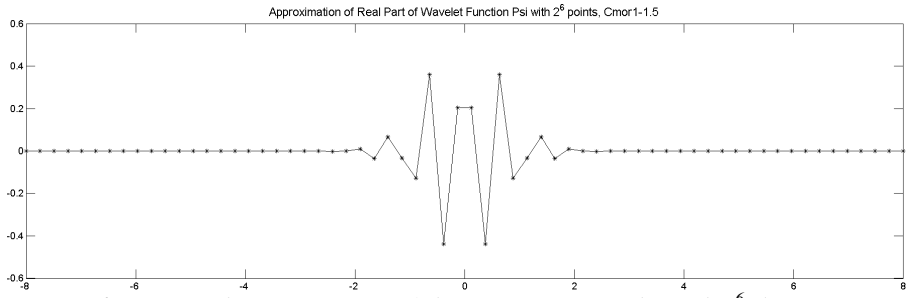

Figure 36. Numerical approximation of the Cmor1-1.5 wavelet with 2^6 data points in the wavelet's support domain from -8 to 8.

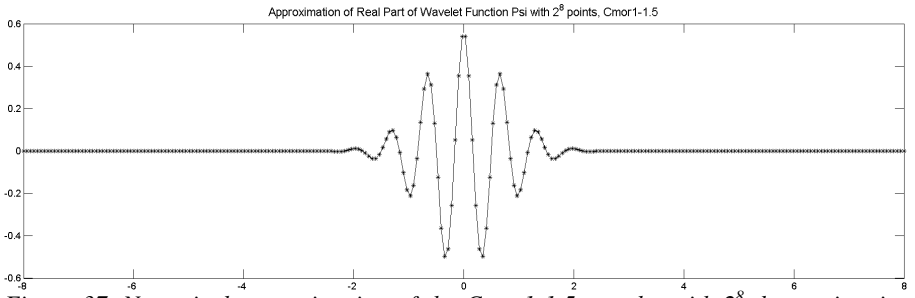

Figure 37. Numerical approximation of the Cmor1-1.5 wavelet with 2^8 data points in the wavelet's support domain from -8 to 8.

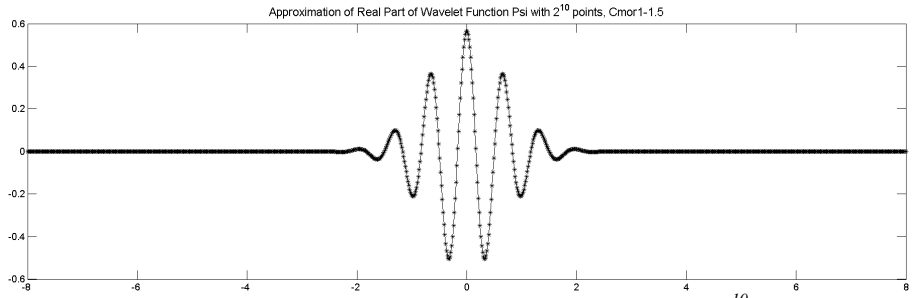

Figure 38. Numerical approximation of the Cmor1-1.5 wavelet with 2^{10} data points in the wavelet's support domain from -8 to 8.

Example of the Analysis

The same impulse response with the frequency of 0.3 Hz and damping of 6 % (Figure 23) is used to illustrate the effect of the wavelet's numerical approximation accuracy on the damping estimates and the same wavelets (Cmor1-1, Cmor1-1.3, and Cmor1-1.5) are used here (Figure 24) than were used before in Section 3.4.1.

To emphasize the effect of the wavelet's approximation accuracy on the wavelet coefficients and damping estimates of the impulse response, the approximation accuracy of 2^6 data points is used in Figure 39 which presents the corresponding wavelet coefficients of the impulse response with the Cmor1-1 and Cmor1-1.5 wavelet. Large oscillations are caused in the wavelet coefficient when the low approximation accuracy of the wavelet is used. This is the case for the both wavelets, but the longer wavelet (Cmor1-1.5) produces larger oscillations in the wavelet coefficient than the shorter one.

The way that these oscillations of the wavelet coefficient affect the damping estimates is dependent on the time difference, T_d (Figure 39). If the value of 0.2 oscillation cycles is used for the time difference, T_d, large oscillations are observed in the damping estimate (Figure 40). On the other hand, if the value of 0.5 oscillation cycles is used for the time difference, T_d, smaller (but still significant) oscillations are observed in the damping estimate (Figure 41). It is clear that larger oscillations in the wavelet coefficient caused by the longer Cmor1-1.5 wavelet are also reflected as larger oscillations in the damping estimate. The points highlighted in Figure 40 and Figure 41 are the points that would have been selected as the impulse response's damping estimates in these cases.

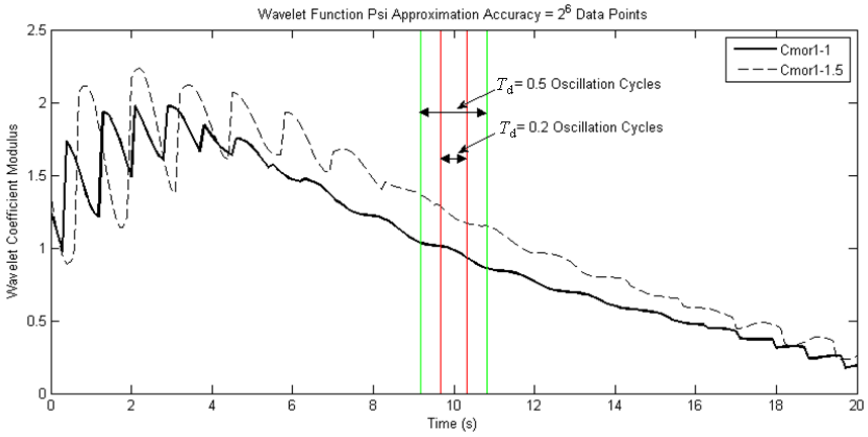

Figure 39. Wavelet coefficient modulus of the example impulse response (Figure 23) with the Cmor1-1 and Cmor1-1.5 wavelets and with the wavelet's approximation accuracy of 2^6 data points in the wavelet's support domain. Two time differences between the wavelet coefficients, T_d, are also shown.

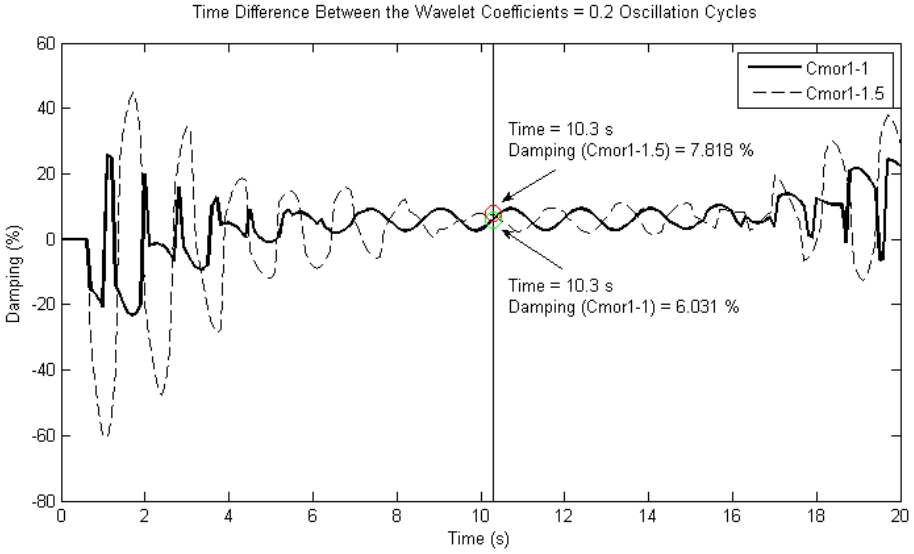

Figure 40. The damping estimate calculated from the wavelet coefficient modulus (Figure 39) of the example impulse response (Figure 23) with the time difference, T_d, of 0.2 oscillation cycles. Damping value and the time instance highlighted in the figure is the midpoint of the damping values.

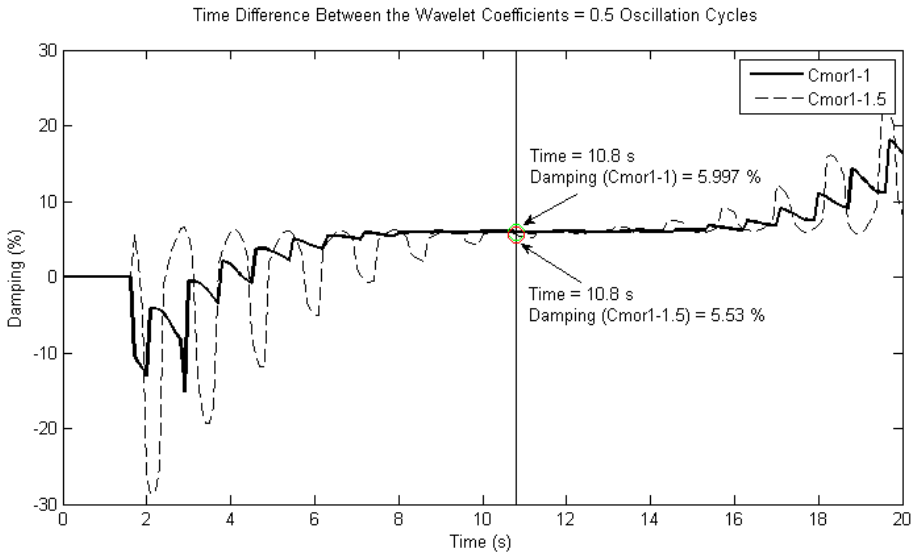

Figure 41. Damping estimate calculated from the wavelet coefficient modulus (Figure 39) of the example impulse response (Figure 23) with the time difference, T_d, of 0.5 oscillation cycles. Damping value and the time instance highlighted in the figure is the midpoint of the damping values.

Analysis Results with Different Approximation Accuracies of the Wavelet, with Multiple Time Differences between the Selected Wavelet Coefficients, and with Different Wavelets

To get a complete picture how the numerical approximation accuracy, 2^{A_A} (A_A is an exponent of approximation accuracy), of the wavelet function affects the damping estimates in case of multiple time differences, T_d, between the selected wavelet coefficients and with different wavelets, the standard deviations of the damping estimates are calculated. The calculation is done with an interval of one oscillation cycle (3.333 s) in the middle of the damping estimate curve for each case. The standard deviation of the damping estimate is a measure of the estimate's accuracy.

The standard deviations for the Cmor1-1, Cmor1-1.3, and Cmor1-1.5 wavelets, for the time difference, T_d, between 0.1 to 3 oscillation cycles, and for the wavelet's approximation accuracies, 2^{A_A}, of 2^6, 2^8, 2^{10}, 2^{12}, 2^{14}, 2^{16}, 2^{18}, and 2^{20} data points in the wavelet's domain from −8 to 8 are shown in Figure 42. In the analysis, the damping of the impulse response is 10 %, which is the worst case giving the largest standard deviations. The results are similar for other damping ratios except the standard deviations are smaller.

The standard deviation often has a local minimum when the time difference, T_d, is an integer multiple of 0.5 oscillation cycles. This is evident especially for the shortest Cmor1-1 wavelet (Figure 42a) and with the low wavelet's approximation accuracies (<

2^{12} data points). The effect of the time difference, T_d, on the damping estimate standard deviation decreases when the approximation accuracy increases. The decrease of the standard deviation "saturates" or it is not decreasing a lot more when the approximation accuracy of the wavelet reaches the level of 2^{14} data points; the value used in this thesis. This can be considered as the minimum level for the wavelet's approximation accuracy in the impulse response's damping estimation. The longer wavelets (Cmor1-1.3, and Cmor1-1.5) produce higher damping standard deviations compared to the shortest wavelet (Cmor1-1). When the damping estimate is observed as a function of time, it is constantly increasing with longer wavelets. The constant increase of the damping estimate increases the standard deviation of the damping estimate, since it deviates from the mean damping although it is not oscillating. However, the constant increase of the damping estimate is only a smaller part of the high standard deviation in the case of longer wavelets. The larger part is due to the larger oscillation of the damping estimate in the case of longer wavelets.

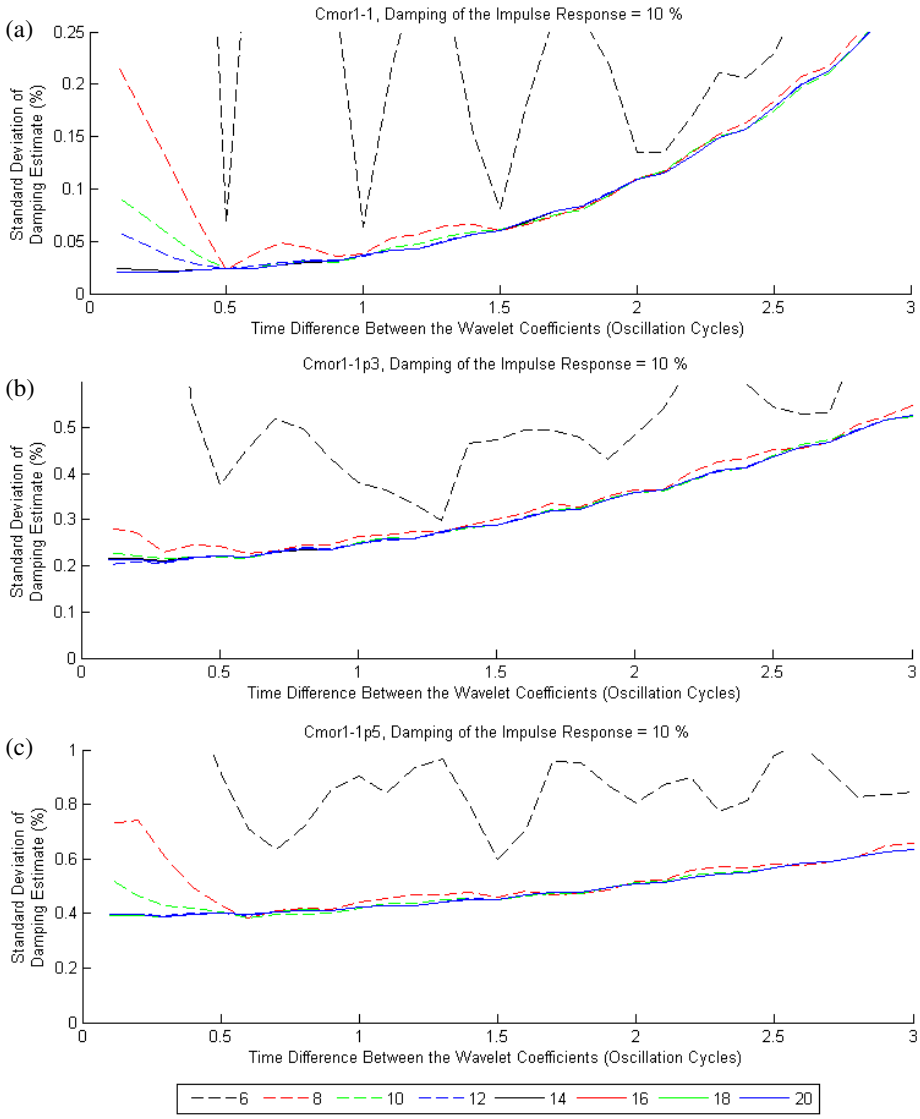

Figure 42. Standard deviations of the damping estimates as a function of time difference between the wavelet coefficients, T_d. The results are presented for the three wavelets Cmor1-1 (a), Cmor1-1.3 (b), and Cmor1-1.5 (c). The standard deviations are calculated in the interval of one oscillation cycle (3.333 s) such that the window is located in the middle of the damping estimate curve. The legend value shows the exponent of the numerical approximation accuracy (approximation accuracy = 2^{A_A} data points, where A_A = exponent of approximation accuracy = legend value) of the wavelet for each curve.

3.5 Summary of the Parameters

The parameters of the damping estimation method are classified as general parameters and the parameters of the different blocks in Figure 14. The general parameters are the *time window length* and *update time* of the method and the signal *sampling frequency*. They are common for all blocks of the method. The frequency estimation, mode extraction, and mode damping estimation blocks each have their own wavelet function as a parameter. The selection of the wavelet functions is studied in detail. The criteria for selecting the wavelet functions for mode extraction and frequency estimation are specified. The Cmor1-1.5 and Gaus20[17] wavelet functions are selected for frequency estimation and mode extraction of the Nordic power system, respectively.

The other parameters of the frequency estimation block are the *frequency band* and *scale resolution*. Frequency band is selected to include the 0.3 Hz mode which is of interest here and a high enough scale resolution is selected. The parameters of the random decrement technique, *threshold* and *sample length*, are specified by analyzing the output of a simple simulation model.

The wavelet function and other parameters of the mode damping estimation block, *time difference* and *selection point*, are studied by analyzing ideal impulse responses with different damping ratios. Also the *frequency deviation* and *accuracy of the wavelet's approximation* is considered. The effect of using three different wavelets[18] and different time differences on the damping estimates is studied. The shortest wavelet (Cmor1-1) produces the least biased estimates for the damping[19]. The bias increases when a longer time difference is used or when the damping ratio of the impulse response increases. The damping ratio affects only the absolute bias, relative bias is not much affected. The selection point for damping estimate is studied and usually the midpoint gives the best results for damping estimates[20]. The effect of selection point increases when the time difference increases. The frequency deviation has a significant effect on the damping estimates via the definition of the damping ratio. The accuracy of the wavelet's approximation has a significant effect on the damping estimates if it is too low. The time difference affects more the damping estimates if the accuracy of the wavelet's approximation is low.

[17] Also the Gaus4 and Gaus44 wavelet functions are used in the performance analysis of the thesis to verify that the selected wavelet function (Gaus20) is optimal for estimating damping under the ambient conditions.
[18] The wavelets are Cmor1-1, Cmor1-1.3, and Cmor1-1.5.
[19] Also the Cmor1-1.5 wavelet function is used in the performance analysis of the thesis to verify the optimality of the wavelet selection under the ambient conditions of the power system.
[20] Also the selection point when the rightmost wavelet is in the middle of the impulse response is used in the performance analysis of the thesis to verify the optimality of the wavelet selection under the ambient conditions of the power system.

4 Performance Analysis of the Damping Estimation Method

4.1 Quantities to Assess Performance

Performance of the damping estimation method can be considered good when the damping estimates are accurate. In order to study the accuracy of the estimation results, three quantities are used: standard deviation of the estimate, mean value of the estimate, and the bias of the estimate from the real (or reference) value. The mean value tells the average damping ratio during the estimation period. The bias determines how much the estimates generally deviate from the reference damping. The standard deviation tells how large the variation of the estimates is and determines how much the individual estimates usually deviate from the reference damping. The accuracy is considered good when the mean value is near the real value and both the bias and the standard deviation are near zero. In this case both the individual estimates, and the estimates in general are near the real value and can be considered accurate. The bias used here is the absolute bias as defined by Equation (16).

In this method to assess the accuracy it is assumed that the real damping is constant during the estimation period. If the real damping changes, the damping estimates should change accordingly. The speed of reaction of the damping estimates is dictated by the time window length of the method. If the time window is long, then the estimates react slower. Therefore, shorter time windows are preferred as long as the accuracy of the estimates is good enough.

4.2 Nordic Power System Simulations in Assessing Performance

The simulations are used to study the performance of the method because the real damping is known and can be compared to the estimated damping. The grid measurements in an almost identical power flow situation are then used to verify if the results for the simulations and measurements agree, as they should if the model describes the power system dynamics well enough.

4.2.1 Simulation Cases and Output Signals

Dynamic Simulation Model and Power Flows

The nonlinear dynamic simulation model of the Nordic power system is used here. The oscillation characteristics of the system are described in Section 1.10.2. When the system is operating under the ambient conditions, the oscillations are small and the dynamic behavior of the system is approximately linear. The simulation model is implemented in PSS®E-software and it has about 6000 buses, 1700 machines and 2600 loads. The number of state variables is about 17000.

The power flow of the Northern AC-lines between Finland and Sweden (presented in Figure 3) affects most the damping ratio of the 0.3 Hz mode. When the power transfer from Finland to Sweden increases the damping of the inter-area mode becomes poorer. Different power flow cases are used in order to find out how the damping estimation method performs with different damping ratios.

Here, a concept *base power flow case*, which represents a winter situation with high load, high power export from Finland to Sweden, and a 7 % damping ratio of the 0.3 Hz mode, is used. Other power flow cases with different damping ratios of the 0.3 Hz mode are used, too. They are modified from the *base power flow case*. The reference damping (the real damping) is calculated in each power flow case by creating a small transient to the system and applying Prony analysis to find out the oscillation modes and their damping (Hauer 1991). Because the simulated transient is small, the power system behavior is linear, and the related damping is the small-signal damping of the power system.

Power System Input

To reflect the real behavior of the power system under ambient conditions, the randomly varying loads excite the oscillations in the system in the simulations, too. The load variation is done only on the Finnish side of the grid where the controllability of the studied 0.3 Hz mode is the largest (Uhlen et al. 2003, Elenius et al. 2005) and therefore the excitation of the mode is the most effective. In this way, the power oscillations in the interconnecting lines between Finland and Sweden become close to the measured values under the ambient conditions (a couple of MWs oscillation).

The individual varying loads follow the uniform distribution. Therefore, the load variation results in the driving noise not being strictly Gaussian, which is assumed in the damping estimation method. However, because the number of varying loads is large, the net effect of the load variation is approximately Gaussian based on the central limit theorem[21] (Cam 1986).

[21] Central limit theorem states that the sum of independent and identically distributed random variables with finite mean and variance approaches the normal distribution (Gaussian distribution) when the number of random variables increases, irrespective of the distribution of the random variables.

Analyzed Output Signals

The analyzed output signals of the simulation represent different geographical areas where the modal observability is different, and physical quantities of the Nordic power system. In Finland, the signals are selected from South and North Finland. In Sweden, they are from North, North/Central, Central/South, and South Sweden. In Norway they are from North, Central, South Western, and South Eastern Norway and in Denmark from East Denmark. The physical quantities are active power flows of the interconnecting lines between Finland and Sweden, generator relative rotor angles (relative to a large generator in South Sweden), generator speed deviations from nominal, local frequency deviations from nominal, and bus voltage magnitudes and phase angles. Although all of these signals are analyzed with the damping estimation method, only some results are presented in order to describe the performance characteristics of the method.

An example of an analyzed output signal under the ambient conditions is presented in Figure 43. The signal is active power of the interconnecting 400 kV line between Finland and Sweden. The simulation duration is here as well as in the other studied cases 1000 s (16.7 min) to achieve enough data for the damping estimation method.

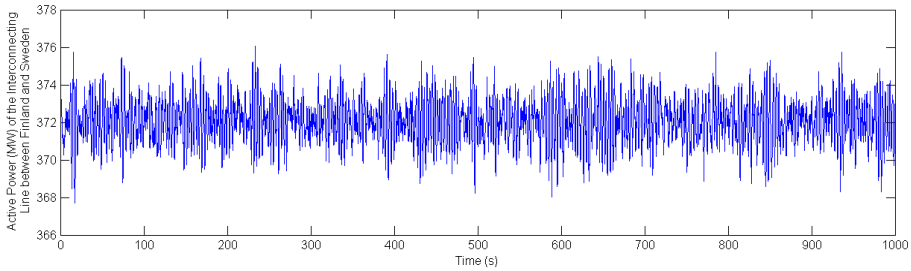

Figure 43. An example of the simulation output signals. The signal is the active power of the interconnecting line between Finland and Sweden. A couple of MWs oscillation is observed in the signal which is close to the measured values in the Nordic power system in the same power flow situation under the ambient conditions.

4.2.2 Cases of Performance Analysis using the Simulated Data

Four cases are analyzed in the performance analyses:

1) Effect of different *time window lengths*, *mode extraction wavelets*, and *signals* on the estimates of damping and frequency
    a. Original parameter set of the method and base power flow case is used
2) Effect of measurement *noise* on the estimates of damping and frequency
    a. Original parameter set of the method and base power flow case is used. Only one signal is used in the analysis, but different time window lengths and mode extraction wavelets are studied
3) Effect of *two different parameter sets* of the method on the damping estimates
    a. Base power flow case and only one signal is used in the analysis, but different time window lengths, and mode extraction wavelets are studied

4) Effect of *different damping conditions* of the power system on the damping estimates
    a. Only one signal and a fixed time window is used in the analysis, but different mode extraction wavelets are studied

The *base power flow case* with a 7 % reference damping ratio of the 0.3 Hz mode is presented in Section 4.2.1. The *original parameter set* means that the Cmor1-1.5 wavelet is an analyzing wavelet of the approximate impulse responses' damping, and the selection point is the one when the rightmost wavelet is in the middle of the impulse response[22]. The four cases are explained in more detail in the following sections.

Case 1: Effect of Different Time Window Lengths, Mode Extraction Wavelets, and Signals on the Estimates of Damping and Frequency

The presented results are used to study the performance characteristics of the method with different signals, time windows (from 1 to 11 minutes) and with different mode extraction wavelets (Gaus4, Gaus20, and Gau44). The studied signals are different physical quantities of the grid and the machine speed measurement, grid frequency measurement and voltage magnitude signals are all from the same generating plant (a large generator in Southern Finland). The machine relative rotor angle signal is between this generator and another large generator in Southern Sweden. The active power flow is that of the interconnecting line between Finland and Sweden. All these signals have a good observability of the 0.3 Hz mode.

Case 2: Effect of Measurement Noise on the Estimates of Damping and Frequency

The measured signals always contain some measurement noise. The effect of different amounts of measurement noise on the damping estimates is studied.

Description of the Noise

Here, all the SNRs are defined in the linear scale with the equation

$$SNR = \frac{P_{\text{signal}}}{P_{\text{noise}}} = \left(\frac{\sigma_{\text{signal}}}{\sigma_{\text{noise}}} \right)^2, \tag{18}$$

where SNR is the signal-to-noise ratio of a signal, P_{signal} and P_{noise} are the average powers of the signal (without mean value) and the noise respectively, and σ_{signal} and σ_{noise} are the standard deviations of the signal and the noise respectively. Before adding the noise, the average values of the signals are removed.

[22] See Section 3.4.2 for an explanation of different selection points used in this thesis.

The measurement noise is caused by the combined measurement inaccuracy of voltages, currents, or frequency. The main sources of the measurement inaccuracy are the measurement errors of the instrument transformers and the PMUs. The measurement accuracies of these devices are known to some extent (e.g. Depablos et al. 2004) and therefore the SNRs of the measurements are also possible to assess. For example, the SNRs in the range from 30 to 5 in the linear scale are realistic values for the accuracy of the PMU's voltage angle measurements (Larsson & Laila 2009). Here, the SNRs of infinity, 10, 5, 2, 1, and 0.1 in the linear scale are studied, in order to illustrate the effect of a wide range of SNRs on the damping estimates. However, the realistic values are above 5 (Larsson & Laila 2009). It is assumed that the measurement errors are white Gaussian noise. It is a realistic assumption for the measurement errors (Phadke & Thorp 2008).

Case 3: Effect of Two Different Parameter Sets of the Method on the Damping Estimates

In this case, the performance of the method is analyzed with two different parameter sets. The intention is to find out which parameter set gives more accurate damping estimation results, and to verify the validity of the parameter selection studies in Section 3.4, when the power system is operating under ambient conditions. The first parameter set is the *original parameter set* with the Cmor1-1.5 wavelet function and the selection point is the one when the rightmost wavelet is in the middle of the impulse response. In the second parameter set, the wavelet function used in the analysis of the approximate impulse response's damping is Cmor1-1 and the selection point is the one when the two wavelets are symmetrically located around the middle of the impulse response.

The results achieved with these two sets of parameters are compared. Only one of the simulation output signals is used in the analysis because the characteristics of the results are similar for the other signals. Grid frequency measurement at a bus in Southern Finland is used in the analysis.

Case 4: Effect of Different Damping Conditions of the Power System on the Damping Estimates

In this case, the correspondence between the reference and the estimated damping values is studied in detail using a 9 minute-long time window. In the study four signals of the simulation are used: Finland–Sweden interconnection line active power flow, local grid frequency and a generator speed deviation in Southern Finland, and the angle difference between the generators in Southern Finland and Sweden.

4.3 Performance in Case of the Measured Grid Data

Damping and frequency estimation results for the measured grid data are considered in this section. The PMU measurements from the Nordic power system are used.

4.3.1 Power System Input and Measured Output Signals

In the measured data cases, the power system operates under ambient conditions; then the inputs are the power system ambient excitations: mainly the ever present load fluctuations in the grid. The measured output signals that are used in the damping estimation are the PMU measurement quantities of the Finnish WAMS which is described in Appendix A. The physical measurement quantities of the PMUs are voltages, currents, local frequency, and local rate of change of frequency (Phadke & Thorp 2008). Active, reactive, and apparent power is calculated from the voltages and currents.

The 0.3 Hz mode, which is of interest in this thesis, is well observable in Southern Finland when voltage magnitude, frequency, or rate of change of frequency is analyzed. The mode is also well observable when current, or active power flow of the AC interconnection path between Finland and Sweden is analyzed. In addition, the voltage angle difference between the oscillating generator groups in Finland and Sweden has a high observability of the mode. (Uhlen et al. 2003, Elenius et al. 2005) Therefore, these measurement locations are used.

The signals which have a high observability of the mode of interest are preferred in the damping and frequency estimation because the results are more reliable compared to the signals with poor observability of the mode. The observabilities can be calculated with the linear analysis of the power system dynamic model (Uhlen et al. 2003, Elenius et al. 2005).

4.3.2 Performance of the Damping Estimation Method with Different Signals, Time Window Lengths, and Mode Extraction Wavelets

The presented results are used to study the performance characteristics of the method with different signals, time windows (from 1 to 31 minutes) and with different mode extraction wavelets (Gaus4, Gaus20, and Gau44).

Power Flow Case

A power flow case in which the power export from Finland to Sweden is nearly constant (Figure 44), and approximately the same as in the simulated case, is studied here. Because the Finland–Sweden AC power flow is a dominant factor affecting the

0.3 Hz mode damping, the damping in the measured data case and in the simulated data case should be about the same.

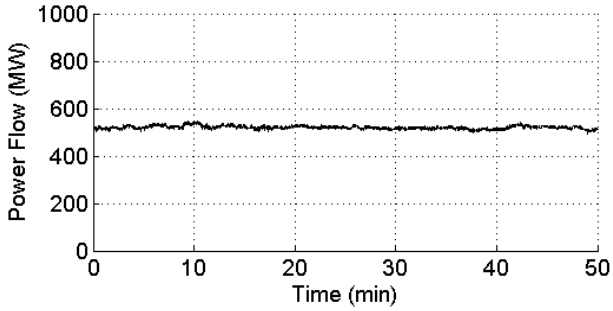

Figure 44. Measured active power flow of an interconnecting line between Finland and Sweden in the studied power flow case.

4.3.3 Detection of Change in Damping

It studied if the changes in the damping level can be observed with the damping estimation method. Two cases are studied: detection of degraded damping and improved damping.

Detection of Degraded Damping

The studied case consists of the SVC test made in Southern Finland. In the test the properties of the SVC and its POD were analyzed. The parameter set of the POD turned out to be wrong during the test and the POD did actually increase the oscillations rather than damp them. During the test the POD was operated both without a dead band and also with a predefined dead band.

Detection of Improved Damping

The studied case is another SVC test made in Southern Finland. In the test the parameter set of the POD was correct. Among other things the operation of the POD was verified to be correct and the damping improved.

5 Results of the Performance Analysis

In this chapter, the performance of the damping estimation method is studied by analyzing the damping estimation results for different simulated and measured signals of the Nordic power system.

5.1 Performance in Case of the Nordic Power System Simulations

5.1.1 Time Evolution of the Damping Estimate and Damping vs. Frequency

The time evolutions of the damping estimates with three different mode extraction wavelets are presented in Figure 45a. The damping estimation results can also be presented as damping vs. frequency (Figure 45b). The shortest (Gaus4) wavelet in the mode extraction produces the most variance in the damping estimate and gives the highest damping estimates. The damping estimate is higher the shorter the mode extraction wavelet is; i.e. the Gaus4 wavelet produces the highest and the Gaus44 produces the smallest damping estimate.

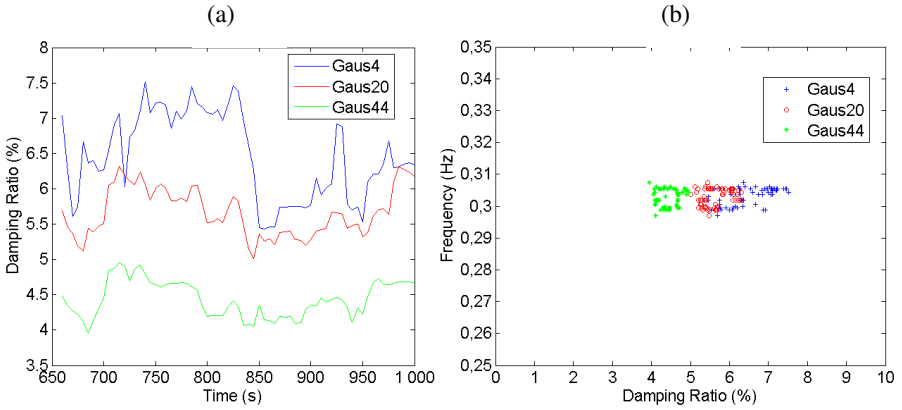

Figure 45. Damping as a function of time (a) and damping vs. frequency (b) with Gaus4, Gaus20, and Gaus44 as mode extraction wavelets. The analyzed signal is the active power of an interconnecting line between Finland and Sweden (Figure 43). The time window length is 11 minutes.

5.1.2 Case 1: Effect of Different Time Window Lengths, Mode Extraction Wavelets, and Signals on the Estimates of Damping and Frequency

Frequency Estimation Results

The frequency estimation results are presented before the damping estimation results because frequency estimation is a preceding step for damping estimation (Figure 14). The mean values and standard deviations of the frequency estimates for different time window lengths and different output signals of the simulation with 7 % reference damping are presented in Figure 46 and Figure 47, respectively. The wavelet function used in the frequency estimation is the Cmor1-1.5 wavelet.

According to Figure 46, the mean values of the frequency estimates are nearly equal for different time window lengths. There is a small difference in the mean values for different signals. Machine relative rotor angle and active power flow on the Finland–Sweden interconnection line (Figure 46) give a slightly lower frequency estimate. These signals are very closely related to each other in the small-signal conditions, because the power flow between the two countries is (approximately) linearly dependent on the angle difference. However, the difference in the frequency estimates is small and can be considered negligible in practice (see Section 3.4.3 where the deviation between the frequency estimate and actual frequency is studied).

The standard deviations of the estimates decrease with the increased time window length. For the one minute time window the frequency estimates are considerably less accurate than for the other time windows.

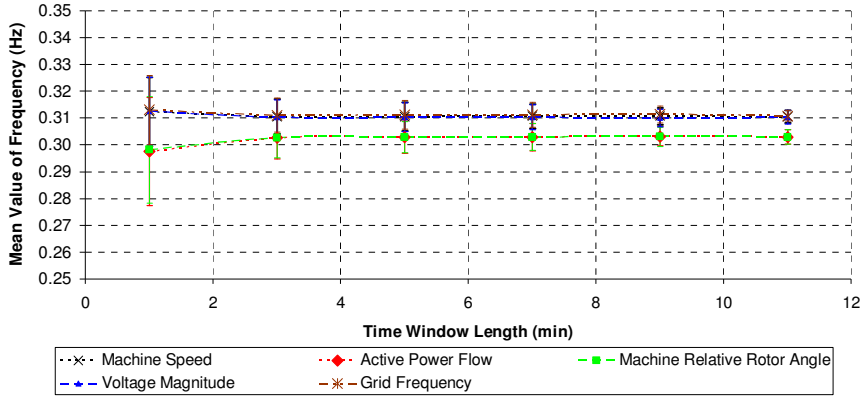

Figure 46. Mean values of the frequency estimates with different time window lengths and analyzed signals. The errorbars show the standard deviation of the estimates. The frequency estimation wavelet is the Cmor1-1.5.

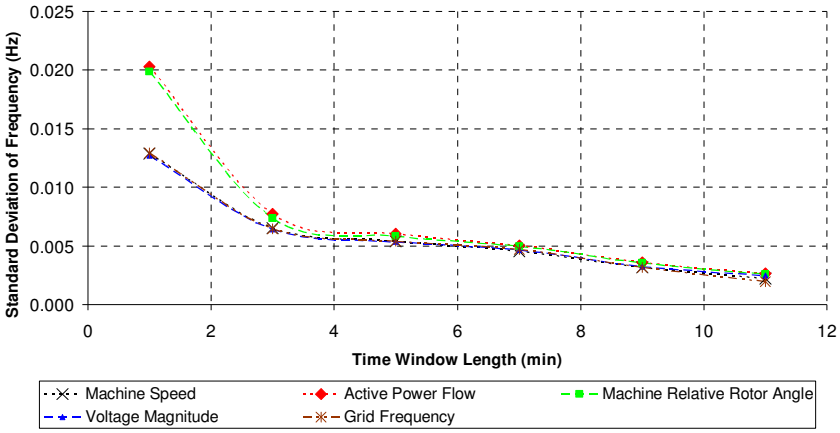

Figure 47. Standard deviations of the frequency estimates with different time window lengths and analyzed signals. The frequency estimation wavelet is the Cmor1-1.5.

Damping Estimation Results

Mean Values of the Damping Estimates

The mean values of the damping estimates with different time window lengths and output signals of the simulation are presented in Figure 48, Figure 49, and Figure 50 for the mode extraction wavelets Gaus4, Gaus20, and Gaus44, respectively. The errorbars of the figures show the standard deviations of the estimates.

The mean values of the damping estimates increase with the increased time window length and approach the real damping value. Error bounds of the damping estimates overlap implying that the same damping is estimated from different signals. However, there is a small difference between the damping estimated from a machine relative rotor angle and the active power flow of an interconnecting line between Finland and Sweden as compared to the damping estimated from the other signals. Most probably the difference is due to the different estimated frequency (see Section Frequency Estimation Results), because for a low frequency the damping ratio is higher than for a high frequency, if the damping is equal in terms of the decay time which describes how much the oscillation is damped in a fixed time interval.

When the results are compared in terms of different mode extraction wavelets, it is evident that the mean value of the damping estimate decreases when the mode extraction wavelet length increases. However, for a very short time window, the mean values are nearly equal. The longer wavelets smooth the sharp variations of a signal more and therefore some of the damping information is lost, and the estimated damping is lower. The estimated damping with the longer wavelets is pessimistic.

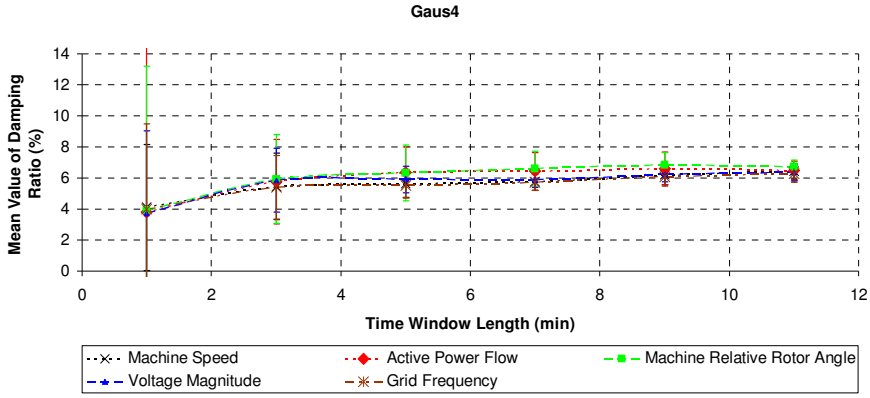

Figure 48. Mean values of the damping estimates with different time window lengths and analyzed signals. The mode extraction wavelet is the Gaus4. The errorbars show the standard deviation of the estimates.

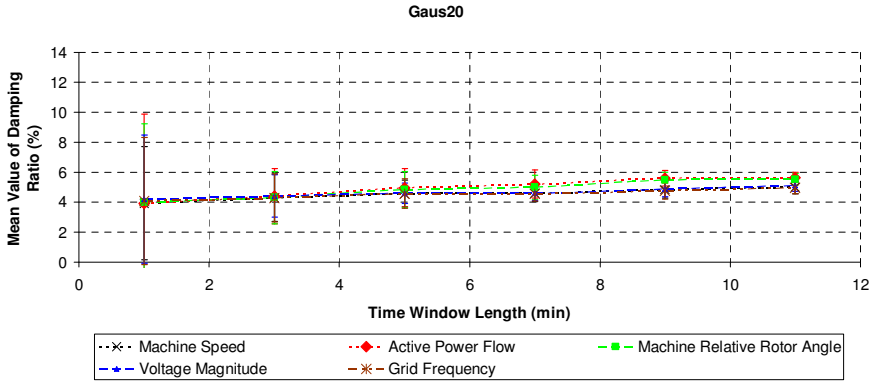

Figure 49. Mean values of the damping estimates with different time window lengths and analyzed signals. The mode extraction wavelet is the Gaus20. The errorbars show the standard deviation of the estimates.

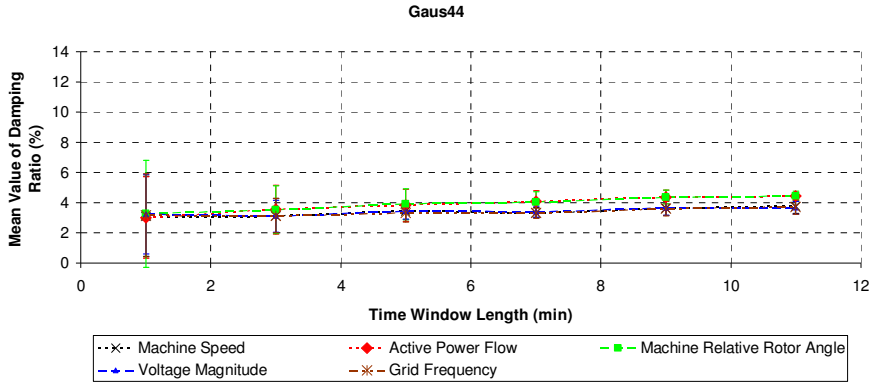

Figure 50. Mean values of the damping estimates with different time window lengths and analyzed signals. The mode extraction wavelet is the Gaus44. The errorbars show the standard deviation of the estimates.

Standard Deviations of the Damping Estimates

The standard deviations of the damping estimates with different time window lengths and output signals are presented in Figure 51, Figure 52, and Figure 53 for the mode extraction wavelets Gaus4, Gaus20, and Gaus44, respectively.

The standard deviations decrease with the increased time window length and they are smaller for the longer mode extraction wavelets (Gaus20 and Gaus44) compared to the shortest one (Gaus4). This is the case especially for short time windows ($\leq$ 5 min). The effect of mode extraction wavelet length on the damping estimate standard deviations decreases with the increased time window length. Almost the same standard deviation level is achieved with all the studied mode extraction wavelets when the time window is long ($\geq$ 9 min).

When the damping is estimated using the machine relative rotor angle and the active power flow of the Finland–Sweden interconnection line, the standard deviations are slightly different compared to the other signals. This is the case especially with the shorter time windows ($\leq$ 7 min).

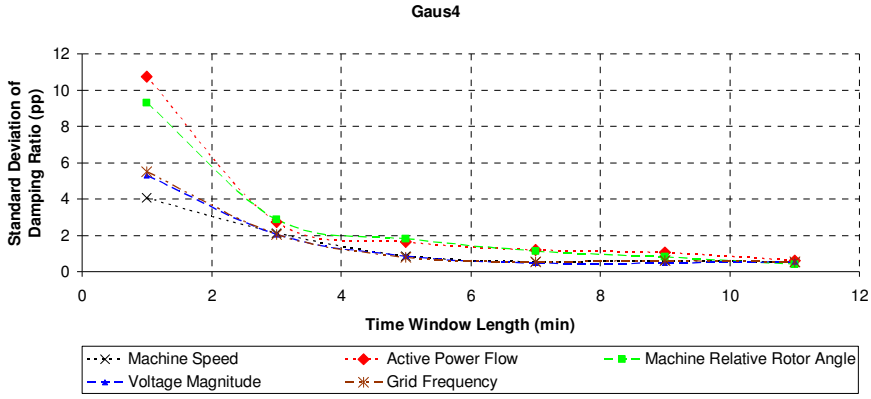

Figure 51. Damping estimate standard deviations with different time window lengths and analyzed signals. The mode extraction wavelet is the Gaus4. pp = percentage point.

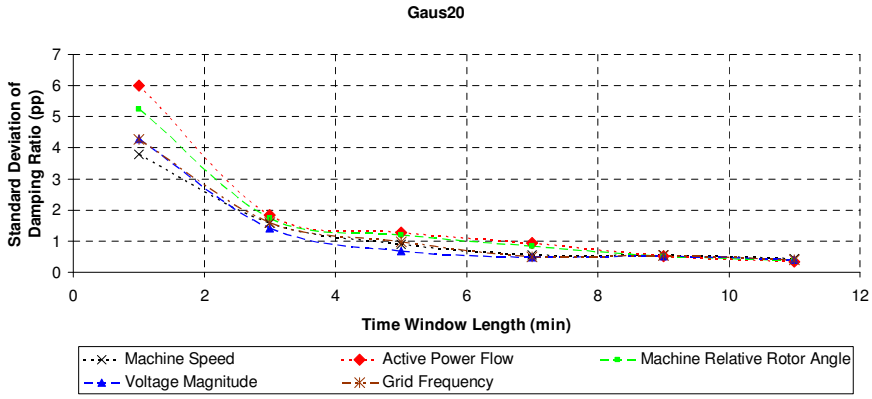

Figure 52. Damping estimate standard deviations with different time window lengths and analyzed signals. The mode extraction wavelet is the Gaus20. pp = percentage point.

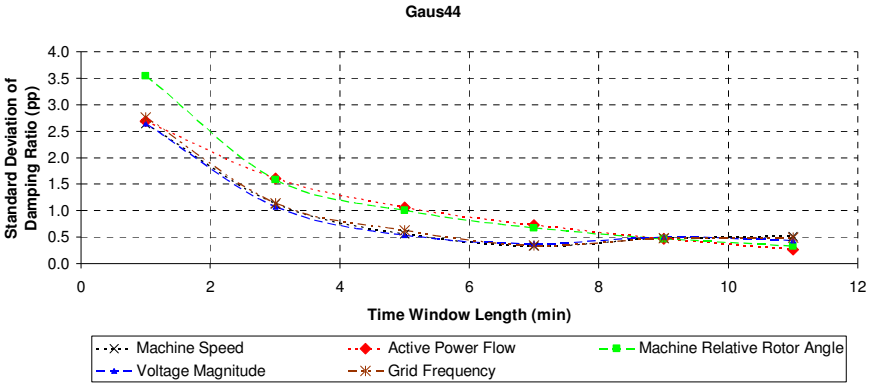

Figure 53. Damping estimate standard deviations with different time window lengths and analyzed signals. The mode extraction wavelet is the Gaus44. pp = percentage point.

Damping estimate standard deviations are further examined in case of the 3 and 11 minutes time windows in Figure 54 and Figure 55, respectively. In the case of the 3 minutes time window, the standard deviation decreases when longer mode extraction wavelets are used. This is valid for all the studied signals. When the time window is lengthened to 11 minutes, the standard deviations become smaller and the wavelet used in the mode extraction has less effect on the results. For the longest time window (11 minutes), the general level of standard deviation achievable with the method is about 0.4 % in this case.

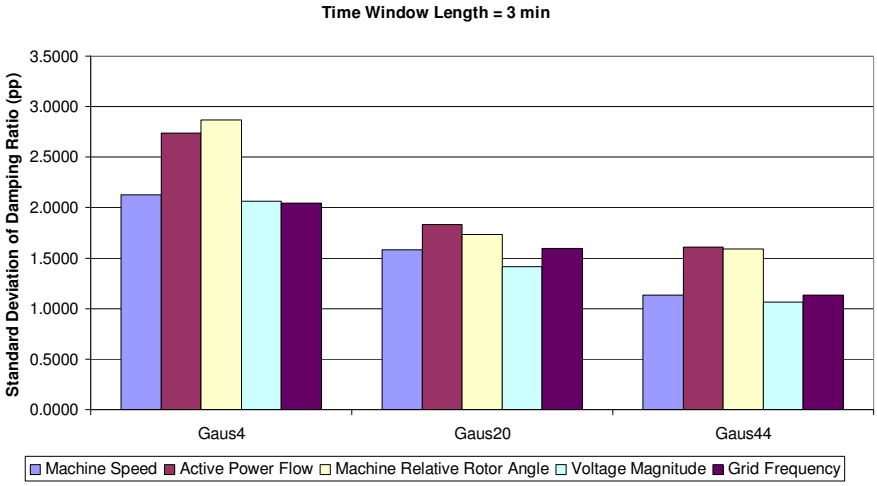

Figure 54. Damping estimate standard deviations with different mode extraction wavelets and analyzed signals. The time window length is 3 minutes.

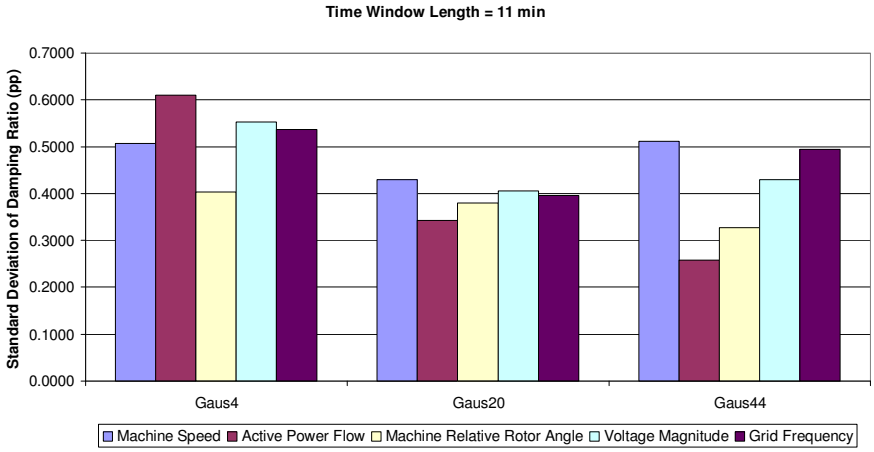

Figure 55. Damping estimate standard deviations with different mode extraction wavelets and analyzed signals. The time window length is 11 minutes (the longest time window).

Biases of the Damping Estimates

The biases of the damping estimates for different time window lengths, output signals of the simulation, and mode extraction wavelets (Gaus4, Gaus20, and Gaus44) are presented in Figure 56, Figure 57, and Figure 58, respectively. The biases in this section are absolute biases as defined by Equation (16). The real damping of the mode for the *base power flow case* is about 7 %, and it is used as a reference value in the calculation of the biases.

The biases are large for all the studied mode extraction wavelets in case of a short time window (1 min). In this case, the number of samples averaged in the random decrement technique is too low and the estimation of the impulse response, and therefore damping, is poor. When the time window length is increased, the biases are decreased because the damping estimates approach the real damping value. The biases do not decrease as much in case of the longer wavelets (Gaus20 and Gaus44) because the mean values of the damping estimates are lower.

There is a difference in biases in the case of different signals. The difference is greatest when the damping is estimated using the machine relative rotor angle or active power flow of the Finland–Sweden interconnection line and compared to the damping estimated using the other signals. The difference is due to the different damping estimate mean value.

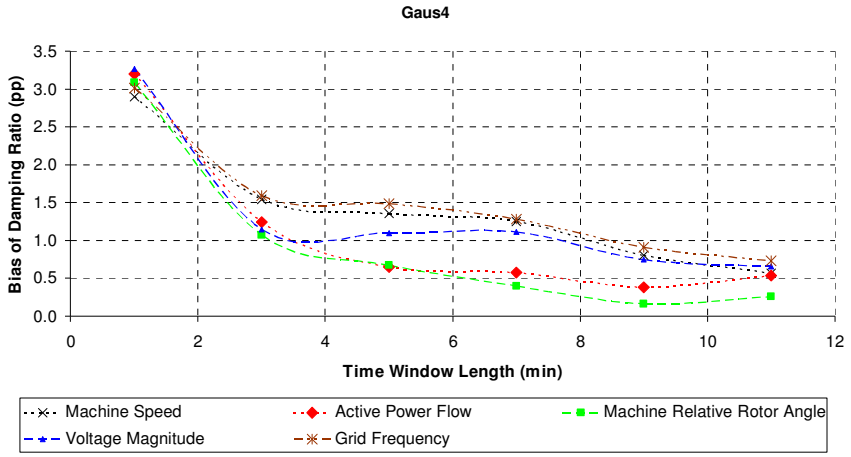

Figure 56. Damping estimate biases with different time window lengths and analyzed signals. The mode extraction wavelet is the Gaus4. The reference value for the bias calculation is 7 %. pp = percentage point.

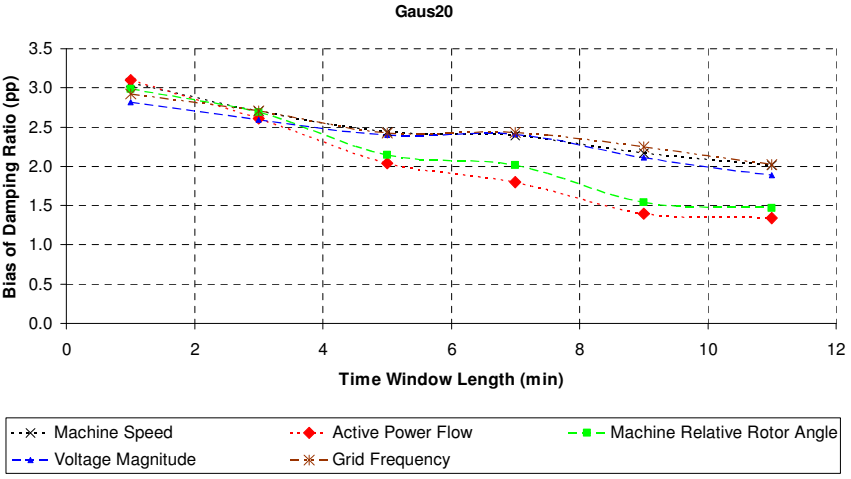

Figure 57. Damping estimate biases with different time window lengths and analyzed signals. The mode extraction wavelet is the Gaus20. The reference value for the bias calculation is 7 %. pp = percentage point.

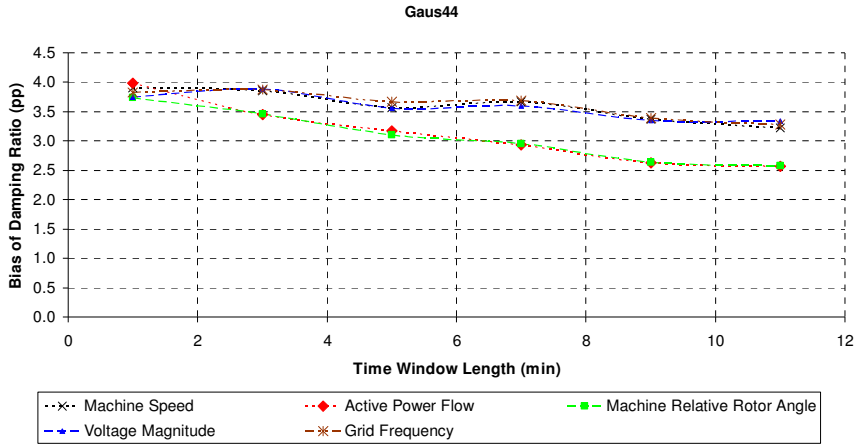

Figure 58. Damping estimate biases with different time window lengths and analyzed signals. The mode extraction wavelet is the Gaus44. The reference value for the bias calculation is 7 %. pp = percentage point.

Damping estimate biases are further examined in the case of the 3 and 11 minutes time windows in Figure 59 and Figure 60, respectively. The biases clearly grow when the mode extraction wavelet length increases in both the 3 and 11 minutes time window cases. This is valid for all the studied signals. When the difference between the 3 and 11 minutes time windows is considered, all the biases decrease roughly 1 % when the time window lengthens from 3 to 11 minutes.

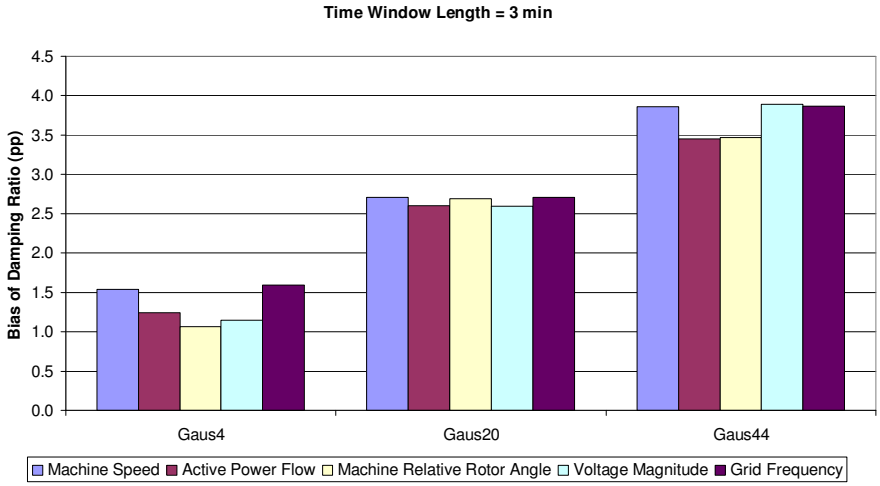

Figure 59. Damping estimate biases with different mode extraction wavelets and analyzed signals. The time window length is 3 minutes. pp = percentage point.

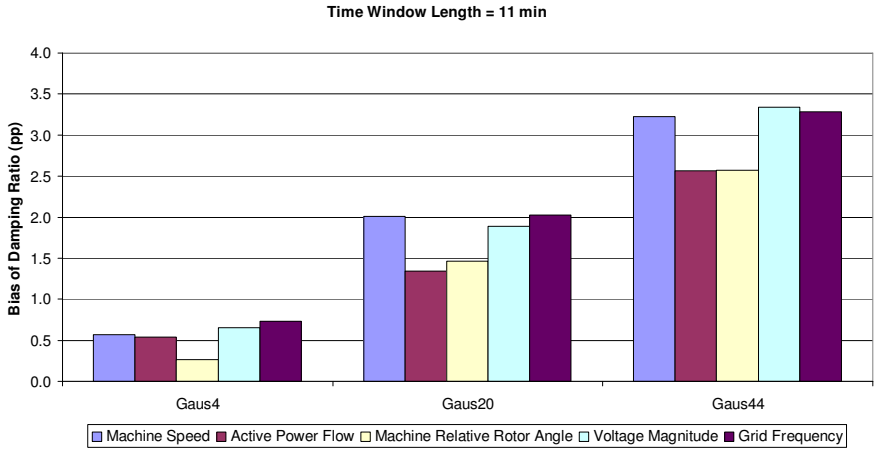

Figure 60. Damping estimate biases with different mode extraction wavelets and analyzed signals. The time window length is 11 minutes. pp = percentage point.

5.1.3 Case 2: Effect of Measurement Noise on the Estimates of Damping and Frequency

Frequency Estimation Results with Measurement Noise

The mean values and standard deviations of the frequency estimates are presented in Figure 61 and Figure 62, respectively, with different SNRs and for different time window lengths. The errorbars show the standard deviations of the estimates in Figure 61.

The SNR has very little effect on the mean values and standard deviations of the frequency estimates. However, with the shortest time window (1 min) the poorest SNR (0.1) produces a slightly different mean value (Figure 61) and a higher standard deviation (Figure 62) for the frequency estimate.

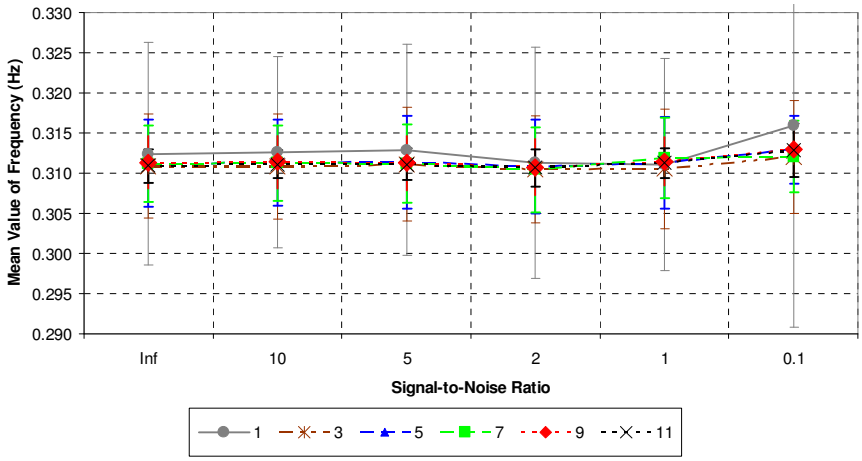

Figure 61. Mean values of the frequency estimates with different signal-to-noise ratios of the analyzed signal and with different time window lengths. The legend value shows the time window length in minutes. The errorbars show the standard deviation of the estimates. The analyzed signal is the grid frequency measurement at a bus in Southern Finland. The frequency estimation wavelet is the Cmor1-1.5.

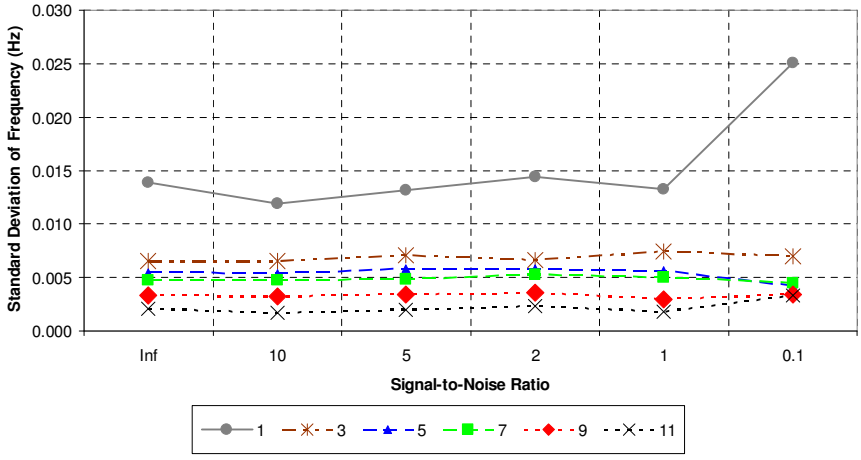

Figure 62. Standard deviations of the frequency estimates with different signal-to-noise ratios of the analyzed signal and with different time window lengths. The legend value shows the time window length in minutes. The analyzed signal is the grid frequency measurement at a bus in Southern Finland. The frequency estimation wavelet is the Cmor1-1.5.

Damping Estimation Results with Measurement Noise

Mean Values of the Damping Estimates

The mean values of the damping estimates with different SNRs and time window lengths for the Gaus4, Gaus20, and Gaus44 mode extraction wavelets are presented in Figure 63, Figure 64, and Figure 65, respectively.

The noise has some effect on the damping estimate mean values, and biases (Appendix E), in the case of the short mode extraction wavelet (Gaus4). The effect of noise is minimized when the longer mode extraction wavelets (Gaus20 and Gaus44) and long time windows (≥ 3 min) are used. The longer wavelets' ability to extract the actual mode from the noisy signal is better than the shorter ones', and the long time window minimizes the random effects caused by the noise although this is evident here only when the time window length increases from one minute to longer.

When the realistic SNRs (≥ 5) and long time windows (≥ 3 min) are considered, the damping estimate mean values and biases are not much affected by the noise. This is the case for all the mode extraction wavelets. However, the effect of noise is even smaller when the longer mode extraction wavelets are used.

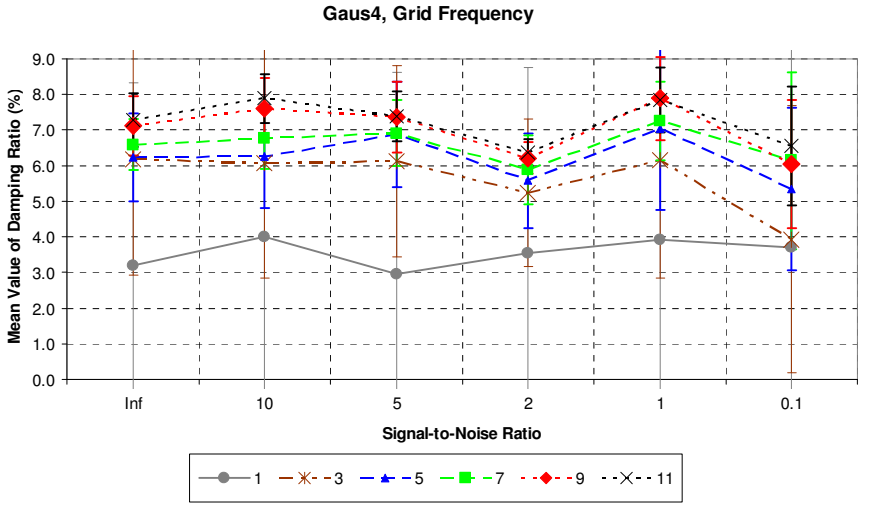

Figure 63. Mean values of the damping estimates with different signal-to-noise ratios of the analyzed signal and with different time window lengths. The legend value shows the time window length in minutes. The errorbars show the standard deviation of the estimates. The mode extraction wavelet is the Gaus4. The analyzed signal is the grid frequency measurement at a bus in Southern Finland.

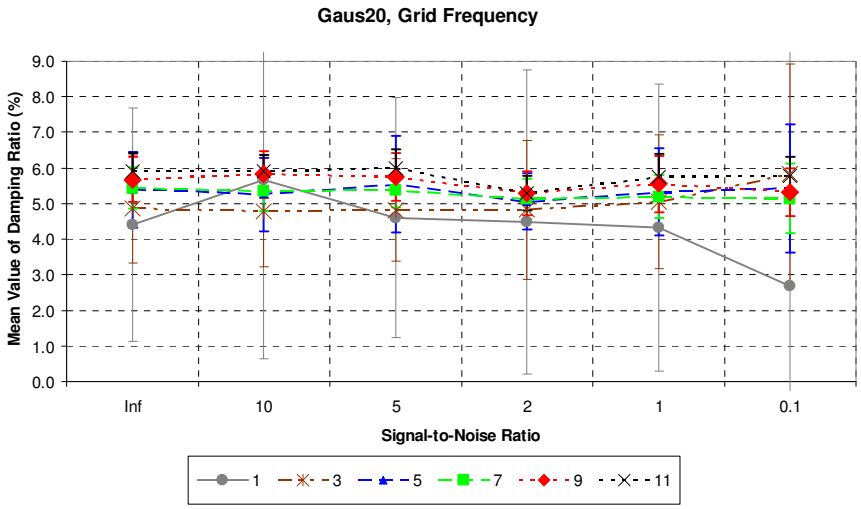

Figure 64. Mean values of the damping estimates with different signal-to-noise ratios of the analyzed signal and with different time window lengths. The legend value shows the time window length in minutes. The errorbars show the standard deviation of the estimates. The mode extraction wavelet is the Gaus20. The analyzed signal is the grid frequency measurement at a bus in Southern Finland.

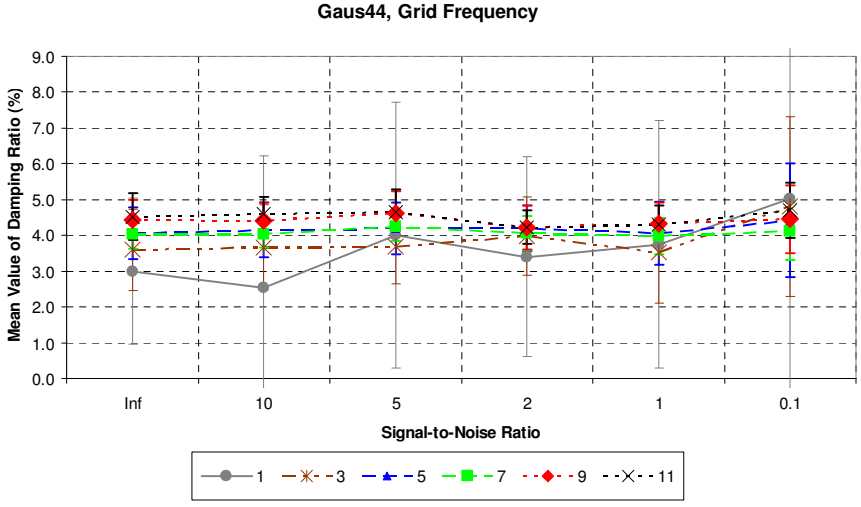

Figure 65. Mean values of the damping estimates with different signal-to-noise ratios of the analyzed signal and with different time window lengths. The legend value shows the time window length in minutes. The errorbars show the standard deviation of the estimates. The mode extraction wavelet is the Gaus44. The analyzed signal is the grid frequency measurement at a bus in Southern Finland.

Standard Deviations of the Damping Estimates

The standard deviations of the damping estimates with different SNRs and time window lengths for the Gaus4, Gaus20, and Gaus44 mode extraction wavelets are presented in Figure 66, Figure 67, and Figure 68, respectively.

The noise has quite little effect on the damping estimate standard deviations. The standard deviations tend to increase slightly with poorer SNRs, especially with shorter time windows. The effect of noise is the greatest for the shortest mode extraction wavelet (Gaus4) and it is minimized when the longer mode extraction wavelets (Gaus20 and Gaus44) are used.

When the realistic SNRs (≥ 5) and long time windows (≥ 3 min) are considered, the damping estimate standard deviations are not much affected by the noise. This is valid for all the studied mode extraction wavelets. However, the effect of noise is even smaller for the longest mode extraction wavelets.

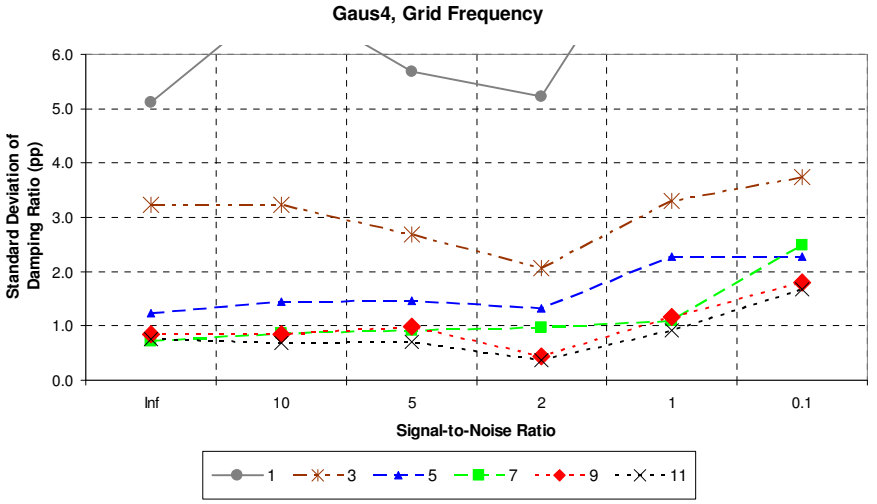

Figure 66. Standard deviations of the damping estimates with different signal-to-noise ratios of the analyzed signal and with different time window lengths. The legend value shows the time window length in minutes. The mode extraction wavelet is the Gaus4. The analyzed signal is the grid frequency measurement at a bus in Southern Finland.

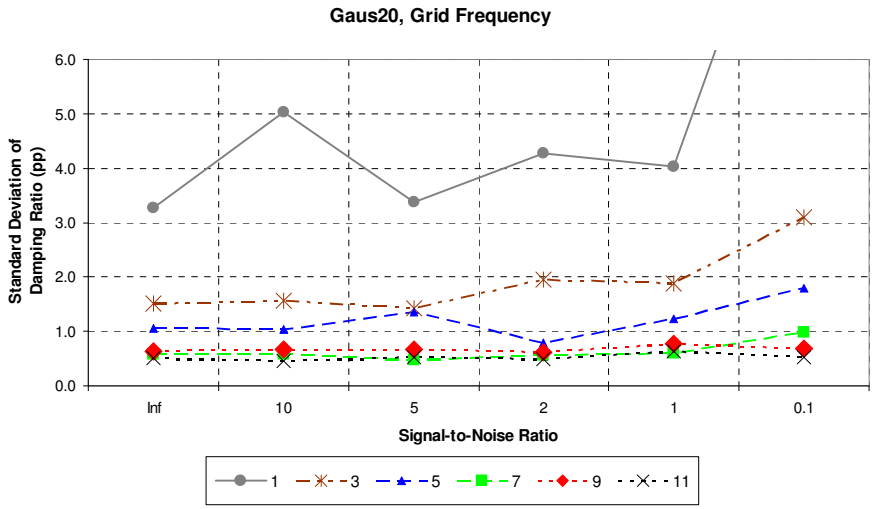

Figure 67. Standard deviations of the damping estimates with different signal-to-noise ratios of the analyzed signal and with different time window lengths. The legend value shows the time window length in minutes. The mode extraction wavelet is the Gaus20. The analyzed signal is the grid frequency measurement at a bus in Southern Finland.

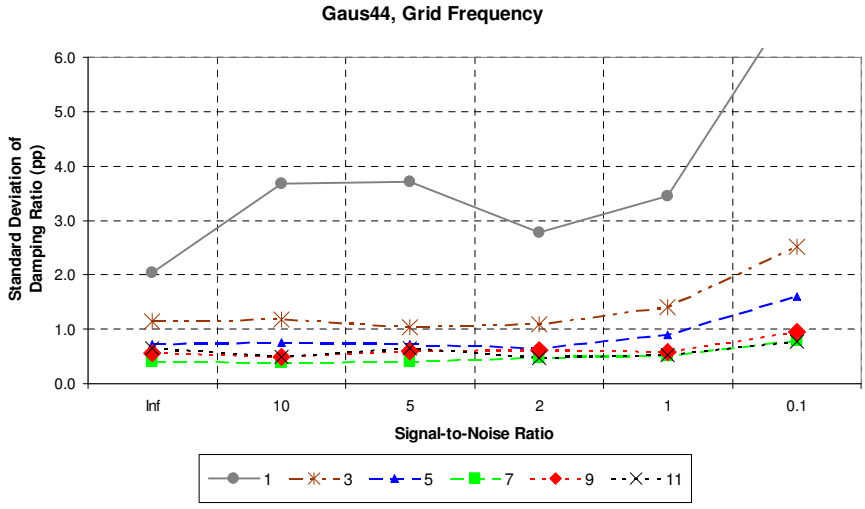

Figure 68. Standard deviations of the damping estimates with different signal-to-noise ratios of the analyzed signal and with different time window lengths. The legend value shows the time window length in minutes. The mode extraction wavelet is the Gaus44. The analyzed signal is the grid frequency measurement at a bus in Southern Finland.

5.1.4 Case 3: Effect of Two Different Parameter Sets of the Method on the Damping Estimates

Mean Values of the Damping Estimates

The mean values of the damping estimates with different time window lengths and the two sets of parameters are presented in Figure 69, Figure 70, and Figure 71 for the mode extraction wavelets Gaus4, Gaus20, and Gaus44, respectively. The errorbars of the figures show the standard deviations of the estimates.

The mean values of the damping estimates are about 1 % higher, and the biases are smaller (Appendix F), for the parameter set in which the damping is estimated from the approximate impulse response using the shorter (Cmor1-1) wavelet and the damping is selected from the midpoint of the approximate impulse response. The difference is slightly lower when a longer mode extraction wavelet (Gaus20 or Gaus44) is used. Then, the estimated damping is lower, too. The difference in the results is evident although the error bounds of the damping estimates overlap.

An exception is encountered with the time window length of 1 minute. With this short time window, the mean values of the damping estimates are higher (in case of the Gaus4 and the Gaus44 mode extraction wavelets), when the original set of parameters is used. When the time window is short, the number of samples averaged in the RDT is low. Then, the beginning of the approximate impulse response is closer to the real impulse response than the end of it because the random components affect more at the end of the approximate impulse response where the amplitude is lower. More weight is put on the beginning of the approximate impulse response when the damping is selected to be the one in which the rightmost wavelet is in the middle of the impulse response curve. Therefore, higher damping estimates are achieved for the short time window with the original set of parameters. The difference in the estimates increases with the time window length because the approximate impulse response approaches the shape of the real impulse response when the number of samples in the RDT's averaging process increases.

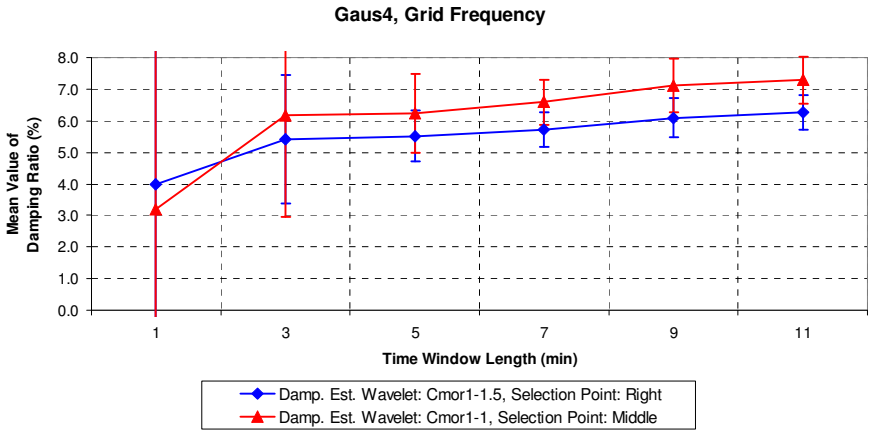

Figure 69. Mean values of the damping estimates with different time window lengths and parameter sets of the damping estimation method. The mode extraction wavelet is the Gaus4. The errorbars show the standard deviation of the estimates. The analyzed signal is the grid frequency measurement at a bus in Southern Finland.

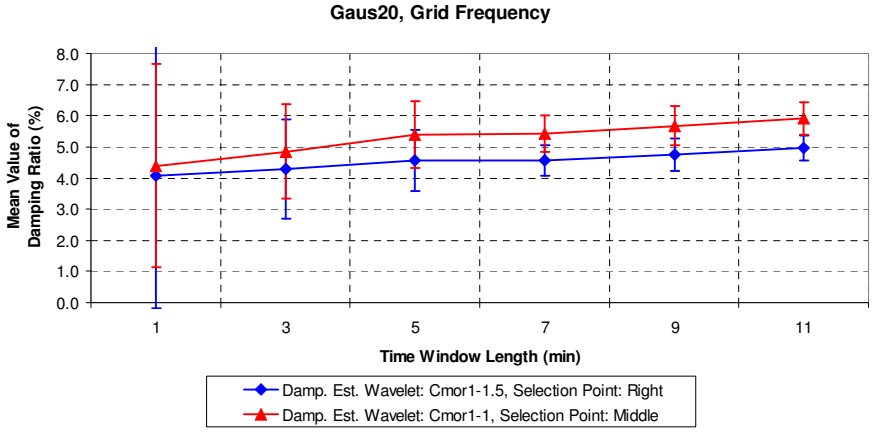

Figure 70. Mean values of the damping estimates with different time window lengths and parameter sets of the damping estimation method. The mode extraction wavelet is the Gaus20. The errorbars show the standard deviation of the estimates. The analyzed signal is the grid frequency measurement at a bus in Southern Finland.

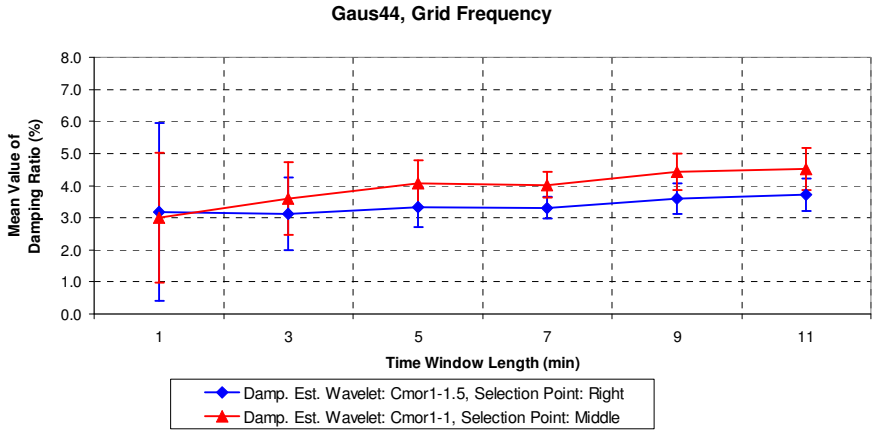

Figure 71. Mean values of the damping estimates with different time window lengths and parameter sets of the damping estimation method. The mode extraction wavelet is the Gaus44. The errorbars show the standard deviation of the estimates. The analyzed signal is the grid frequency measurement at a bus in Southern Finland.

Standard Deviations of the Damping Estimates

The damping estimate standard deviations with different time window lengths and the two sets of parameters are presented in Figure 72, Figure 73, and Figure 74 for the mode extraction wavelets Gaus4, Gaus20, and Gaus44, respectively.

When longer time windows are considered ($\geq$ 5 min), the standard deviations are slightly higher for the parameter set in which the damping is estimated from the approximate impulse response using the shorter (Cmor1-1) wavelet and the damping is selected from the midpoint of the impulse response. Generally, when the estimated damping is higher, its standard deviation is higher, too. However, when the longer mode extraction wavelets and the long time windows are considered, the differences in the standard deviations are negligible.

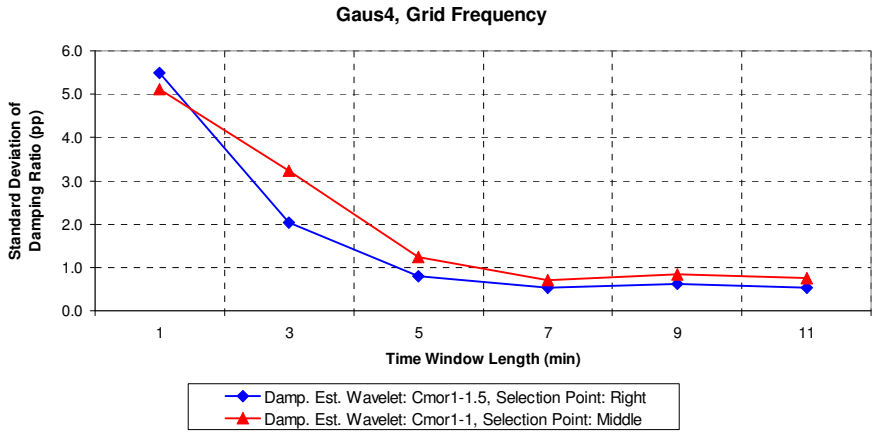

Figure 72. Standard deviations of the damping estimates with different time window lengths and parameter sets of the damping estimation method. The mode extraction wavelet is the Gaus4. The analyzed signal is the grid frequency measurement at a bus in Southern Finland.

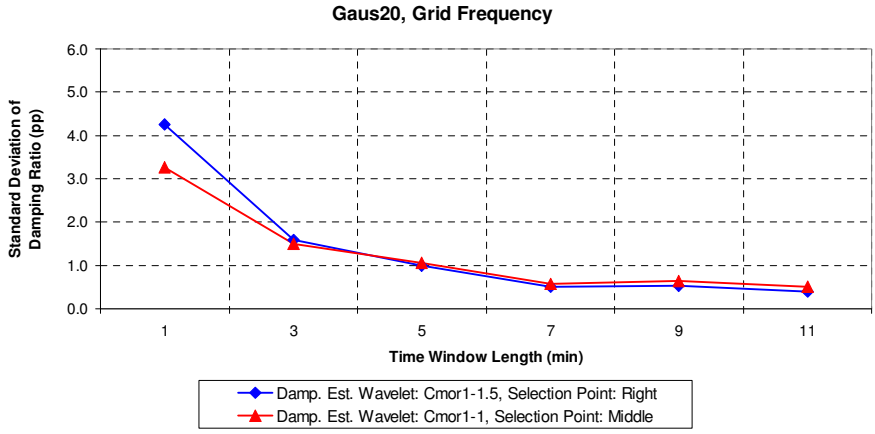

Figure 73. Standard deviations of the damping estimates with different time window lengths and parameter sets of the damping estimation method. The mode extraction wavelet is the Gaus20. The analyzed signal is the grid frequency measurement at a bus in Southern Finland.

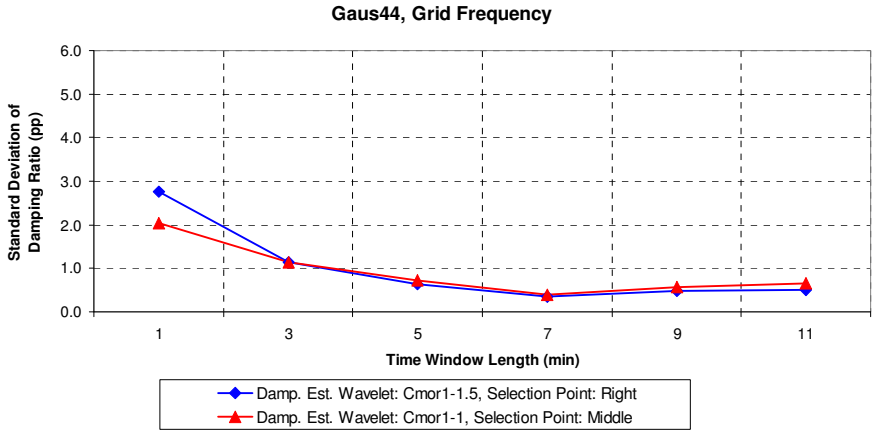

Figure 74. Standard deviations of the damping estimates with different time window lengths and parameter sets of the damping estimation method. The mode extraction wavelet is the Gaus44. The analyzed signal is the grid frequency measurement at a bus in Southern Finland.

5.1.5 Case 4: Effect of Different Damping Conditions of the Power System on the Damping Estimates

Mean Values of the Damping Estimates

The correspondence between the mean value of the damping estimate and the reference damping is presented for the Gaus4, Gaus20, and Gaus44 mode extraction wavelets in Figure 75, Figure 76, and Figure 77, respectively. With a low reference damping (below 4 %), the mean values are close to the reference damping ratio for all the mode extraction wavelets. However, when the reference damping increases, the damping estimates of the longer mode extraction wavelets (Gaus20 and Gaus44) become lower than the reference damping. The longer the mode extraction wavelet and the higher the reference damping, the greater the bias is. With the shortest, Gaus4, mode extraction wavelet, the estimates might be even slightly higher than the reference damping.

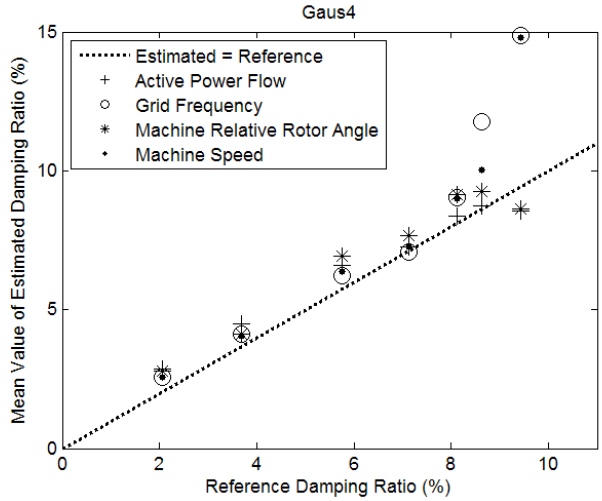

Figure 75. Estimated damping vs. reference damping with different simulated signals. The mode extraction wavelet is the Gaus4 and the time window length is 9 minutes. The dotted straight line corresponds to the ideal case that the estimated damping is equal to the reference damping.

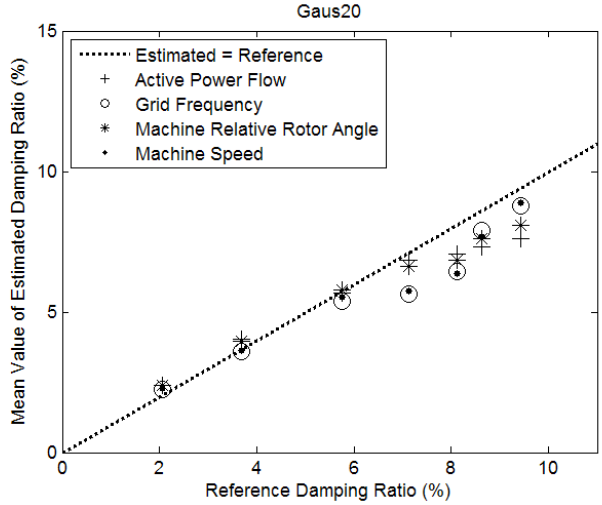

Figure 76. Estimated damping vs. reference damping with different simulated signals. The mode extraction wavelet is the Gaus20 and the time window length is 9 minutes. The dotted straight line corresponds to the ideal case that the estimated damping is equal to the reference damping.

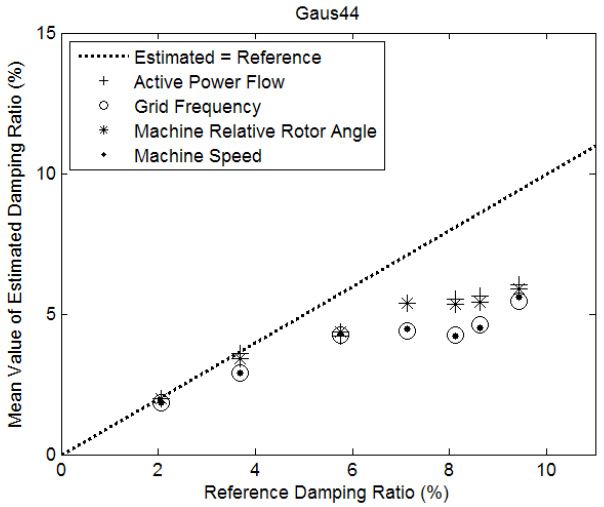

Figure 77. Estimated damping vs. reference damping with different simulated signals. The mode extraction wavelet is the Gaus44 and the time window length is 9 minutes. The dotted straight line corresponds to the ideal case that the estimated damping is equal to the reference damping.

Standard Deviations of the Damping Estimates

The correspondence between the standard deviation of the damping estimate and the reference damping is presented for the Gaus4, Gaus20, and Gaus44 mode extraction wavelets in Figure 78, Figure 79, and Figure 80, respectively. Generally, the standard deviations grow with the reference damping and usually the standard deviations are lower the longer the mode extraction wavelet is.

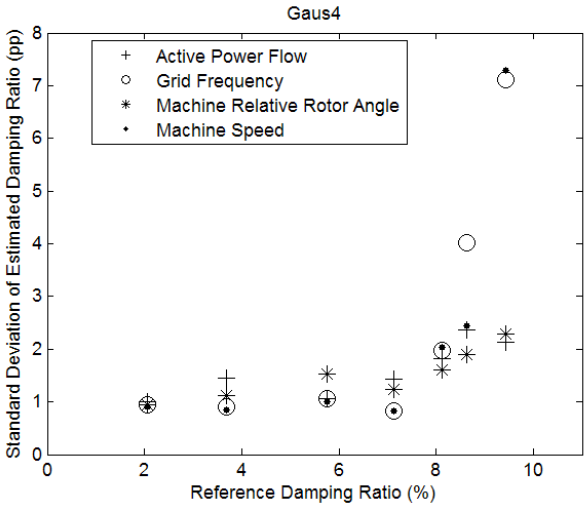

Figure 78. Damping estimate standard deviation vs. reference damping with different simulated signals. The mode extraction wavelet is the Gaus4 and the time window length is 9 minutes.

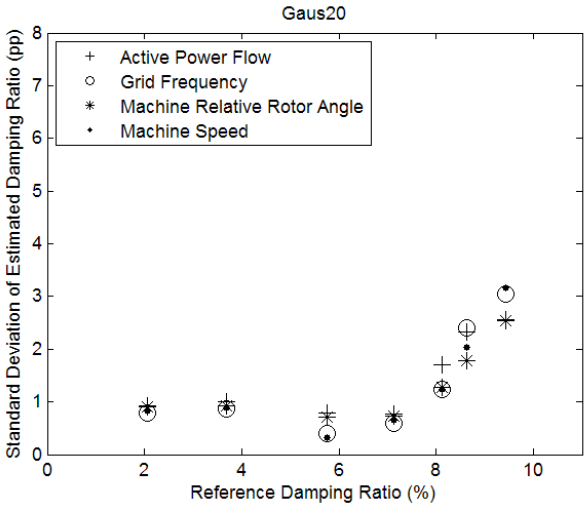

Figure 79. Damping estimate standard deviation vs. reference damping with different simulated signals. The mode extraction wavelet is the Gaus20 and the time window length is 9 minutes.

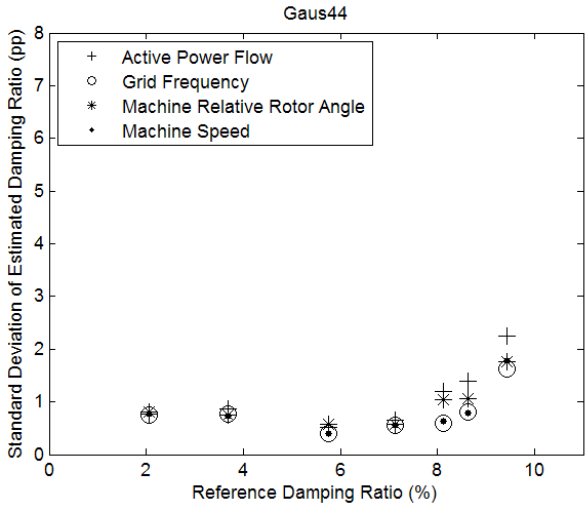

Figure 80. Damping estimate standard deviation vs. reference damping with different simulated signals. The mode extraction wavelet is the Gaus44 and the time window length is 9 minutes.

Comparison between the Mode Extraction Wavelets

The mean values of the damping estimates with the different reference damping ratios and mode extraction wavelets are presented in Figure 81. The mean values are consistently lower the longer the mode extraction wavelet is. With the Gaus20 wavelet the mean values are accurate until the damping ratio of about 7 % and with the Gaus44 wavelet until the damping ratio of about 4 %. The standard deviations, Figure 82, are generally lower the longer the mode extraction wavelet is.

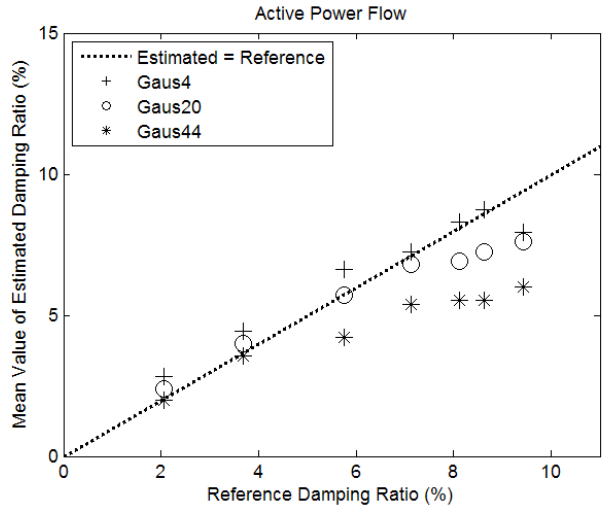

Figure 81. Estimated damping vs. reference damping with the Gaus4, Gaus20, and Gaus44 mode extraction wavelets. The analyzed signal is the active power flow of the Finland–Sweden interconnection line. The time window length is 9 minutes. The dotted straight line corresponds to the ideal case that the estimated damping is equal to the reference damping.

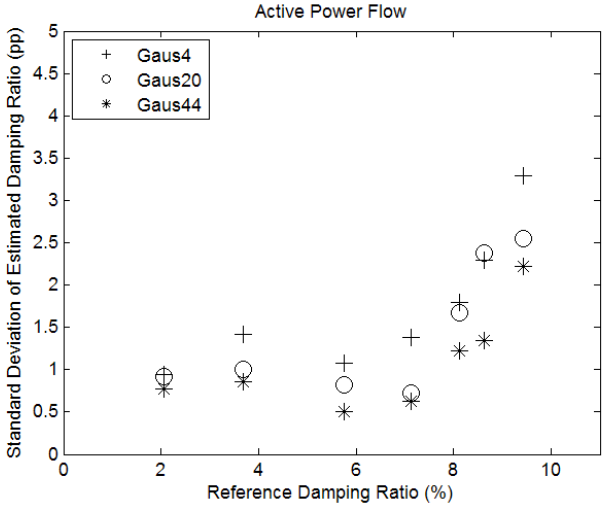

Figure 82. Damping estimate standard deviation vs. reference damping with the Gaus4, Gaus20, and Gaus44 mode extraction wavelets. The analyzed signal is the active power flow of the Finland–Sweden interconnection line. The time window length is 9 minutes.

5.2 Performance in Case of the Measured Grid Data

5.2.1 Time Evolution of the Damping Estimate and Damping vs. Frequency

Time evolution of the 0.3 Hz mode damping estimate is presented with the three mode extraction wavelets (Gaus4, Gaus20, and Gaus44) in Figure 83a. The damping vs. frequency is presented for the studied wavelets in Figure 83b. There is much more variation in the damping estimate when the shortest (Gaus4) wavelet is used as compared to the longer (Gaus20 and Gaus44) wavelets. On the other hand, the Gaus20 and Gaus44 wavelets produce about the same amount of variation in the damping estimates but the Gaus20 wavelet produces a much higher mean value of the damping estimate.

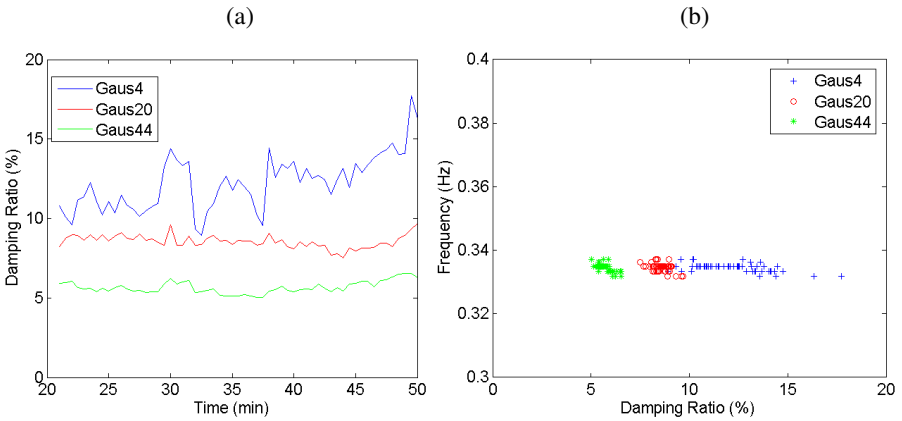

Figure 83. The time evolution of the damping estimate (a) and damping vs. frequency (b) with the Gaus4, Gaus20, and Gaus44 mode extraction wavelets. The measured signal is the active power of the interconnecting line between Finland and Sweden (Figure 44). The time window length is 21 minutes.

5.2.2 Performance of the Damping Estimation Method with Different Signals, Time Windows, and Mode Extraction Wavelets

Frequency Estimation Results

The mean values and standard deviations of the frequency estimates are presented in Figure 84 and Figure 85, respectively, with different time window lengths and measured signals.

The mean values of the frequency estimates are almost equal for different time window lengths although the mean values increase slightly from the shortest time windows compared to the longer ones. There are small differences between the mean values of the estimates when different signals are used. The difference is due to the slightly changing mean value of the voltage magnitude and active power flow signals. However, the difference in the frequency estimates is small, and negligible in practice.

The standard deviations of the frequency estimates decrease with the increased time window length. For the one minute time window, the frequency estimates have much higher standard deviations than for the longer time windows.

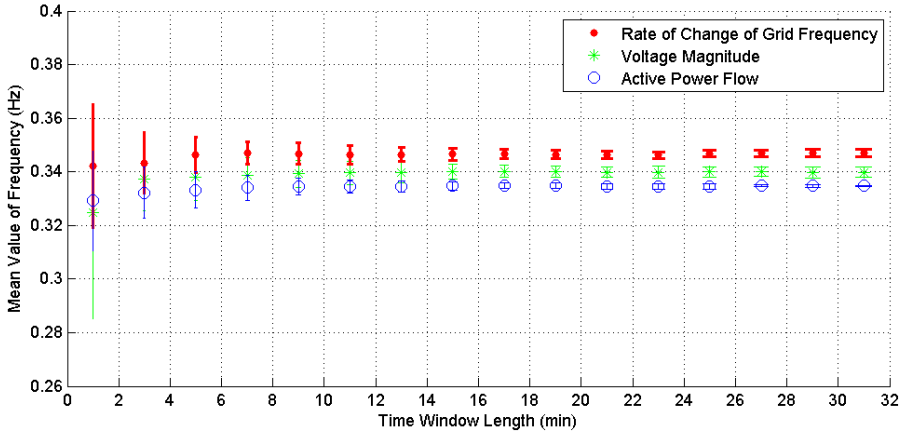

Figure 84. Mean values of the frequency estimates with different time window lengths and measured signals. The errorbars show the standard deviation of the estimates. The frequency estimation wavelet is the Cmor1-1.5.

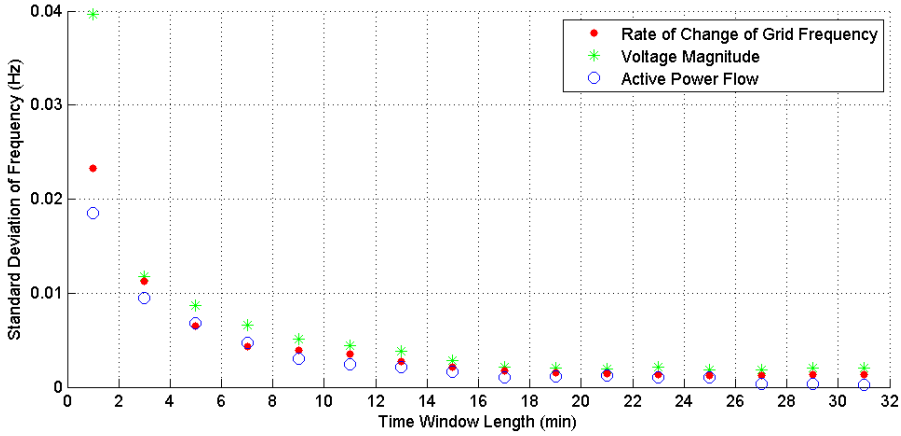

Figure 85. Standard deviations of the frequency estimates with different time window lengths and measured signals. The frequency estimation wavelet is the Cmor1-1.5.

Damping Estimation Results

Mean Values of the Damping Estimates

The mean values of the damping estimates with different time window lengths and measured signals are presented in Figure 86, Figure 87, and Figure 88 for the mode extraction wavelets Gaus4, Gaus20, and Gaus44, respectively. The errorbars of the figures show the standard deviations of the estimates.

The mean values of the damping estimates first increase with the increased time window length and then stabilize to a constant level. In case of the shortest mode extraction wavelet (Gaus4), a different damping estimate mean value is achieved from the voltage magnitude signal as compared to the other signals (Figure 86). The voltage magnitude signal has poorer observability and more other modes than the other measurements. However, the error bounds of the damping estimates overlap and account well for the difference in the estimates. When longer mode extraction wavelets (Gaus20 and Gaus44) are used, the difference in the damping estimates is minimal between the different signals (Figure 87 and Figure 88).

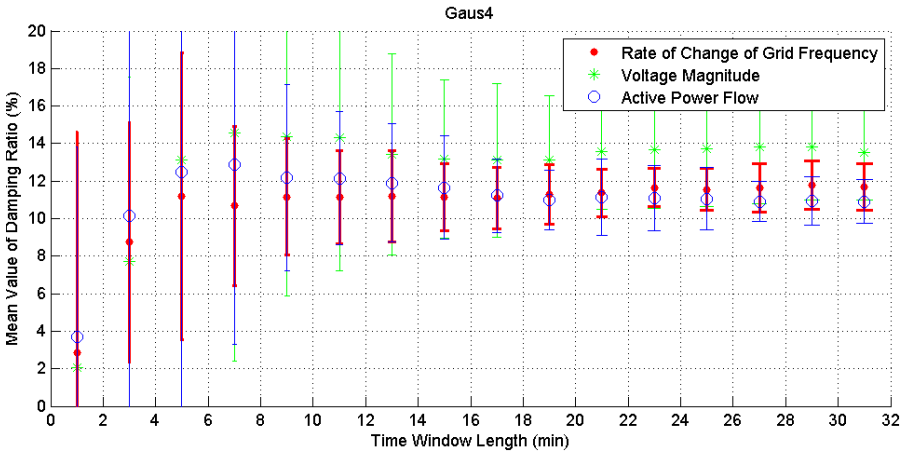

Figure 86. Mean values of the damping estimates with different time window lengths and measured signals. The mode extraction wavelet is the Gaus4. The errorbars show the standard deviation of the estimates.

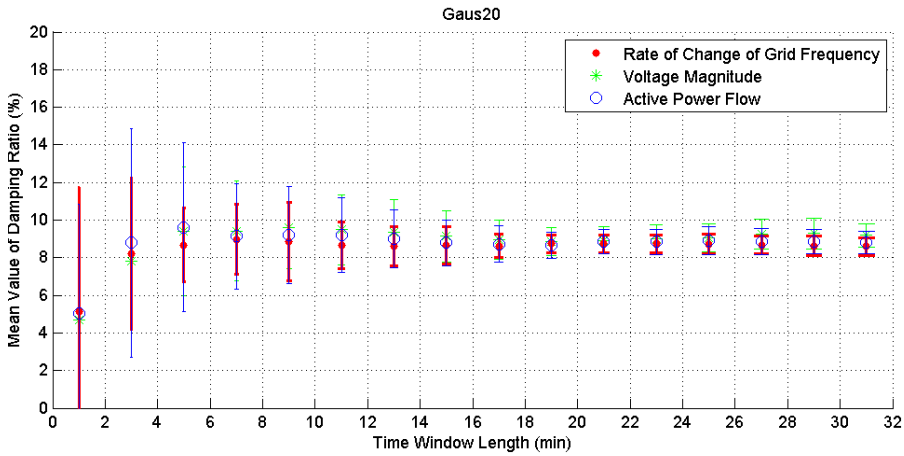

Figure 87. Mean values of the damping estimates with different time window lengths and measured signals. The mode extraction wavelet is the Gaus20. The errorbars show the standard deviation of the estimates.

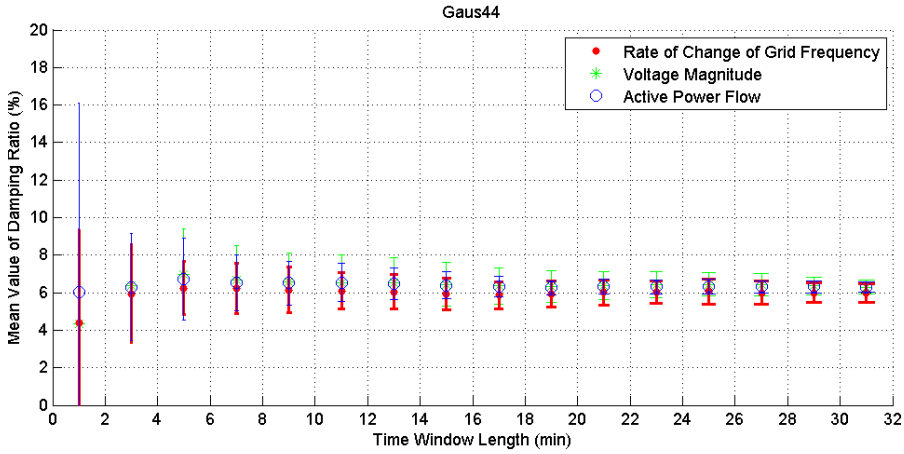

Figure 88. Mean values of the damping estimates with different time window lengths and measured signals. The mode extraction wavelet is the Gaus44. The errorbars show the standard deviation of the estimates.

Standard Deviations

The standard deviations of the damping estimates with different time window lengths and measured signals are presented in Figure 89, Figure 90, and Figure 91 for the mode extraction wavelets Gaus4, Gaus20, and Gaus44, respectively.

The standard deviations decrease with the increased time window length until a certain time window length (about 20 min). Different signals give slightly different standard deviations for the damping estimates. Generally, the voltage magnitude signal is the

poorest, and the other studied signals give better results. The voltage magnitude signal has poorer observability and more other modes than the other measurements. However, the difference between the signals decreases with the increased time window length when all the standard deviations decrease. When longer mode extraction wavelets (Gaus20 and Gaus44) are used, the difference in the standard deviations is small between the different signals (Figure 90 and Figure 91).

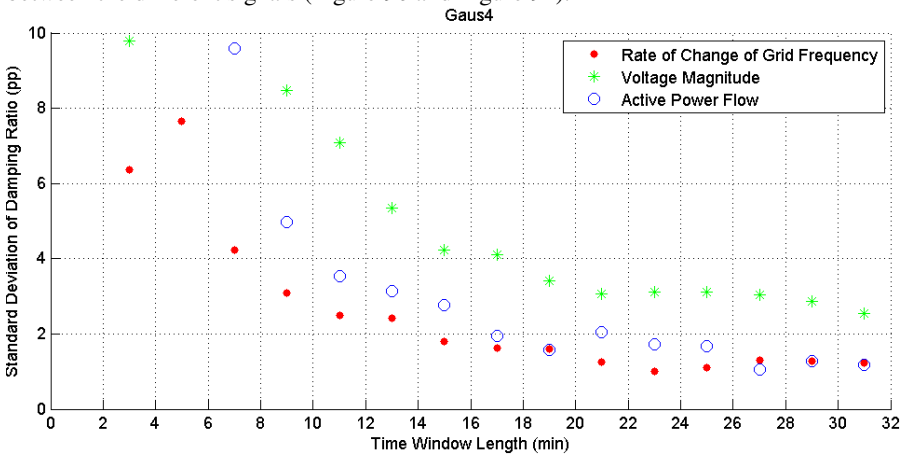

Figure 89. Standard deviations of the damping estimates with different time window lengths and measured signals. The mode extraction wavelet is the Gaus4.

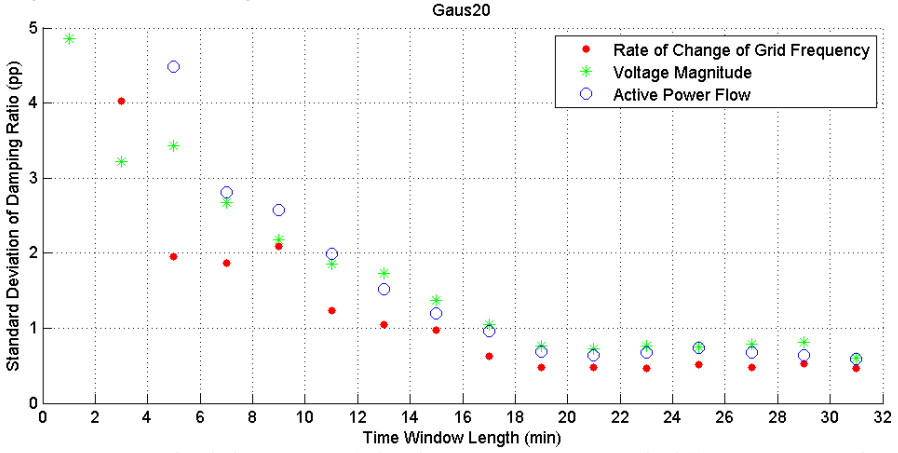

Figure 90. Standard deviations of the damping estimates with different time window lengths and measured signals. The mode extraction wavelet is the Gaus20.

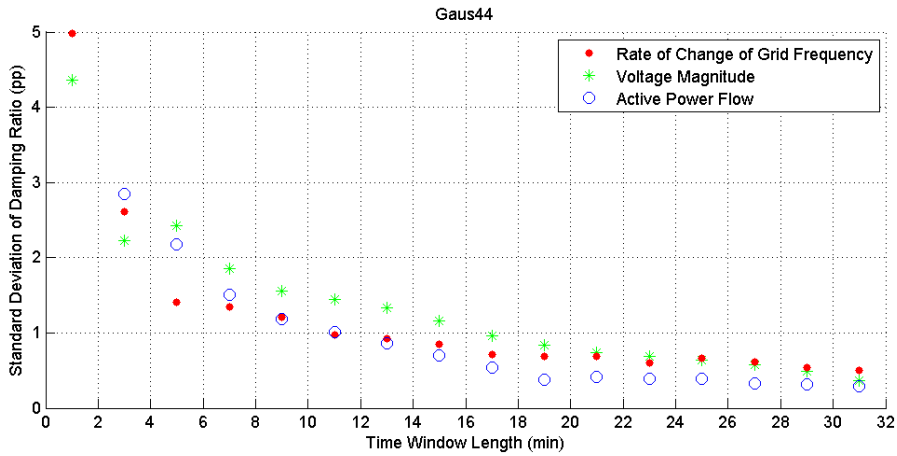

Figure 91. Standard deviations of the damping estimates with different time window lengths and measured signals. The mode extraction wavelet is the Gaus44.

Comparison between the Mode Extraction Wavelets

Damping estimate mean values and standard deviations in the case of different mode extraction wavelets are compared in Figure 92 and Figure 93, respectively. The mean values are consistently lower the longer the mode extraction wavelet is, except with the shortest time window (1 min). The longer wavelets smooth the sharp variations of the signal and cause the approximate impulse response to decay more slowly, and therefore the estimated damping is lower. The mean values stabilize roughly to constant levels when the time window length is about 5 minutes.

The standard deviations are higher for the shortest Gaus4 mode extraction wavelet and roughly the same for the longer Gaus20 and Gaus44 mode extraction wavelets. The effect of mode extraction wavelet length on the damping estimate standard deviations decreases with the increased time window length.

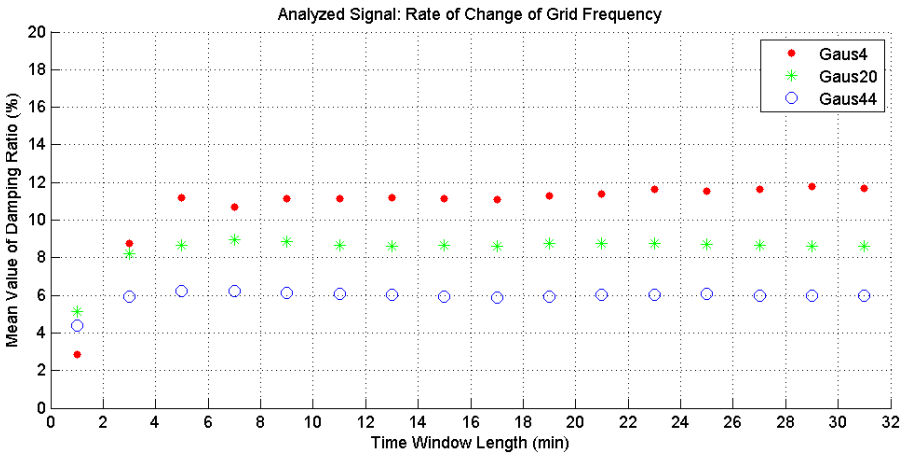

Figure 92. Mean values of the damping estimates with different time windows and mode extraction wavelets (Gaus4, Gaus20, and Gaus44). The measured signal is the rate of change of grid frequency at a bus in Southern Finland.

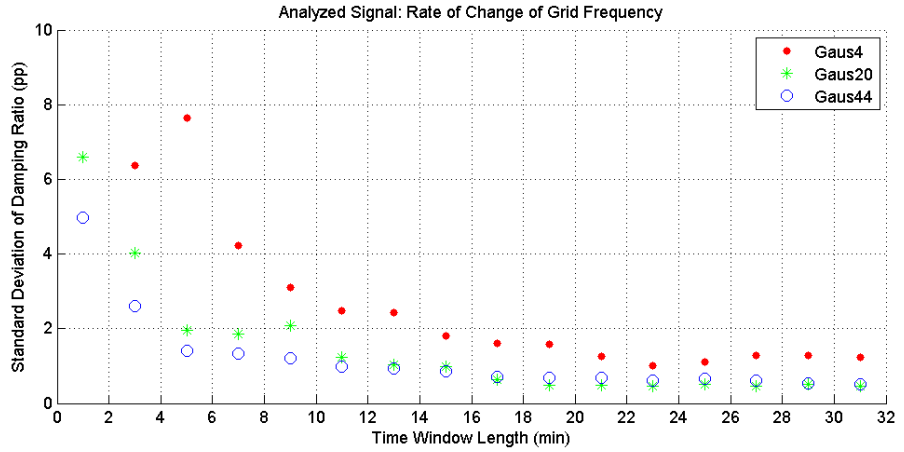

Figure 93. Standard deviations of the damping estimates with different time windows and mode extraction wavelets (Gaus4, Gaus20, and Gaus44). The measured signal is the rate of change of grid frequency at a bus in Southern Finland.

5.2.3 Detection of Change in Damping

Detection of Degraded Damping

The growth in the oscillation amplitude of the SVC's voltage magnitude indicates the periods when the POD was operating; Figure 94b. The period when the POD was operated *without* a dead band is clearly observable both in the amplitude of the oscillation and in the estimated damping curve, see Figure 94 and the segment indicated

with number 6. Due to an incorrect parameter set for the SVC POD, the observed damping is clearly lower than the damping would be otherwise. The damping estimates from all signals stabilize when the damping gets poorer indicating that the damping estimates are more reliable then.

The periods when the POD was operated *with* the dead band are not so evident but still observable. Such periods are, for instance, the segments indicated by the numbers 7 and 9 in Figure 94. The observed damping is significantly lower during periods when the POD is operated with the dead band, although the increase in the amplitude is much lower, and therefore it does react only occasionally to the oscillations of the grid.

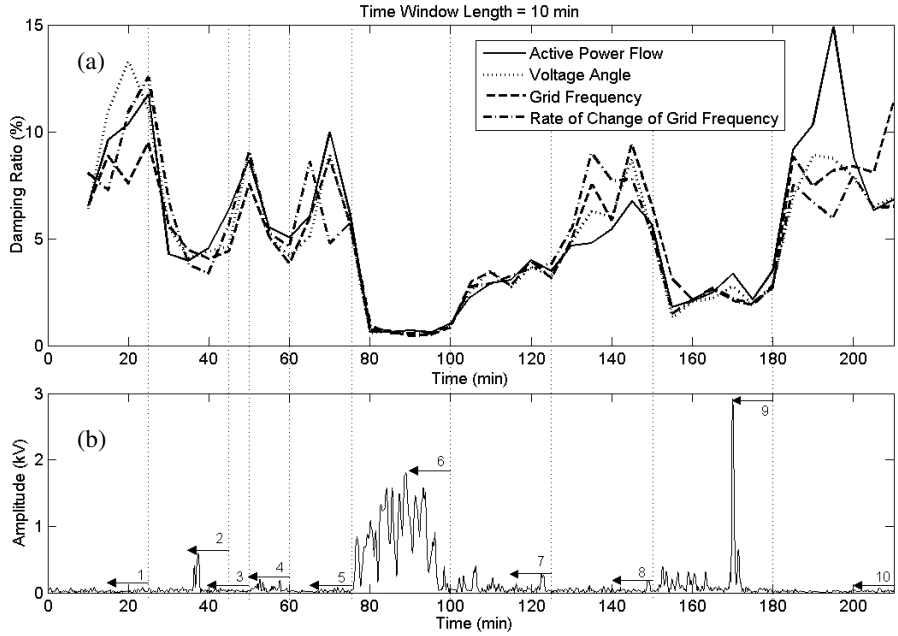

Figure 94. Damping vs. time (a) and amplitude vs. time (b) of the 0.3 Hz mode during the SVC test measurement period in which the parameter set of the POD was incorrect. The numbered segments indicate time periods of different oscillation amplitude and the length of the arrows indicates the length of the time window of the damping estimation method.

Detection of Improved Damping

In Figure 95, the vertical lines indicate when the POD was turned on and off. A slight improvement in the damping ratio can be observed when the POD is turned on and a slight degradation can be observed when the POD is turned off (Figure 95a).

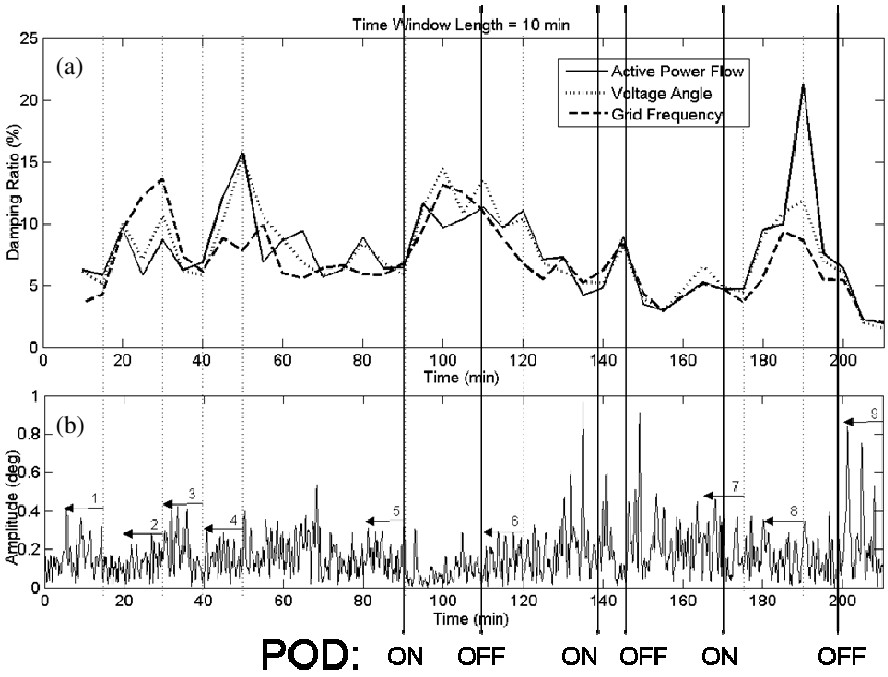

Figure 95. Damping vs. time (a) and amplitude vs. time (b) of the 0.3 Hz mode during the SVC test measurement period in which the parameter set of the POD was correct. The vertical lines show when the SVC POD was turned on and off. The numbered segments indicate time periods of different oscillation amplitude and the length of the arrows indicates the length of the time window of the damping estimation method.

6 Discussion

6.1 General Issues

Electromechanical oscillation damping must always be high enough in order to guarantee the stable and secure operation of the power system. Conventionally, the stability of the power system has been managed by extensive simulation studies. However, measurement-based damping estimation methods have advantages compared to the simulations. The estimation does not rely on the power system simulation model, which does not necessarily reflect the behavior of the real power system perfectly. In addition, the damping estimates are based on the up-to-date operating condition, when the damping estimation is applied to real-time data. Because of the advantages of the measurement-based damping estimation, a new damping estimation method is developed in this thesis. In developing the method, the main emphasis is on the damping estimation of the Nordic power system 0.3 Hz inter-area mode that limits the power transfer capacity from Finland to Sweden. However, the performance characteristics and applicability of the method is discussed also at the general level and the estimation error sources are identified.

6.2 Performance of the Method

The performance analyses in this thesis are conducted by studying the damping estimation results achieved for simulated and measured data of the Nordic power system. The most accurate damping estimates are achieved when maximal information of the oscillations is available; i.e. when all the following conditions are fulfilled. These conditions are that the signal has good observability of the mode of interest, poor observability or no other modes, the damping ratio of the mode of interest is low and a long time window is used. When the damping ratio is low, the oscillations decay slowly and a long mode extraction wavelet with good frequency resolution can be used because the time resolution of the wavelet is not an issue. In this case the effect of other modes (if they exist) and measurement noise is minimized and the analysis is concentrated on the mode of interest. When selecting the mode extraction wavelet function for the Nordic power system (Section 3.2.3), it is assumed that there are two inter-area modes (0.3 Hz and 0.5 Hz) present in the system. In this case, for example, the Gaus20 wavelet function provides good enough frequency resolution to separate the modes at 0.3 Hz and 0.5 Hz from each other. The time resolution of the Gaus20 wavelet function is well enough for estimating damping ratios accurately until about 7 % (Figure 81). However, if there are modes closer to each other than the 0.3 Hz and 0.5 Hz, then a longer mode extraction wavelet (e.g. Gaus44) with better frequency resolution is needed. Then, the time resolution is lower, and the damping estimation method can only be used to estimate accurately lower damping ratios (e.g. about 4 % in case of the Gaus44 wavelet, Figure 81). On the other hand, if there is only one inter-area mode present in the system, then a shorter wavelet than the Gaus20 can be used and higher damping ratios can be estimated accurately. In this case the wavelet function only needs to separate the mode

well enough from the measurement noise. The effect of modal observability affects the damping estimation results in such a way that the voltage magnitude signal usually gives poorer results than the other signals, because the voltage magnitude is affected by local phenomena (e.g. reactive loads and voltage controls of the grid) more than other, global signals, like voltage angle differences between the oscillating areas. Finally, using a long time window makes the random decrement technique collect enough samples and the estimation of the impulse response, and therefore damping, is good.

It is important to be able to estimate the poor damping accurately because then the damping is more critical to the system stability. However, using long time windows brings a delay and causes the estimates to become less real-time, i.e. the estimates react more slowly to the changes in the real damping. If the damping estimation is applied in real-time damping monitoring, this is evidently a drawback. However, when the damping ratio gets lower, the amplitude of the ambient oscillations increases and the estimates react faster to the changed damping than the time window length indicates. The faster reaction is because the threshold condition of the random decrement technique is crossed more often in that part of the signal where the damping is poorer. When the damping ratio increases, the estimates react slower to the change in damping, compared to the case when the damping ratio decreases. It is a beneficial property of the method that the decreased damping (power system less stable) is estimated faster than the increased damping. A limit for the longest possible time window length is set by the time period during which the power system operating condition, and therefore the real damping of the mode, remains nearly constant. This time period is not constant though. However, usually accurate enough damping estimates are achieved with a considerably shorter time window than the time interval between substantial changes in the power system operating condition. After a substantial transition in the power system operating condition, it takes some time before the damping estimates are adapted to the new damping level. Further research is needed to determine how fast the damping estimates react to change in damping in different situations.

Damping estimation is useful even though the damping would be good; for example in verification of the simulation model and in verifying the correct operation of the damping controllers of the grid. Therefore, the very long mode extraction wavelets (e.g. Gaus44) are not applicable because they have too poor time resolution when the oscillations damp out quickly. The poor time resolution causes errors (a large bias) for the damping estimates. When shorter mode extraction wavelets (e.g. Gaus20 or Gaus4) are used, higher damping ratios can be estimated accurately assuming that the frequency resolution of the wavelets is high enough. When high enough frequency resolution is guaranteed by the user, the damping estimation method gives either accurate or conservative estimates; i.e. the estimates are lower than the real damping. This characteristic is beneficial because then the estimates do not lead to reduced system security.

Frequency estimates, received with the method, are more accurate (percentual error smaller) than the damping estimates. This characteristic is of a fundamental nature because the frequency of the oscillation is related to the time instants of the peaks or zero crossings of the signal while the damping is related to the temporal changes in the amplitude of the signal. Observing the temporal amplitude is harder than observing the time instants of the peaks or zero crossings, and the amplitude is more affected by the

random effects due to random load variations. Therefore, the frequency estimates are naturally of better quality than the damping estimates.

6.3 Variance of the Damping Estimates

When analyzing the electromechanical oscillation mode damping using the measured grid data, the estimates always have some variance. Part of the variance comes from the changes that happen in the power system (changes in loads, production, power flows and grid configuration) and affect the real damping. From the grid operator's point of view, it is interesting how damping changes during the operation.

However, the main part of the damping estimates' variance comes from the methods' inability to correctly estimate the mode damping. This is an undesirable property and it is inherent to the damping estimation method. When considering the causes of the variance of the estimation method, the power system is assumed to remain in the same operating point: load, production, power flows, and grid configuration the same, and therefore the damping is the same. In assessing the possible causes of the variance, general representation of the damping estimation procedure (Figure 96) is used. The possible causes of variance in the damping estimates are changes in the excitation (e), changes in the measurement noise (d) and changes in the damping estimation method.

The measurement noise has very little effect on the damping estimate variances especially when longer mode extraction wavelets (e.g. Gaus20 or Gaus44) are used (Figure 67 and Figure 68, respectively), and the noise causes only a fraction of the damping estimation variance. The damping estimation method does not have any variable parameters, so the changes in the damping estimation method do not cause variance in the damping estimates. The method produces always the same damping estimate for the same input data.

Therefore, most of the damping estimates' variance is due to the changing properties of the excitation and the interaction between the excitation and the power system. During ambient operation, oscillations are excited mainly by constantly varying loads in the grid and the assumption is that the excitation is random Gaussian noise. The random load variations can be considered approximately Gaussian distributed based on the central limit theorem (Cam 1986) because the number of loads in a power system is large, fulfilling the conditions of the theorem. The central limit theorem states that the sum of independent and identically distributed random variables with finite mean and variance approaches the normal distribution (Gaussian distribution) when the number of random variables increases, irrespective of the distribution of the random variables. Although the Gaussianity assumption can be considered valid, the damping estimation accuracy generally improves (the variance decreases) when the time window of the method extends (Figure 51, Figure 52, Figure 53, Figure 66, Figure 67, Figure 68, Figure 72, Figure 73, Figure 74, Figure 89, Figure 90, and Figure 91). The information of the oscillations increases with the extended time window. When random Gaussian noise is assumed, the extended time window reduces the effect of random departures from this assumption. Also the possible nonlinear behavior of the power system can cause variance in the damping estimates because linear behavior is assumed.

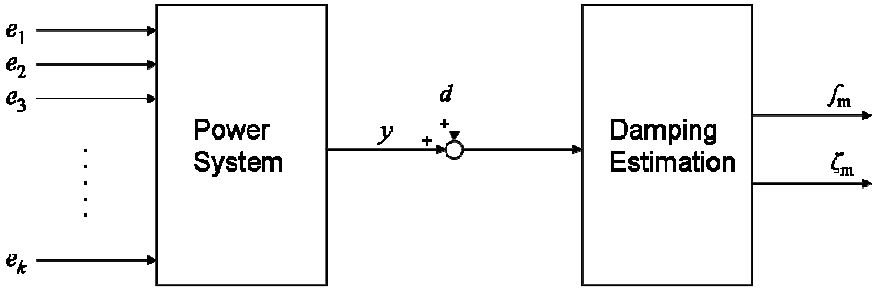

Figure 96. General representation of the damping estimation procedure, where e_1, e_2, e_3, … e_k are the excitations of the oscillations, y is the output signal of the power system, d is the measurement noise, ζ_m is the estimated mode damping ratio, and f_m is the estimated mode frequency.

Another general characteristic of the damping estimates' variance is that it increases when the damping ratio of the mode increases (Figure 78, Figure 79, and Figure 80). When the mode damping increases, the oscillations vanish faster from the signals and their damping is therefore harder to estimate. (Turunen et al. 2008) However, it is beneficial that the poor damping can be estimated reliably because the information of the mode damping is more important for a TSO when the mode damping is low. This is evident from Figure 97 where the dependence of the 0.3 Hz mode damping and the standard deviation of the damping estimate are presented as a function of the Finland–Sweden active power flow. The damping estimates are more accurate when the power transfer is large (and close to the transfer limit) and the damping is low; or when the correct damping information is more important for the system stability.

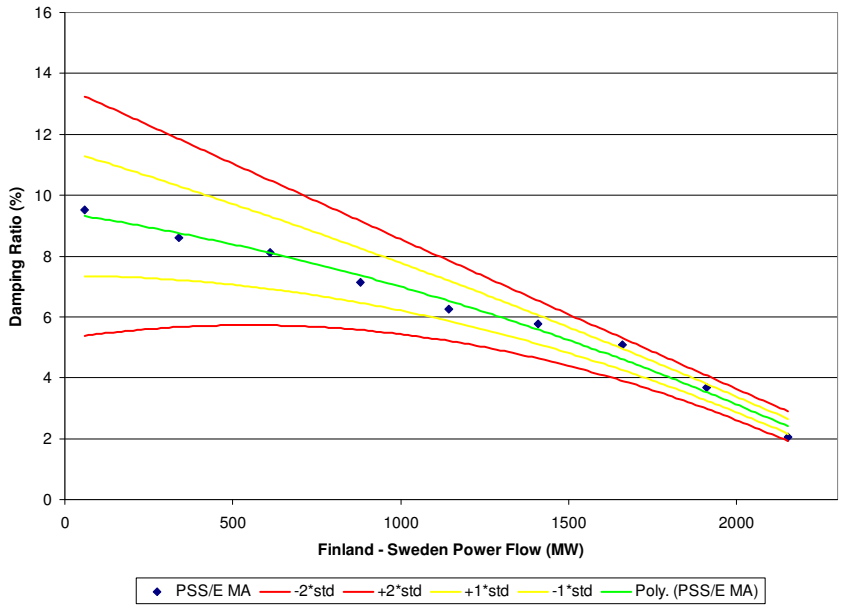

Figure 97. Damping ratio of the 0.3 Hz mode small-signal oscillations as a function of Finland–Sweden power flow according to the time domain (PSS®E) simulations (blue dots). Polynomial trendlines show the dependence between the power flow and damping ratio (green line), the power flow and the ± one standard deviation error bounds of the damping estimates (yellow lines), and the power flow and the ± two standard deviation error bounds of the damping estimates (red lines). The figure is schematic and is based on the results of using about 10 minutes time window in the damping estimation.

6.4 Applicability and Limitations

The emphasis of the thesis is on the Nordic power system 0.3 Hz mode damping estimation. However, the method can be applied to any other oscillation mode and power system too if there are no other modes too close to the mode of interest. The frequency band of the method needs to be adjusted to include the mode of interest and a signal with good observability of the mode of interest needs to be selected. When these conditions are fulfilled, the method analyses other modes similarly to the 0.3 Hz mode in this thesis, and the characteristics of the results for the other modes would be similar to those achieved in this thesis for the 0.3 Hz mode. This is because the method is based on using the wavelet transform in the frequency estimation, mode extraction, and mode damping estimation (Figure 14). The wavelet transform analyses different frequency components of a signal by stretching and compressing the same mother wavelet function and therefore the characteristics of the method are similar for different modes. The characteristics of the random decrement technique are not dependent on the mode frequency either.

However, the method of this thesis is not applicable if there is another dominant mode too close to the mode of interest. In this case the wavelet function used in the mode extraction has too low frequency resolution to separate the modes from each other. For example, the Gaus20 wavelet function has good enough frequency resolution to separate the modes at 0.3 Hz and 0.5 Hz well enough from each other and it has good enough time resolution to estimate damping ratios up to 7 %. If there would be another mode closer to the 0.3 Hz than the 0.5 Hz, then another wavelet function with better frequency resolution (e.g. Gaus44) could be selected but the time resolution of this wavelet function would be poorer and there would be a high bias in the damping estimates when the real damping ratio would be higher than 4 %. Bias increases when the mode extraction wavelet length increases, this is evident in the results achieved for the simulated data (e.g. Figure 59 and Figure 60). For the measured data the real damping is not known, but the longer the mode extraction wavelet the lower the estimate of the damping ratio (e.g. Figure 92) and presumably the higher the bias is. Also the time window length of the method affects the bias because of the characteristics of the random decrement technique. If a short time window is used, the number of samples averaged in the random decrement technique is too low, the estimation of the impulse response is poor, and the damping estimates are poor, too.

The performance analyses of this thesis are based on the simulation studies and analysis of the measured data. Because of the complexity of the damping estimation procedure, the performance of the method cannot be assessed with analytic means. The damping estimation method assumes linear behavior of the power system dynamics. However, in the studies of this thesis, the nonlinear simulation model of the Nordic power system is used and therefore the damping estimation results are very realistic. Even though some nonlinearity would exist under the ambient conditions, its effect on the damping estimates is negligible since the excitations are small in amplitude. The explicit study of the effect of the nonlinearity on the damping estimates is not in the scope of this thesis. In addition, the effect of different input characteristics other than the Gaussian noise is not studied, although the input in the simulation studies is not strictly Gaussian and should be reflected in the results.

The selection of correct parameters for the damping estimation method is an important part of the damping estimation presented in this thesis. Although detailed studies are made, it is recognized that the parameter selection is based on the analysis of a limited number of combinations between the different parameters. Also the number of operating conditions of the power system, applied in the study, is limited. However, the studied cases represent the real conditions where the damping estimation is applied and therefore the parameter selection is at least nearly optimal.

7 Conclusions

7.1 General Conclusions

This thesis presented a novel approach into electromechanical oscillation damping estimation during ambient operation of the power system. The method is based on utilizing the wavelet transform and the random decrement technique. The method can be applied to monitor any oscillation mode although the main emphasis in this thesis was in estimation of the Nordic power system 0.3 Hz inter-area mode. The only limitation is that there should not be other modes too close to the mode of interest. The closer the other mode is to the mode of interest, the better frequency resolution is required for the mode extraction wavelet function. The better frequency resolution leads to poorer time resolution, because there is a tradeoff between the frequency and time resolutions of a wavelet function. The poorer time resolution further leads to higher bias (deviation from the real value) of the damping estimates. The amount of bias depends on the real damping ratio of the mode in such a way that when the real damping ratio is lower, the bias is lower too. The mean values of the estimates are either correct or lower than the real damping; therefore the damping estimates do not lead to reduced system security.

The parameters of the damping estimation method were selected with detailed studies. The properties of the different wavelet functions in case of oscillation monitoring were considered. General criteria for selecting the optimal mother wavelets in oscillation monitoring were specified and the criteria were quantitatively defined for the Nordic power system.

The damping estimation method's capability to estimate the damping was studied both in the case of the simulated and measured data of the Nordic power system. When the simulated data is used, the real damping of the mode is known and it can be compared to the estimated damping. The results show that when the parameters (especially the mother wavelets and time window length but also the other parameters shown in Figure 14) of the damping estimation method are selected correctly, the method can estimate the damping reasonably well both in terms of the mean value of the estimate and the standard deviation. The most accurate damping estimation results are achieved when the damping ratio is low (below 5 %), a long time window (above 5 minutes) and a long mode extraction wavelet (Gaus20 or Gaus44) is used. In addition, the analyzed signal should have good observability of the mode of interest (and preferably poor observability of the other modes). The measurement noise of the analyzed signals does not have much effect on the estimates especially when the longer mode extraction wavelets (Gaus20 and Gaus44) are used.

When the damping ratio is higher than 5 %, the longest mode extraction wavelets (e.g. Gaus44) are not applicable because the time resolution is too poor and therefore the estimates have too large bias. In the thesis, an optimal compromise between the frequency and time resolutions of the mode extraction wavelet function was studied and the wavelet functions for damping estimation of the Nordic power system were identified. With these wavelet functions (e.g. Gaus20), accurate estimates of the

damping can be achieved when the damping ratio is rather low (below 7 %), and for the higher damping ratios the estimates are conservative; i.e. they are lower than the real damping. If the analyzed signal contains only the mode of interest, even higher damping ratios than 7 % can be estimated with the method, when a shorter mode extraction wavelet than Gaus20 is used. The wavelet transform can be applied to find out the different modes in the signals at different time instances. However, the Gaus20 wavelet function produces a good compromise if the wavelet function is kept fixed.

When the measured data is studied, the real damping of the mode is not known and the focus is on the variation of the estimates around the mean value. The variation is measured by the standard deviation of the estimates because it is a measure of how much the individual estimates generally deviate from the mean value. The smaller the standard deviation is, the more accurate the estimates are. The results for the measured data show, that the time window should be roughly 20 minutes long in order to minimize the standard deviation of the estimates. It was also shown that the degraded damping due to the incorrect operation of the damping controller can be observed with the damping estimation method. The detection of improved damping due to the new damping controller (or better tuned controller) was observed to be harder.

The mode frequency estimates were more accurate than the damping estimates both for the simulated and the measured data. It has also been recognized in the other studies of the field that the mode frequency estimation is more accurate than the damping estimation (Turunen et al. 2008, Messina 2009).

The general sources of the damping estimate inaccuracy were discussed in the thesis. It was concluded that the main part of the inaccuracy is generally due to the differences between the real and the assumed excitation of the power system oscillations. The method assumes the excitation to be random Gaussian noise (see Section 2.2.3), but random departures from this assumption cause variance to the estimates. Using longer time windows reduces the variance, because the assumption becomes more valid.

A similar kind of performance characteristics as found in this thesis has been reported, for instance, by Liu & Venkatasubramanian (2008), Trudnowski et al. (2008), and Trudnowski & Pierre (2009); i.e. the damping estimates are more accurate for a poorly damped mode. The standard deviations of the damping estimates are usually slightly higher than those observed in this thesis (e.g. Wies et al. 2003, Liu & Venkatasubramanian 2008) indicating that the accuracy of the developed method is well comparable to the other methods of the field. The method of this thesis produces conservative results for the damping estimates; this is not the case for all methods (e.g. Wies et al. 2003, Anderson et al. 2005, Trudnowski et al. 2008, Turunen et al. 2008). The conservative estimates are beneficial because they do not lead to reduced system security. Usually, the performance of the commercial damping monitoring systems is not well reported. However, the test period that was carried out at Fingrid did show that improved performance is required (Turunen 2005). This thesis presents a method towards significantly more accurate damping estimates.

7.2 Future Work

In general terms, the future work in the area of electromechanical oscillation damping estimation includes the search for new and preferably better damping estimation methods, improvement of the existing methods, and finding the utilizations of the methods.

7.2.1 Damping Estimation under the Ambient Conditions

In the field of damping estimation under the ambient conditions it would be important to study the validity of the assumptions of the methods with real data. For example, the random load variations under the ambient conditions are commonly assumed to be Gaussian distributed. Another common assumption is the linear behavior of the power system when it is subjected to small excitations. However, some of the approaches in damping estimation do not necessarily carry these assumptions; see, for example, Messina (2009).

When the specific future work areas of the wavelet-based damping estimation method are considered, the main topic would be the extension of the method to allow multiple input signal analysis, and therefore possibly more accurate damping estimates. The observabilities of the modes in different measurements can be achieved from the linear analysis of the simulation model or they can possibly be estimated from the measured data. The signals with the best observabilities can then be used in the analysis. However, if the signal is carefully selected for the univariate method, the benefit of using multiple inputs in the analysis should be small.

The thesis focused on introducing a new method for damping estimation, and studying its performance characteristics. The comparison to other published methods is an area of future work. However, the method's performance is assessed to be comparable to other methods.

7.2.2 Online Utilization of Damping Estimation

In the thesis it was shown that the degraded damping due to the incorrect operation of the damping controller can be observed with the damping estimation method. The detection of improved damping due to the new damping controller (or better tuned controller) was observed to be harder but might be possible. Future research is needed to find out how the method can be utilized most optimally in practice.

Another online application of the damping estimation method could possible be online transfer limit monitoring. In this approach the power transfer limit would be set based on the estimated damping in such a way that the damping estimate must remain above a certain level. However, when the system is operated with the n – 1 criterion, the damping after the n – 1 contingency must be positive to maintain system stability. Because the damping estimation is done when the grid is operating intact, it should be

possible to predict the decrease in damping due to the n – 1 contingency. Even if the prediction could be done with good enough accuracy (based on a detailed simulation study of the grid), the variance of the damping estimate might be an obstacle.

7.2.3 Offline Utilization of Damping Estimation

A possible offline use of damping estimation could be the verification of the dynamic simulation model of the power system. This could be implemented by comparing the estimated damping with the simulated damping in the same power flow situation in which the damping is poor. Here, about 9 % damping ratio is estimated for the measured data case (Figure 87) while the simulated damping with the approximately same power transfer from Finland to Sweden is about 7 %. Because the estimation error is about 0.5 pp (estimation error in terms of standard deviation, pp is percentage point), the difference between the damping in simulation and measurement is significant. There is also a clear difference in the estimated mode frequency of simulation (about 0.3-0.31 Hz, Figure 46) and measurement (about 0.33-0.35 Hz, Figure 84).

The simulation model used in the studies is somewhat outdatet: many components[23], which increase the damping, have been added to the power system. These components explain the difference in the damping in this case. Because the damping estimation method is capable of indicating the difference in damping in this case, a topic of future work is to study in detail if the method can be used for verification of the simulation model.

7.2.4 Damping Estimation under the Transient Conditions

Utilization of the wavelet-based damping estimation method under the transient conditions is a possible topic of future work. The transients can be caused for example by faults or switching events in the grid. The assumption is that if the system behaves linearly during the transient and the damping remains constant, the performance of the method improves during the transient because the signal-to-noise ratio of the oscillations increases. However, if the damping is different before and after the transient, the damping ratios produced by the method lie in between the pre-transient and post-transient damping ratios and approach the post-transient damping when the time window moves forward.

[23] For example, several series compensators in the AC transmission path between Finland and Sweden, several other reinforcements in the grid, and an HVDC-link between Finland and Estonia with a power oscillation damper.

8 References

Anderson, M. G., Zhou, N., Pierre, J. W., Wies, R. W. 2005. Bootstrap-Based Confidence Interval Estimates for Electromechanical Modes From Multiple Output Analysis of Measured Ambient Data. IEEE Trans. Power Systems. vol. 20. no. 2. pp. 943-950. May 2005.

Banejad, M., Ledwich, G. 2002. Correlation Based Mode Shape Determination of a Power System. Proc. 2002 IEEE Int. Conf. on Acoustics, Speech, and Signal Processing. vol. 4. pp. 3832-3835.

Brincker, R., Krenk, S., Kirkegaard, P.H., Rytter, A. 1992. Identification of Dynamical Properties from Correlation Function Estimates. Bygningsstatiske Meddelelser. vol. 63. no. 1. pp. 1-38.

Bronzini, M., Bruno, S., De Benedictis, M., La Scala, M. 2007. Power system modal identification via wavelet analysis. Proc. 2007 IEEE Lausanne Power Tech, pp. 2041-2046.

Cai, J. Y., Huang, Z., Hauer, J., Martin, K. 2005. Current Status and Experience of WAMS Implementation in North America. Proc. 2005 IEEE/PES Transmission and Distribution Conference & Exhibition: Asia and Pacific. Dalian, China. 7 pp.

Cam, L. L. 1986. The central limit theorem around 1935. Statistical Science. vol. 1. no. 1. pp. 78–91.

Chang, C. S. 1975. Study of Dynamic Characteristics of Aerodynamic Systems Utilizing Randomdec Signatures. NASA. CR-132563.

Cirio, D., Danelli, A., Pozzi, M., Cecere, S., Giannuzzi, G., Sforna, M. 2006. Wide Area Monitoring and Control System: the Italian research and development. CIGRE 2006 Session, SC C2-208, Paris 27th Aug. – 1st Sep.

Cole, A. H. 1971. Failure Detection of a Space Shuttle Wing Flutter by Random Decrement. NASA. TMX-62, 041.

Cole, A. H. 1973. On-line Failure Detection and Damping Measurement of Space Structures by Random Decrement Signatures. NASA. CR-2205.

Crow, M. L., Singh, A. The Matrix Pencil for Power System Modal Extraction. IEEE Trans. Power Systems. vol. 20. no. 1. pp. 501-502. Feb 2005.

Daubechies, I. 1992. Ten Lectures on Wavelets. Philadelphia, PA: SIAM. pp. 1-7.

Depablos, J., Centeno, V., Phadke, A. G., Ingram, M. Comparative Testing of Synchronized Phasor Measurement Units. Proc. 2004 IEEE Power Engineering Society General Meeting. vol. 1. pp. 948-954.

Doraiswami, R., Liu, W. 1993. Real-time Estimation of the Parameters of Power System Small Signal Oscillations. IEEE Trans. Power Systems. vol. 8. pp. 74-83. Feb. 1993.

Elenius, S., Uhlen, K., Lakervi, E. 2005. Effects of Controlled Shunt and Series Compensation on Damping in the Nordel System. IEEE Trans. Power Systems. vol. 20. no. 4. pp. 1946-1957. Nov. 2005.

Ghasemi, H., Cañizares, C. 2007. On-Line Damping Torque Estimation and Oscillatory Stability Margin Prediction. IEEE Trans. Power Systems. vol. 22. no. 2. pp. 667-674. May 2007.

Glickman, M., O'Shea, P., Ledwich, G. 2005. Damping Estimation in Highly Interconnected Power Systems. Proc. 2005 IEEE Region 10 TENCON. pp. 1-4. Nov. 2005.

Glickman, M., O'Shea, P., Ledwich, G. 2007. Estimation of Modal Damping in Power Networks. IEEE Trans. Power Systems. vol. 22. no. 3. pp. 1340-1350. Aug. 2007.

Grund, C. E., Paserba, J. J., Hauer, J. F., Nilsson, S., 1993. Comparison of Prony and Eigenanalysis for Power System Control Design. IEEE Trans. Power Systems. vol. 8. no. 3. pp. 964-971. Aug. 1993.

Hashiguchi, T., Yoshimoto, M., Mitani, Y., Saeki, O., Tsuji, K., Hojo, M., Ukai, H. 2003. Analysis of Power System Dynamics Based on Multiple Synchronized Phasor Measurements. Proc. 2003 IEEE Power Engineering Society General Meeting, vol. 2, pp. 615-620.

Hauer, J. F. 1991. Application of Prony Analysis to the Determination of Modal Content and Equivalent Models for Measured Power System Response. IEEE Trans. Power Systems. vol. 6. no. 3. pp. 1062-1068. Aug. 1991.

Hauer, J. F., Mittelstadt, W. A., Martin, K. E., Burns, J. W., Lee, H., Pierre, J. W., Trudnowski, D. J. 2009. Use of the WECC WAMS in Wide-Area Probing Tests for Validation of System Performance and Modeling. IEEE Trans. Power Systems. vol. 24. pp. 250-257. Feb. 2009.

Hemmingsson, M. Power System Oscillations: Detection, Estimation & Control. 2003. Doctoral thesis. Lund University, Faculty of Engineering. Department of Industrial Electrical Engineering and Automation. 158 pp.

Hemmingsson, M., Samuelsson, O., Pedersen, K. O. H., Nielsen, A. H. 2001. Estimation of Electro-Mechanical Mode Parameters using Frequency Measurements. Proc. 2001 IEEE Power Engineering Society Winter Meeting. vol 3. pp. 1172-1177.

Ibrahim, S. R. 1977. Random Decrement Technique for Modal Identification of Structures. Journal of Spacecrafts. 14(11).

Kang, P., Ledwich, G. 1999. Estimating Power System Modal Parameters using Wavelets. Proc. 5th Int. Symposium on Signal Processing and Its Applications. vol. 2. pp. 563-566. Aug. 1999.

Kim, C. H., Aggarwal, R. 2001. Wavelet transforms in power systems. Part 2 Examples of application to actual power system transients. Power Engineering Journal. vol. 15, issue 4. pp. 193-202. Aug. 2001.

Korba, P. 2007. Real-time monitoring of electromechanical oscillations in power systems: first findings. IET Generation, Transmission & Distribution, vol. 1, issue 1, pp. 80-88.

Korba, P., Larsson, M., Rehtanz, C. 2003. Detection of Oscillations in Power Systems using Kalman Filtering Techniques. Proc. 2003 IEEE Conf. on Control Applications. vol. 1. pp. 183-188.

Korba, P., Uhlen, K. 2010. Wide-area monitoring of electromechanical oscillations in the Nordic power system: practical experience. IET Generation, Transmission & Distribution, vol. 4, issue 10, pp. 1116-1126.

Kundur, P. 1993. Power System Stability and Control. McGraw-Hill Inc. 1176 p.

Laila, D. S., Larsson, M., Pal, B. C., Korba, P. 2009. Nonlinear damping computation and envelope detection using Hilbert transform and its application to power systems wide area monitoring. Proc. 2009 IEEE Power & Energy Society General Meeting, 7 pp.

Larsson, M., Korba, P., Zima, M. 2007. Implementation and Applications of Wide-area monitoring systems. Proc. 2007 IEEE Power Engineering Society General Meeting. 6 pp.

Larsson, M., Laila, D. S. 2009. Monitoring of Inter-Area Oscillations under Ambient Conditions using Subspace Identification. Proc. 2009 IEEE Power & Energy Society General Meeting. 6 pp.

Ledwich, G. 2007. Decoupling for improved Modal Estimation. Proc. 2007 IEEE Power Engineering Society General Meeting. 6 pp.

Ledwich, G., Geddey, D., O'Shea, P. 2008. Phasor Measurement Unit's for system diagnosis and load identification in Australia. Proc. 2008 IEEE Power Engineering Society General Meeting. 6 pp.

Ledwich, G., Palmer, E. 2000. Modal Estimates from Normal Operation of Power Systems. Proc. 2000 IEEE Power Engineering Society Winter Meeting. vol. 2. pp. 1527-1531.

Leirbukt, A., Breidablik, Ø., Gjerde, J. O., Korba, P., Uhlen, K., Vormedal, L. K. 2008. Deployment of a SCADA Integrated Wide Area Monitoring System. Transmission and Distribution Conference and Exposition: Latin America, 2008 IEEE/PES. 6 pp.

Leirbukt, A. B., Gjerde, J. O., Korba, P., Uhlen, K., Vormedal, L. K., Warland, L. 2006. Wide Area Monitoring Experiences in Norway. Proc. 2006 IEEE PES PSCE. pp. 353-360.

Li, W., Gardner, R. M., Dong, J., Wang, L., Xia, T., Zhang, Y., Liu, Y., Zhang, G., Xue, Y. 2009. Wide Area Synchronized Measurements and Inter-Area Oscillation Study. IEEE PES PSCE, 15-18 March 2009. 8 pp.

Liu, G., Venkatasubramanian, V. 2008. Oscillation Monitoring from Ambient PMU Measurements by Frequency Domain Decomposition. Proc. 2008 IEEE Int. Symposium on Circuits and Systems. pp. 2821-2824.

Machowski, J., Bialek, J. W., Bumby, J. R. 1997. Power System Dynamics and Stability. John Wiley & Sons Ltd. 461 p.

Mallat, S. 1999. A Wavelet Tour of Signal Processing. Academic Press.

Mallat, S. G. 1989. A Theory for Multiresolution Signal Decomposition: The Wavelet Representation. IEEE Trans. Pattern Analysis and Machine Intelligence. vol. 11. no. 7. pp. 674-693. Jul. 1989.

Mei, K., Rovnyak, S. M., Ong, C.-M. 2006. Dynamic Event Detection Using Wavelet Analysis. Proc. 2006 IEEE Power Engineering Society General Meeting, 7 pp.

Messina, A. R. (Editor). 2009. Inter-area Oscillations in Power Systems. A Nonlinear and Nonstationary Perspective. Springer Science+Business Media LLC. 267 p.

Messina, A. R., Vittal, V. 2006. Nonlinear, Non-Stationary Analysis of Interarea Oscillations via Hilbert Spectral Analysis. IEEE Trans. Power Systems. vol. 21. no. 3. pp. 1234-1241. Aug 2006.

Messina, A. R., Vittal, V., Ruiz-Vega, D., Enríquez-Harper, G. 2006. Interpretation and Visualization of Wide-Area PMU Measurements Using Hilbert Analysis. IEEE Trans. Power Systems. vol. 21. no. 4. pp. 1763-1771. Nov 2006.

Misiti, M., Misiti, Y., Oppenheim, G., Poggi, J.-M. 2009. Wavelet Toolbox™ 4. User's Guide. Natick, MA: The MathWorks, Inc. Mar. 2009.

Mithulananthan, N., Canizares, C. A., Reeve, J., Rogers, G. J. 2003. Comparison of PSS, SVC, and STATCOM Controllers for Damping Power System Oscillations. IEEE Trans. Power Systems. vol. 18. no. 2. pp. 786-792. May 2003.

Padiyar, K. R. 1996. Power System Dynamics. Stability and Control. John Wiley & Sons (Asia) Pte Ltd. 629 p.

Pal, B., Chaudhuri, B. 2005. Robust Control in Power Systems. Springer Science+Business Media Inc. 190 p.

Paserba, J. (Convenor). 1996 Analysis and Control of Power System Oscillations: CIGRE Special Publication 38.01.07. vol. Technical Brochure 111.

Phadke, A. G., Thorp, J. S. 2008. Synchronized Phasor Measurements and Their Applications: Springer Science.

Pierre, D. A., Trudnowski, D. J., Hauer, J. F. 1992. Identifying Linear Reduced-Order Models for Systems with Arbitrary Initial Conditions Using Prony Signal Analysis. IEEE Trans. Automatic Control. vol. 37. no. 6. pp. 831-835. Jun. 1992.

Pierre, J. W., Trudnowski, D. J., Donnelly, M. K. 1997. Initial Results in Electromechanical Mode Identification from Ambient Data. IEEE Trans. Power Systems. vol. 12. pp. 1245-1251. Aug. 1997.

Pierre, J. W., Zhou, N., Tuffner, F. K., Hauer, J. F., Trudnowski, D. J., Mittelstadt, W. A. 2010. Probing Signal Design for Power System Identification. IEEE Trans. Power Systems. vol. 25. no. 2. pp. 835-843. May 2010.

Poon, K. P., Lee, K. C. 1988. Analysis of Transient Stability Swings in Large Interconnected Power Systems by Fourier Transformation. IEEE Trans. Power Systems. vol. 3. no. 4. pp. 1573-1581. Nov. 1988.

Pourbeik, P. (Working Group Convenor), Morison, K. (Task Force Convenor). 2007. Review of on-line dynamic security assessment tools and techniques: CIGRE Working Group C4.601. vol. Technical Brochure 325.

Pourbeik, P. (Working Group Convenor), Rehtanz, C. (Task Force Convenor). 2007. Wide Area Monitoring and Control for Transmission Capability Enhancement: CIGRE Special Publication C4.601. vol. Technical Brochure 330.

Rogers, G. 2000. Power System Oscillations. Kluwer Academic Publishers. 328 p.

Ruiz-Vega, D., Messina, A. R., Enríquez-Harper, G. 2005. Analysis of Inter-Area Oscillations via Non-Linear Time Series Analysis Techniques. 2005 PSCC, session 32, paper 2, 7 pp.

Ruiz-Vega, D., Messina, A. R., Pavella, M. 2003. On-Line Assessment and Control of Poorly Damped Transient Oscillations. Proc. 2003 IEEE Power Engineering Society General Meeting. pp. 2084-2089.

Ruiz-Vega, D., Messina, A. R., Pavella, M. 2004. On-Line Assessment and Control of Transient Oscillations Damping. IEEE Trans. Power Systems. vol. 19. no. 2. pp. 1038-1047. May 2004.

Sanchez-Gasca, J. J., Chow, J. H. 1999. Performance Comparison of Three Identification Methods for the Analysis of Electromechanical Oscillations. IEEE Trans. Power Systems. vol. 14. no. 3. pp. 995-1002. Aug. 1999.

Sattinger, W., Bertsch, J., Reinhardt, P. 2006. Operational Experience with Wide Area Monitoring Systems. CIGRE 2006 Session. SC B5-216. Paris 27th Aug. – 1st Sep. 2006.

Siviter, R., Pollard, M. G. 1985. Measurement of Railway Vehicle Kinetic Behaviour Using the Random Decrement Technique. Vehicle System Dynamics. 14(1-3).

Su, C.-L., Jau, B.-Y. 2007. Visualization of Wide Area Dynamics in Power Network for Oscillatory Stability Assessment. Proc. 2007 Int. Conf. on Intelligent Systems Applications to Power Systems. 6 pp.

Terzija, V., Cai, D., Fitch, J. 2009. Monitoring of Inter-Area Oscillations in Power Systems with Renewable Energy Resources using Prony Method. CIRED 20th International Conference on Electricity Distribution. Prague, 8-11 June 2009.

Thambirajah, J., Barocio, E., Thornhill, N. F. 2010. Comparative review of methods for stability monitoring in electrical power systems and vibrating structures. IET Generation, Transmission & Distribution, vol. 4, issue 10, pp. 1086-1103.

Thambirajah, J., Thornhill, N., Pal, B. 2010. A Multivariate Approach Towards Inter-Area Oscillation Damping Estimation Under Ambient Conditions Via Independent Component Analysis And Random Decrement. IEEE Trans. Power Systems, vol. 25, issue 4, 8pp, June 2010.

Trudnowski, D. J. 2008. Estimating Electromechanical Mode Shape From Synchrophasor Measurements. IEEE Trans. Power Systems. vol. 23. no. 3. pp. 1188-1195. Aug. 2008.

Trudnowski, D. J., Johnson, J. M., Hauer, J. F. 1998. SIMO System Identification from Measured Ringdowns. Proc. 1998 American Control Conference, pp. 2968-2972.

Trudnowski, D. J., Johnson, J. M., Hauer, J. F. 1999. Making Prony Analysis More Accurate using Multiple Signals. IEEE Trans. Power Systems. vol. 14. no. 1. pp. 226-231. Feb. 1999.

Trudnowski, D. J., Pierre, J. W. 2009. Overview of Algorithms for Estimating Swing Modes from Measured Responses. Proc. 2009 IEEE Power & Energy Society General Meeting, 8 pp.

Trudnowski, D. J., Pierre, J. W., Zhou, N., Hauer, J. F., Parashar, M. 2008. Performance of Three Mode-Meter Block-Processing Algorithms for Automated Dynamic Stability Assessment. IEEE Trans. Power Systems. vol. 23. no. 2. pp. 680-690. May. 2008.

Turunen, J. 2005. Tehoheilahtelujen vaimennuksen seuranta voimansiirtoverkossa. M.Sc thesis at Helsinki University of Technology. (In Finnish, abstract in English).

Turunen, J., Larsson, M., Korba, P., Jyrinsalo, J., Haarla, L. 2008. Experiences and Future Plans in Monitoring the Inter-area Power Oscillation Damping. Proc. 2008 IEEE Power Engineering Society General Meeting. 8 pp.

Uhlen, K., Elenius, S., Norheim, I., Jyrinsalo, J., Elovaara, J., Lakervi, E. 2003. Application of Linear Analysis for Stability Improvements in the Nordic Power Transmission System. Proc. 2003 IEEE Power Engineering Society General Meeting. vol. 4. pp. 2097-2103.

Uhlen, K., Warland, L., Gjerde, J. O., Breidablik, Ø., Uusitalo, M., Leirbukt, A. B. Korba, P. 2008. Monitoring Amplitude, Frequency and Damping of Power System Oscillations with PMU Measurements. Proc. 2008 IEEE Power Engineering Society General Meeting. 7 pp.

Vanfretti, L., Garcia-Valle, R., Uhlen, K., Johansson, E., Trudnowski, D., Pierre, J. W., Chow, J. H., Samuelsson, O., Østergaard, J., Martin, K. E. 2010. Estimation of Eastern

Denmark's Electromechanical Modes from Ambient Phasor Measurement Data. Proc. 2010 IEEE Power & Energy Society General Meeting, 8 pp.

Venkatasubramanian, M. V. 2003. Analyzing Blackout Events: Experience from the Major Western Blackouts in 1996. Power Systems Engineering Research Center. Background Paper.

Welch, P. D. 1967. The Use of Fast Fourier Transform for the Estimation of Power Spectra: A Method Based on Time Averaging Over Short, Modified Periodograms. IEEE Transactions on Audio Electroacoustics. vol. AU-15. pp 70–73. June 1967.

Wies, R. W., Balasubramanian, A., Pierre, J. W. 2006. Combining Least Mean Squares Adaptive Filter and Auto-Regressive Block Processing Techniques for Estimating the Low-Frequency Electromechanical Modes in Power Systems. Proc. 2006 IEEE Power Engineering Society General Meeting. 8 pp.

Wies, R. W., Balasubramanian, A., Pierre, J. W. 2006. Using Adaptive Step-Size Least Mean Squares (ASLMS) for Estimating Low-Frequency Electromechanical Modes in Power Systems. Proc. 2006 9th Int. Conf. on Probabilistic Methods Applied to Power Systems. pp. 1-8. Jun. 2006.

Wies, R. W., Balasubramanian, A., Pierre, J. W. 2007. Adaptive Filtering Techniques for Estimating Electromechanical Modes in Power Systems. Proc. 2007 IEEE Power Engineering Society General Meeting. 8 pp.

Wies, R. W., Pierre, J. W., Trudnowski, D. J. 2003. Use of ARMA Block Processing for Estimating Stationary Low-Frequency Electromechanical Modes of Power Systems. IEEE Trans. Power Systems. vol. 18. pp. 167-173. Feb. 2003.

Wies, R. W., Pierre, J. W., Trudnowski, D. J. 2004. Use of Least Mean Squares (LMS) Adaptive Filtering Technique for Estimating Low-Frequency Electromechanical Modes in Power Systems. Proc. 2004 IEEE Power Engineering Society General Meeting. vol. 2. pp. 1863-1870.

Wilson, D. H. 2007. Wide-Area Measurement and Control for Dynamic Stability. Proc. 2007 IEEE Power Eng. Soc. General Meeting. 5 pp.

Wiltshire, R. A., Ledwich, G., O'Shea, P. 2007. A Kalman Filtering Approach to Rapidly Detecting Modal Changes in Power Systems. IEEE Trans. Power Systems. vol. 22. no. 4. pp. 1698-1706. Nov. 2007.

Xie, X., Xin, Y., Xiao, J., Wu, J., Han, Y. 2009. WAMS Applications in Chinese Power Systems. IEEE Power & Energy Magazine. pp. 54-63. Jan/Feb 2009.

Zhang, C. L., Ledwich, G. F. 2003. A New Approach to Identify Modes of the Power System Based on T-Matrix. Proc. 2003 APSCOM 6th Int. Conf. on Advances in Power System Control, Operation and Management. vol. 2. pp. 496-501.

Zhang, X.-P., Rehtanz, C., Pal, B. 2006. Flexible AC Transmission Systems: Modelling and Control. Springer Berlin Heidelberg. 383 p.

Zhou, N., Pierre, J. W., Hauer, J. F. 2006. Initial Results in Power System Identification From Injected Probing Signals Using a Subspace Method. IEEE Trans. Power Systems. vol. 21. no. 3. pp. 1296-1302. Aug. 2006.

Zhou, N., Pierre, J. W., Trudnowski, D. 2006. A Bootstrap Method for Statistical Power System Mode Estimation and Probing Signal Selection. Proc. 2006 IEEE PES PSCE. pp. 172-178.

Zhou, N., Pierre, J. W., Trudnowski, D. J., Guttromson, R. T. 2007. Robust RLS Methods for Online Estimation of Power System Electromechanical Modes. IEEE Trans. Power Systems. vol. 22. no. 3. pp. 1240-1249. Aug. 2007.

Zhou, N., Trudnowski, D. J., Pierre, J. W., Mittelstadt, W. A. 2008. Electromechanical Mode Online Estimation Using Regularized Robust RLS Methods. IEEE Trans. Power Systems. vol. 23. no. 4. pp. 1670-1680. Nov. 2008.

Zima, M., Larsson, M., Korba, P., Rehtanz, C., Andersson, G. 2005. Design Aspects for Wide-Area Monitoring and Control Systems. Proc. of the IEEE. vol. 93. no. 5. pp. 980-996. May 2005.

Appendix A – WAMS and PMUs

The Wide-Area Monitoring System (WAMS), presented in Figure 1, consists of the measurement devices, the data concentrator, the communication infrastructure between the two and of the data handling and analyzing functions (Cai et al. 2005, Xie et al. 2009). The measurement devices are usually the Phasor Measurement Units (PMU) which provide voltage and current measurements synchronized to within a microsecond (Phadke & Thorp 2008).

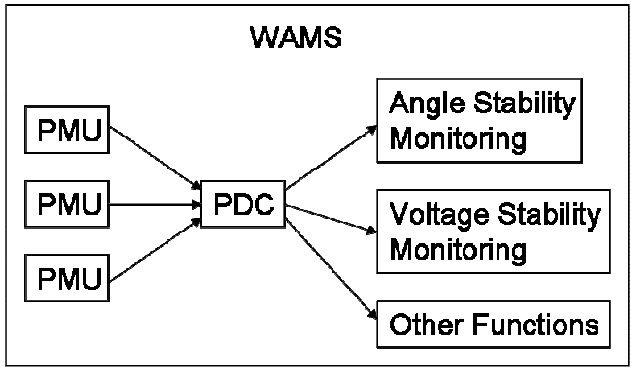

Figure 1. General structure of the wide-area monitoring system. PMU = Phasor Measurement Unit, PDC = Phasor Data Concentrator.

PMUs have been installed in the Finnish main grid since 2006. At the moment, the number of PMUs is eleven (Figure 2, two PMUs not shown in the figure) and they gather information for the Finnish WAMS. In addition, some PMU measurements from other parts of the Nordic power system are available in the Finnish WAMS. The WAMS functions used are power oscillation monitoring, phase angle monitoring, and event driven data archiving. The WAMS and especially the power oscillation monitoring function are still more or less in the development phase and are not used in the control center.

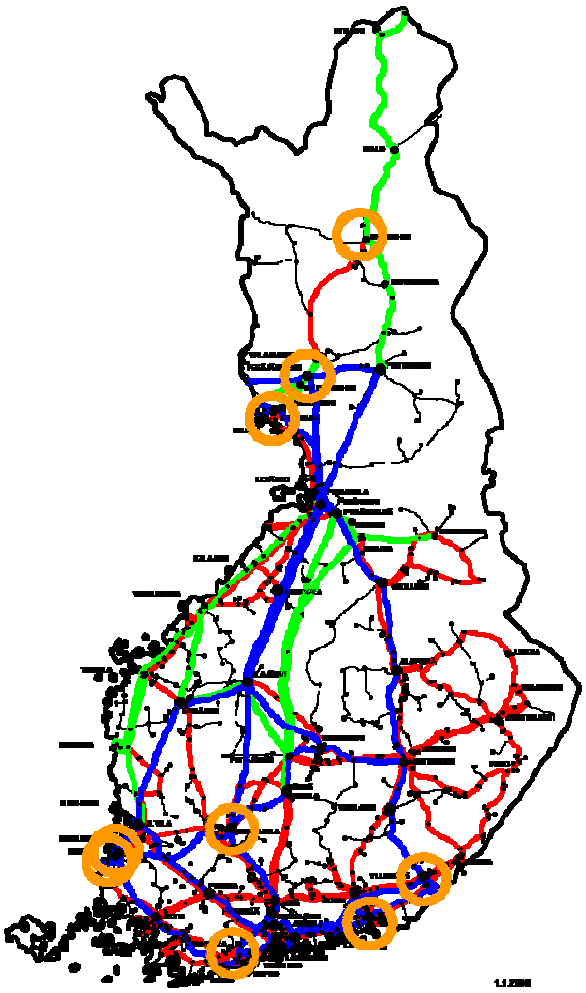

Figure 2. Finnish PMU installation status in the spring 2010.

Appendix B – Some Examples of Wavelets

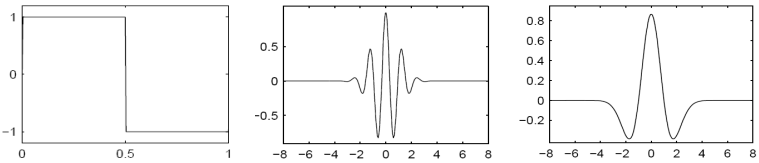

Figure 1. Haar wavelet, Morlet wavelet, and Mexican hat wavelet, respectively (Matlab® Wavelet Toolbox™ version 4.1).

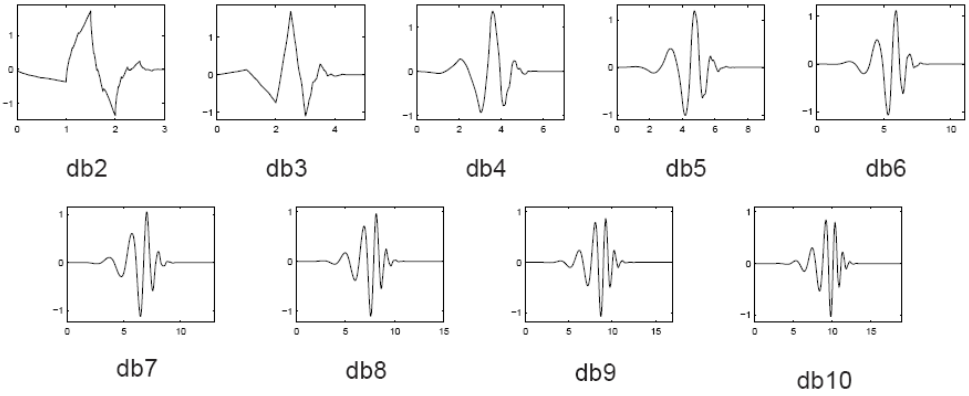

Figure 2. Some wavelets of Daubechies wavelet family (Matlab® Wavelet Toolbox™ version 4.1).

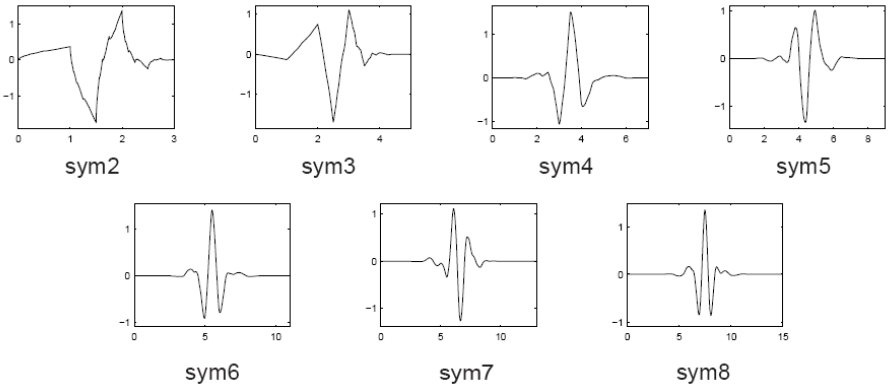

Figure 3. Some wavelets of symlets wavelet family (Matlab® Wavelet Toolbox™ version 4.1).

Appendix C – Illustration of the Uncertainty Principle

The uncertainty principle can be illustrated in practice for the original signal in Figure 7 (body text of the thesis) by presenting the 0.3 Hz and the 0.5 Hz wavelet coefficients of the original signal with the three wavelets in Figure 10 (body text of the thesis). The wavelet coefficients for the Gaus4, Gaus20, and Gaus44 wavelet are shown in Figure 1, Figure 2, and Figure 3, respectively.

When the original signal in Figure 7 (body text of the thesis) is analyzed with the 0.5 Hz Gaus4[24] wavelet, the wavelet coefficients (blue line) are much greater compared to the Gaus20 and Gaus44 wavelets. This implies that the frequency resolution of the Gaus4 wavelet is too poor to separate the 0.3 Hz and 0.5 Hz modes from each other. On the other hand, the Gaus4 wavelet coefficients react to changes in the original signal's amplitude much faster than the longer Gaus20 and Gaus44 wavelets. This is due to the better time resolution of the shorter wavelet. When the wavelet length increases, the time resolution worsens and the wavelet coefficient curve becomes "smoother."

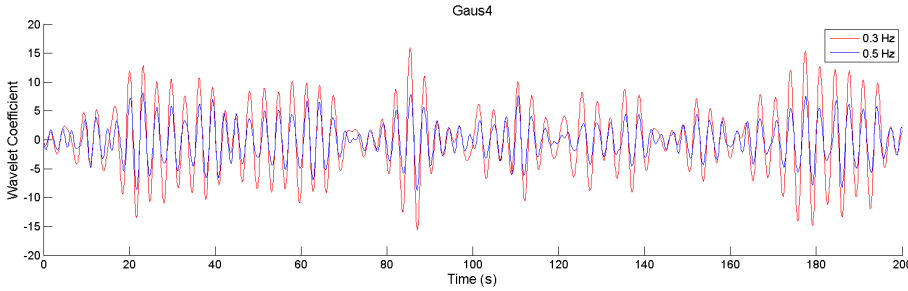

Figure 1. Wavelet coefficients of the original signal (Figure 7, body text of the thesis) with the 0.3 Hz and 0.5 Hz Gaus4 wavelet function.

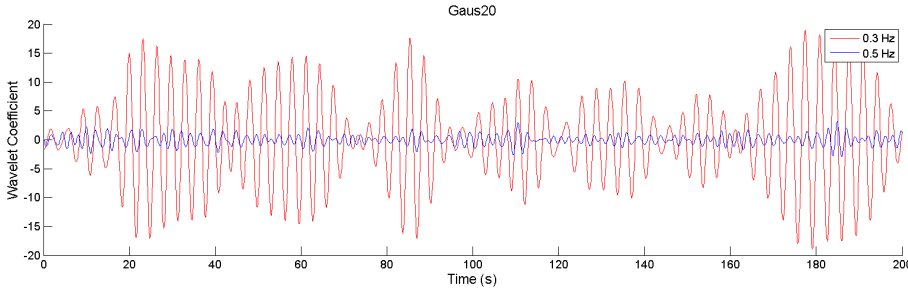

Figure 2. Wavelet coefficients of the original signal (Figure 7, body text of the thesis) with the 0.3 Hz and 0.5 Hz Gaus20 wavelet function.

[24] Gaus20 wavelet function having the center frequency of 0.5 Hz.

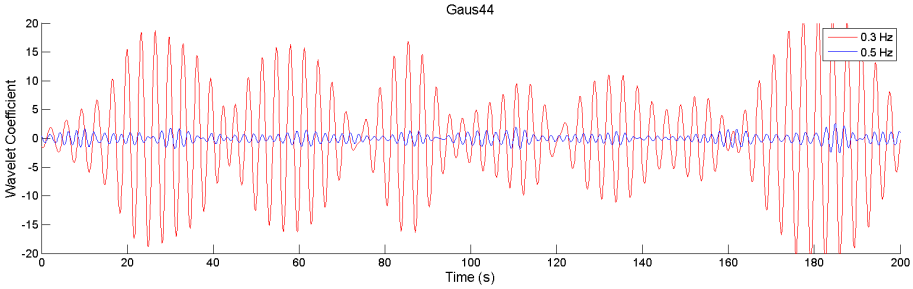

Figure 3. Wavelet coefficients of the original signal (Figure 7, body text of the thesis) with the 0.3 Hz and 0.5 Hz Gaus44 wavelet function.

Appendix D – Wavelet Transform Comparison to Short Time Fourier Transform

Short time Fourier transform (STFT, or windowed Fourier transform) and wavelet transform can be written as inner products with their respective time-frequency atoms (Mallat 1999)

$$Sy(c,b) = \int_{-\infty}^{\infty} y(t) g_{c,b}^{*}(t)\, dt = \left\langle y, g_{c,b} \right\rangle \tag{1}$$

and

$$Wy(a,b) = \int_{-\infty}^{\infty} y(t) \psi_{a,b}^{*}(t)\, dt = \left\langle y, \psi_{a,b} \right\rangle, \tag{2}$$

where $Sy(c,b)$ and $Wy(a,b)$ are STFT and WT of $y(t)$ respectively, c and a are the scaling parameters of STFT and WT respectively, b is the position of the time-frequency atom g or ψ in case of STFT and WT respectively, and $\langle\ \rangle$ denotes the inner product.

Equation (1) and Equation (2) are similar to each other except that the time-frequency atoms (g and ψ) are different. STFT's time-frequency atom, g, consists of a sinusoidal signal multiplied with a separate windowing function that is fixed for various frequency components of the signal. On the other hand, WT's time-frequency atom, ψ, inherently utilizes the variable window length for various frequency components of the signal. The variable window length of ψ comes from stretching or compressing the wavelet function to analyze different frequency components of the signal. Thus low frequency components are analyzed with longer time windows than the high frequency components when the same mother wavelet is considered. This beneficial property of wavelet transform leads to an equal number of oscillation cycles to be used in the wavelet transform independent of the analyzed frequency (Daubechies 1992).

Appendix E – Biases of the Damping Estimates

Damping estimate biases with different SNRs and time window lengths for the Gaus4, Gaus20, and Gaus44 mode extraction wavelets are presented in Figure 1, Figure 2, and Figure 3, respectively.

The noise has some effect on the damping estimate biases especially in case of the short mode extraction wavelet (Gaus4). The effect of noise is minimized when the longer mode extraction wavelets (Gaus20 and Gaus44) are used. When the time window length increases, the effect of noise on the damping estimate biases decreases. However, this is evident here only when the time window length increases from one minute to longer.

When the realistic SNRs (≥ 5) and longer time windows (≥ 3 min) are considered, the damping estimate biases are not much affected by the noise. This is the case for all the studied mode extraction wavelets. However, the effect of noise is even smaller when the longer mode extraction wavelets are used.

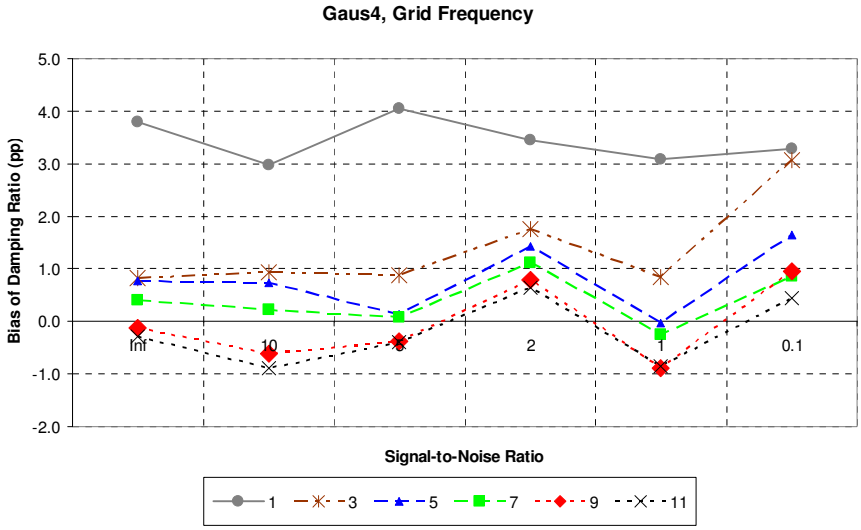

Figure 1. Damping estimate biases with different signal-to-noise ratios of the analyzed signal and with different time window lengths. The legend value shows the time window length in minutes. The mode extraction wavelet is the Gaus4. The analyzed signal is the grid frequency measurement at a bus in Southern Finland.

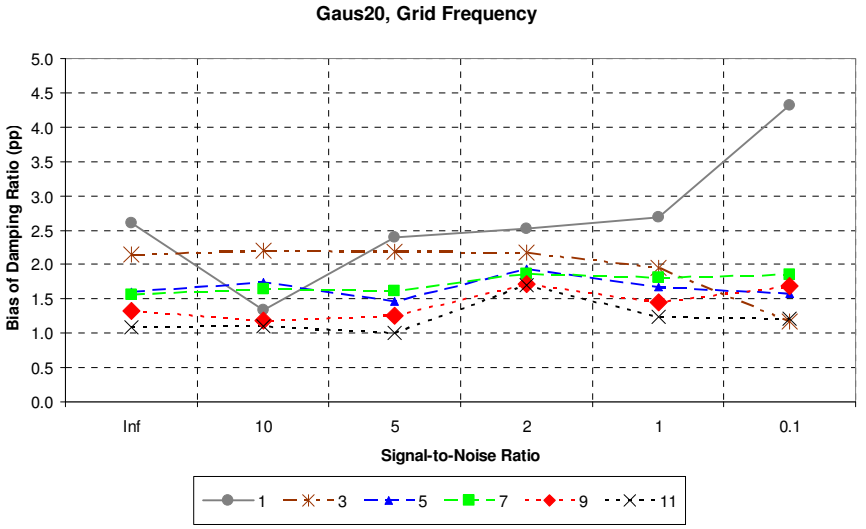

Figure 2. Damping estimate biases with different signal-to-noise ratios of the analyzed signal and with different time window lengths. The legend value shows the time window length in minutes. The mode extraction wavelet is the Gaus20. The analyzed signal is the grid frequency measurement at a bus in Southern Finland.

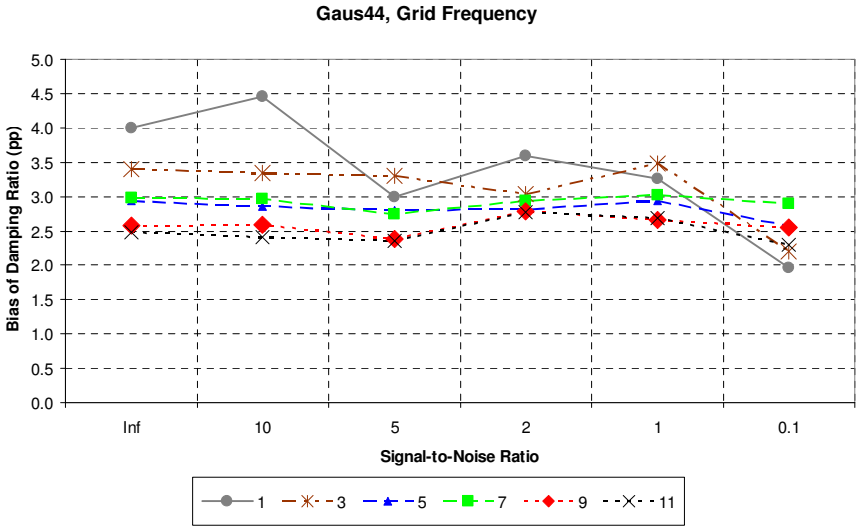

Figure 3. Damping estimate biases with different signal-to-noise ratios of the analyzed signal and with different time window lengths. The legend value shows the time window length in minutes. The mode extraction wavelet is the Gaus44. The analyzed signal is the grid frequency measurement at a bus in Southern Finland.

Appendix F – Biases of the Damping Estimates

The damping estimate biases with different time window lengths and two sets of parameters are presented in Figure 1, Figure 2, and Figure 3 for the mode extraction wavelets Gaus4, Gaus20, and Gaus44, respectively.

The biases are smaller for the parameter set in which the damping is estimated from the approximate impulse response using the shorter (Cmor1-1) wavelet and the damping is selected from the midpoint of the impulse response. With this short time window, the biases of the damping estimates are lower (in the case of the Gaus4 and the Gaus44 mode extraction wavelets) with the original set of parameters.

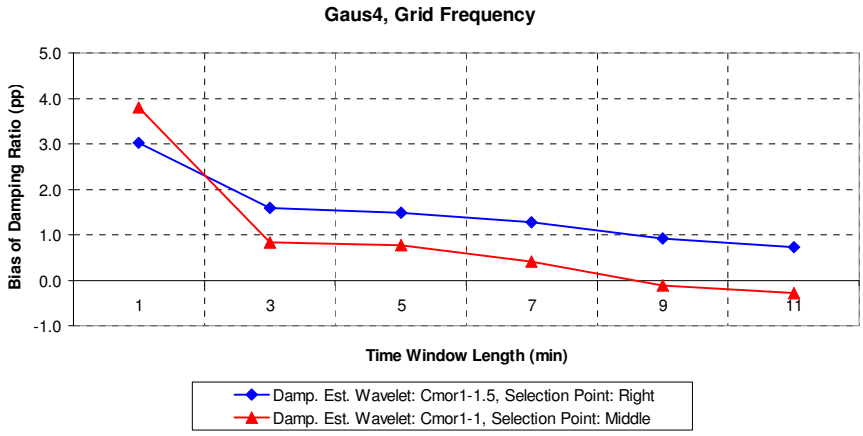

Figure 1. Damping estimate biases with different time window lengths and parameter sets of the damping estimation method. The mode extraction wavelet is the Gaus4. The analyzed signal is the grid frequency measurement at a bus in Southern Finland.

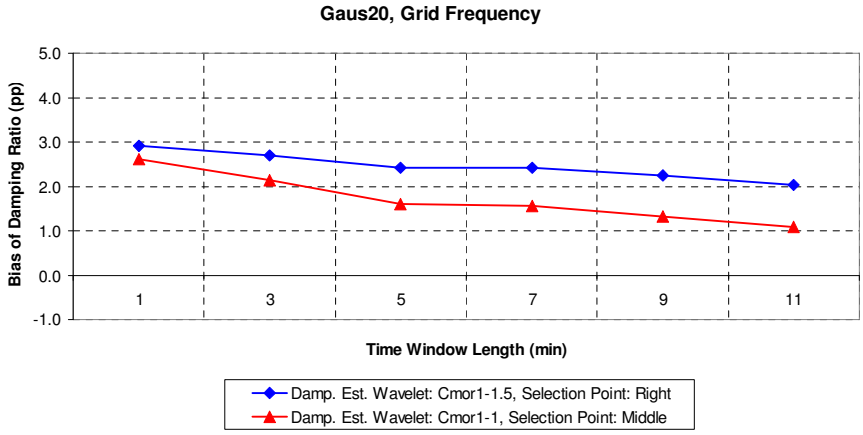

Figure 2. Damping estimate biases with different time window lengths and parameter sets of the damping estimation method. The mode extraction wavelet is the Gaus20. The analyzed signal is the grid frequency measurement at a bus in Southern Finland.

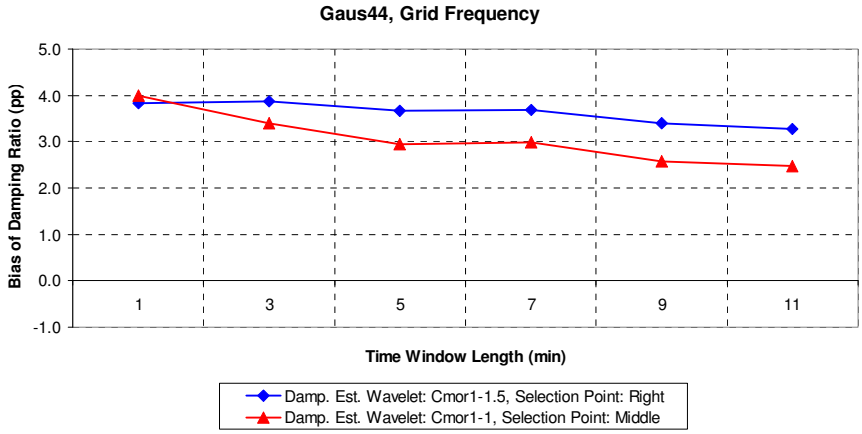

Figure 3. Damping estimate biases with different time window lengths and parameter sets of the damping estimation method. The mode extraction wavelet is the Gaus44. The analyzed signal is the grid frequency measurement at a bus in Southern Finland.

Errata

Add here the errata.

Some challenges are faced in the traditional way to manage the stability of a power system by extensive simulation studies: the studies can only be done for a limited set of operating conditions and the simulation model does not reflect the behavior of the real power system perfectly. Therefore, a specific margin has to be maintained between the allowed power transfer capacity and the theoretical maximum power transfer capacity. Even so, instabilities of the power systems have been recorded in the past, basically due to the discrepancies between the simulated and the real dynamic behavior of the power systems. The challenges in grid operation and planning pointed out above have led the transmission system operators to seek for new and innovative ways to manage the power system stability issue, use the grid efficiently, and keep the security high. One approach, a new wavelet-based method for damping estimation, is introduced and thoroughly studied in this thesis.

ISBN: 978-952-60-4051-6 (pdf)
ISBN: 978-952-60-4050-9
ISSN-L: 1799-4934
ISSN: 1799-4942 (pdf)
ISSN: 1799-4934

Aalto University
School of Electrical Engineering
Department of Electrical Engineering
aalto.fi

BUSINESS + ECONOMY

ART + DESIGN + ARCHITECTURE

SCIENCE + TECHNOLOGY

CROSSOVER

DOCTORAL DISSERTATIONS

Aalto-DD 16/2011